Hyphenation of a Microfluidic Platform with MALDI-TOF Mass Spectrometry for Single Cell Analysis

by

Mian Yang

A Dissertation Presented in Partial Fulfillment
of the Requirements for the Degree
Doctor of Philosophy

Approved April 2016 by the
Graduate Supervisory Committee:

Alexandra Ros, Chair
Randall Nelson
Mark Hayes

ARIZONA STATE UNIVERSITY

May 2016

ABSTRACT

Cell heterogeneity is widely present in the biological world and exists even in an isogenic population. Resolving the protein heterogeneity at the single cell level is of enormous biological and clinical relevance. However, single cell protein analysis has proven to be challenging due to extremely low amount of protein in a single cell and the huge complexity of proteome. This requires appropriate sampling and sensitive detection techniques. Here, a new approach, microfluidics combined with MALDI-TOF mass spectrometry was brought forward, for the analysis of proteins in single cells. The detection sensitivity of peptides as low as 300 molecules and of proteins as low as 10^6 molecules has been demonstrated. Furthermore, an immunoassay was successfully integrated in the microfluidic device for capturing the proteins of interest and further identifying them by subsequent enzymatic digestion. Moreover, an improved microfluidic platform was designed with separate chambers and valves, allowing the absolute quantification by employing iTRAQ tags or an isotopically labeled peptide. The study was further extended to analyze a protein in MCF-7 cell lysate. The approach capable of identifying and quantifying protein molecules in MCF-7 cells is promising for future proteomic studies at the single cell level.

ACKNOWLEDGMENTS

First of all, I want to express my sincere gratitude towards my research advisor, Professor Alexandra Ros, for her professional instruction to my research and support in my Ph.D. career.

I also express my sincere thanks to my advisory committee members Professor Mark Hayes and Professor Randall W. Nelson for their concern and advice on my research project and thesis.

I want to thank Dr. Tzu-Chiao Chao for his insightful comments and suggestions in my project especially in the first two years of my Ph.D.

I thank Dr. Chad Borges and Dr. Matthew Schaab at the Biodesign Institute at Arizona State University for technical assistance on Bruker Ultraflex III MALDI-TOF/TOF instrument, Dr. Robert Ros and Nethmi Ariyasinghe for donating MCF-7 samples and their help for MCF-7 culturing, Nicole Hansmeier for providing a tryptic BSA digest for this study.

I am grateful to my family and friends. My parents have supported me at every step in my life. And I am especially thankful to my husband Jitao Zhang for his understanding and support in these five years at ASU.

TABLE OF CONTENTS

Page

LIST OF TABLES vii

LIST OF FIGURES viii

CHAPTER

1 INTRODUCTION 1

1.1 Significance of Single Cell Analysis 1

1.2 Challenge of Single Cell Proteome Analysis 4

1.3 Current Single Cell Proteome Analysis Status 5

1.4 Dissertation Objective 12

2 FUNDERMENTALS AND THEORY 15

2.1 Immunoassays 15

2.2 MALDI Mass Spectrometry 20

2.3 Quantitative Proteome Analysis by MALDI MS 26

3 DIRECT DETECTION OF PEPTIDES AND PROTEINS REACHING SINGLE CELL SENSITIVITY 31

3.1 Introduction 31

3.2 Materials and Methods 32

3.2.1 Materials 32

3.2.2 Microchip Fabrication 33

3.2.3 Protein Digestion 35

3.2.4 Chip Loading and Manifold Removal 35

CHAPTER Page

3.2.5 MS Analysis.....36

3.2.6 Immobilization of IgG and Insulin Immunoassay.....37

3.3 Results and Discussion.....37

3.3.1 Hyphenation of a Microfluidic Device with MALDI-TOF Instrument.....37

3.3.2 Detection and Identification of Peptides and Proteins.....40

3.3.3 Affinity Capture and MS Detection in a Microfluidic Channel.....44

3.4 Section Conclusions.....48

4 A MICROFLUIDIC PLATFORM FOR PROTEIN IDENTIFICATION AND PROTEIN QUANTIFICATION 50

4.1 Introduction.....50

4.2 Materials and Methods.....51

4.2.1 Materials.....51

4.2.2 Microchip Fabrication.....52

4.2.3 Bcl-2 Immunoassay, Digestion and iTRAQ Tagging.....55

4.2.4 Bcl-2 Quantification in the Ladder-Like Device.....56

4.2.5 MS analysis.....57

4.3 Results and Discussion.....58

4.3.1 Chip Fabrication and Valve Actuation.....58

4.3.2 Affinity Capture and Identification of Bcl-2 in Microfluidic Channels.....60

CHAPTER Page

4.3.3 iTRAQ Tagging of Bcl-2.....64

4.3.4 Quantification of Bcl-2 in the Ladder-like Device.....66

4.4 Section Conclusions.....71

5 IMPROVEMENT OF ABSOLUTE PROTEIN QUANTIFICATION BY AN ISOTOPICALLY LABLED PEPTIDE 72

5.1 Introduction.....72

5.2 Materials and Methods..... 73

5.2.1 Materials.....73

5.2.2 Digestion Efficiency Test of Bcl-2 in Solution.....74

5.2.3 Absolute Protein Quantification by Using an Isotope Labeled Peptide.....74

5.3 Results and Discussion.....75

5.3.1 Solution Digestion Efficiency.....76

5.3.2 Bcl-2 Quantification On-chip by Using an Isotope Labeled Peptide.....78

5.4 Section Conclusions.....81

6 DETECTION AND QUANTIFICATION OF BCL-2 IN CANCER CELLS.....83

6.1 Introduction.....83

6.2 Materials and Methods.....84

6.2.1 Materials.....84

6.2.2 Cell Lysis.....85

6.2.3 Detection of Spiked Bcl-2 in MCF-7 Cell Lysate.....86

CHAPTER Page

6.2.4 Coupling Cell Loading, Lysis with Protein Affinity Capture, Identification and Quantification on Chip....86

6.3 Results and Discussion....88

6.3.1 MCF-7 Cell Lysis....88

6.3.2 Influence of Sample Complexity on Detection of Bcl-2 in Cell Lysate....90

6.3.3 Bcl-2 Identification and Quantification in single MCF-7 cells....93

6.4 Section Conclusions....96

7 CONCLUSION AND OUTLOOK....98

REFERENCES....103

APPENDIX

A SUPPLEMENTAL MATERIAL FOR CHAPTER 4 120

LIST OF TABLES

Table Page

4-1 Identification of Peaks from 1.4 μM in the Spectrum 63

4-2 Dilution series for iTRAQ quantification on Bcl-2 66

LIST OF FIGURES

Figure Page

1-1 Examples of Cellular Heterogeneity....2

1-2 Workflow of β-galactosidase Analysis in a Single *Escherichia Coli* Bacterial....7

1-3 Antibody Detection from Single Mouse Hybridoma Cells....8

1-4 Workflow of FACS....10

1-5 Scheme of Entire Microfluidic Platform for Single Cell Analysis.... 12

2-1 Scheme of Antibody-antigen Interaction.... 16

2-2 General Principle of MALDI.... 21

2-3 Scheme of MALDI-TOF Mass Spectrometer.... 23

2-4 Workflow for the Sample in MALDI TOF/TOF Instrument....24

2-5 Application of MALDI Imaging on a Human Breast Carcinoma Section..... 25

2-6 A Diagram Showing the Multiplexed iTRAQ Tagging Strategy....29

3-1 Workflow of Photolithography.... 34

3-2 Workflow of Making a Chip.... 35

3-3 Schematic Workflow of Microfluidic-Based MALDI-TOF-MS.... 39

3-4 MALDI-TOF-MS Spectra of Peptides and Protein Digest Obtained from the Combined Microfluidic and MALDI-MS Approach.... 41

3-5 MALI-TOF-MS Spectra of Proteins Obtained from the Combined Microfluidic and MALDI-MS Approach.... 43

3-6 Fluorescence Intensity of Fluorescently Labeled IgG for Various Incubation Concentrations Immobilized on ITO Slides.... 45

Figure Page

3-7 MALDI-TOF-MS Analysis of Anti-Insulin Immunoassays..... 46

3-8 Schematics of the Insulin Immunoassay Performed on an ITO Surface within a Microfluidic Channel..... 47

4-1 Top View of the Ladder-Like Device with Pneumatic Valves.....54

4-2 Schematics of the Bcl-2 Immunoassay and Tryptic Digestion Peformed on an ITO Surface within a Microfluidic Channel..... 61

4-3 MALDI-TOF-MS Analysis of an Anti-Bcl-2 Immunoassay followed by Bcl-2 On-chip Tryptic Digestion and MALDI-TOF-MS Analysis Employing an Immunoassay on Chip followed by iTRAQ Labeling during Digestion..... 62

4-4 Averaged Fluorescence Intensity in One Well in Fluidic Channel I and the Opposed Well in Fluidic Channel II when Valve B was Repeatedly Opened and Closed..... 68

4-5 Representative MS/MS Spectrum of the Two iTRAQ Labels from a Bcl-2 On-chip Quantification with an Anti-Bcl-2 Immunoassay..... 70

5-1 Representative MS Spectrum of Bcl-2 in Solution Digestion with 12h Incubation..... 77

5-2 Digestion Efficiencies for Various Incubation Times Ranging from 4h to 36h..... 77

5-3 Representative MS Spectrum of Sample peptide from Bcl-2 Digest and the Internal Standard Peptide..... 79

Figure Page

6-1 Structure of Ladder-Like Device..... 88

6-2 Bright Field Microscope Images for Cells..... 90

6-3 Signal to Noise of Bcl-2 Peptides in MCF-7 Cell Lysate with Bcl-2 (140nM) Spiked.....92

6-4 Signal to Noise of Bcl-2 Peptides in MCF-7 Cell Lysate with Bcl-2 (14nM) Spiked.....92

6-5 MALDI-TOF-MS Analysis of an Anti-Bcl-2 Immunoassay with Treating Antibody by Freezing and Thawing Cycles.....94

6-6 Representative MS Spectrum of Spiked Bcl-2 Detection in MCF-7 Cells.....96

7-1 Synthesis of the hyperbranched polymer used for antibody immobilization in the immunosensor.....101

CHAPTER 1

INTRODUCTION

1.1 Significance of Single Cell Analysis

Cellular heterogeneity within a given cell type or in an ensemble of isogenic cells is a widespread event. Understanding such heterogeneity in single cells promotes development in many fields including molecular biology, cancer diagnostics, pathology and therapy. Protein detection and quantification of individual cells are mainly performed with large cell populations averaging quantitative information over a large cellular ensemble, or is limited to the investigation of few cells at a time. However, in many instances, the qualitative and quantitative information obtained from the measurement of an averaged cell population mask the true behavior of the individual cells. Thus, single cell analysis is crucial for resolving cellular heterogeneity and understanding cell-to-cell variations.

A striking example between single cell and population cell measurements is exemplified in Figure 1-1a. In response to DNA double strand breaks (DSBs), undamped p53 pulses with fixed amplitude and duration are seen in individual cells. By contrast, measurements averaged over populations of cells show damped oscillations of p53(Batchelor, Loewer, and Lahav 2009). Cellular heterogeneity among single cells is also shown with hormones. Individual oocytes show discrete all or nothing response for an intermediate level of progesterone stimulation while the physical models predict an intermediate level of commitment for an intermediate level of progesterone stimulation for oocytes (Ferrell and Machleder 1998; Altschuler and Wu 2010). Another example related to siRNA GAPDH (Glyceraldehyde 3-phosphate dehydrogenase) gene expression

also shows that the behavior of individual cells is different from the population average (Figure 1-1b). The last example is about individual Jurkat cells which present two distinct populations of cells with either partial knockdown (~50%) or complete knockdown (~0%) however averaged bulk measurements from 50 cells show GAPDH expression at ~21% (Toriello et al. 2008). These examples clearly demonstrate that single cell analysis offers fascinating possibilities to illuminate cellular heterogeneity and diversity.

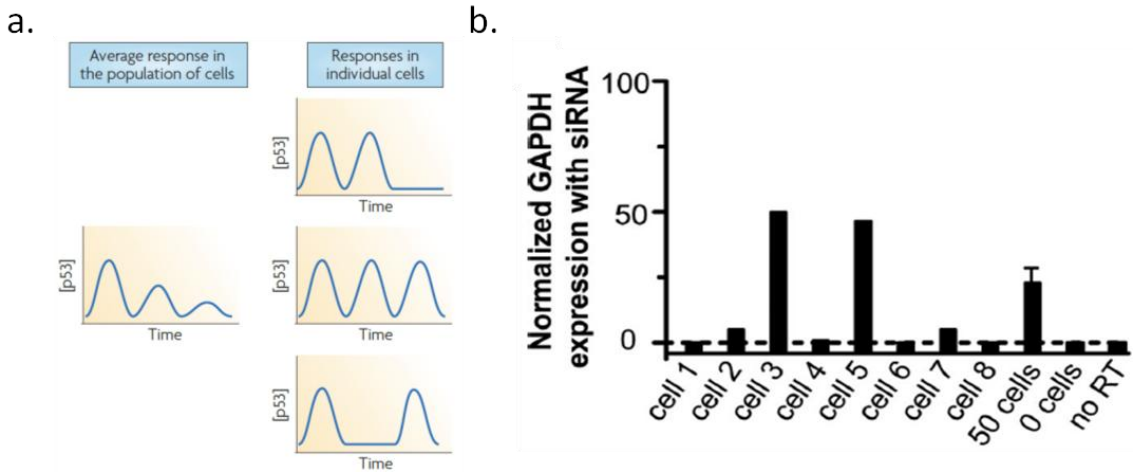

Figure 1-1: Examples of cellular heterogeneity. a. Average response in the population of cells show p53 damped oscillations but responses in individual cells show different numbers of undamped pulses. Adapted with permission from Batchelor et al.(Batchelor, Loewer, and Lahav 2009). b. GAPDH gene expression for Jurkat cells. 8 individual cells exhibit either ~50% or~ 0% GAPDH expression level. A control with no cell (0 cells) exhibit no products. A PCR control without reverse transcriptase (no RT) show no signal. Averaged bulk measurements from 50 cells show GAPDH expression at ~21%. Adapted with permission from Toriello et al. (Toriello et al. 2008).

Three more application-driven examples are cited here. First example is about understanding the steps of cell development such as assessing individual stem cells. Stem cells have the remarkable potential for treating disease (referred to as regenerative medicine) due to their unique long-term self-renewal and proliferation abilities (Hirschi, Li, and Roy 2014; Mull, Zolekar, and Wang 2015; Nakajima-Takagi, Osawa, and Iwama

2014). However, stem cells are all heterogeneous populations such as embryonic stem cells or adult stem cells (Graf and Stadtfeld 2008; Takahashi et al. 2007). Single cell analysis can target specific cell populations and thus allows unraveling the signaling pathways and networks for self-renewal and for differentiation (Wang and Bodovitz 2010).

The Second example is in cancer diagnostics and treatment. Fundamental insights of cancer research are also offered through single cell analysis since cancer is a heterogeneous disease. Acquainting with tumor initiation, metastasis and response to a drug in single tumor cells is extremely important for cancer treatment (Wang and Bodovitz 2010; Martinkova et al. 2009; Majewski and Bernards 2011). Circulating tumor cells (CTCs) have been demonstrated to be prognostic for metastatic breast cancer (Massimo Cristofanilli 2004). Single cell analysis can analyze single CTCs enriched from patient blood samples such as based on RT-MLPA (Reverse Transcriptase Multiplex Ligation-dependent Probe Amplification) assay (Kvastad et al. 2015). This can potentially be a diagnostic tool for cancer genomics. Other examples for single cell analysis of CTCs were summarized in a good review by XiXi et al. (XiXi Chen 2015). In addition, it has been proven that the protein expression level in single cells is highly associated to cancer progression and metastasis. For example, the elevation of c-Src level is known to be associated to cancer progression. Moskaluk et al. reported that the c-Src protein expression was increased by 30-fold in human breast cancer cells compared to normal breast tissue (Verbeek et al. 1996) and thus c-Src could be potentially a biomarker for human breast cancer. Sano et al. demonstrated that over- expression of p16 was associated with cervical cancer (Shapiro et al. 1995). Similarly, quantitative analysis of a

particular protein in a single cell can improve the early diagnosis of diseases like cancer originating from a single cell (Roncador et al. 2005).

The third example is in neuroscience. Neurons are the basic unit of the nervous system which are extremely heterogeneous. The molecular complexity of neuropeptides and neuroproteins are just being understood (Odowd and Smith 1996). Sweedler's group analyzed releases from a single neuron which helped elucidate neural communication and neurological disorders (Fuller et al. 1998; Fan et al. 2013; Page, Rubakhin, and Sweedler 2002; Rubakhin, Greenough, and Sweedler 2003).

1.2 Challenge of Single Cell Proteome Analysis

Although currently available approaches can potentially provide snapshots of single cells, there is still an increasing need for analysis of extremely low sample amount at the level of single cells. This need is particularly urgent when the number of cells is limited (e.g. stem cells, early stage embryos). The vast majority of commercial products for single cell analysis focus on DNA and RNA. An example is Fluidigm Inc. (www.fluidigm.com) selling different polymerase chain reaction (PCR) systems providing automated solution for single-cell genomics. Single cell genomic analysis has been greatly aided by amplification techniques such as PCR (Li et al. 1988; Lambolez et al. 1992) and isothermal amplification (Kurn et al. 2005). This was recently reviewed by Quake et al. (Kalisky, Blainey, and Quake 2011). Compared with single cell genome analysis, protein analysis on the single cell level has proven to be more challenging due to extremely small amounts of protein in a single cell (Beck et al. 2011) and the tremendous complexity of the proteome. Copy numbers of proteins in single mammal

cells vary from several tens to a million copies (Xie et al. 2008; Hanke et al. 2008), which is vanishingly low. The lack of amplification techniques makes analysis of proteins in a single cell more difficult. Moreover, one gene does not only produce one protein. One example is that a single gene in Drosophila can potentially encode more than 30000 closely related but distinct proteins (Clark et al. 2007). This kind of complexity stems from many attributes including protein abundance and expression levels, enzymatic activity, post-translational modification, interaction with other proteins, and protein secretion and translocation (Wu and Singh 2012).

1.3 Current Single Cell Proteome Analysis Status

The traditional methods for single-cell sample processing such as microdissection and micromanipulators have a disadvantage of low throughput. Microfluidic or lab-on-a-chip devices can achieve high throughput analysis and are especially suitable for handling ultra-small sample volumes (in the *nano* to *pico* liter range) comparable to the size of a single cell (Whitesides 2006). In comparison to alternative capillary-based approaches (Arcibal, Santillo, and Ewing 2007; Cannon, Winograd, and Ewing 2000; Stuart and Sweedler 2003), microfluidic devices simplify cell-handling techniques and more importantly allow parallelization as well as the integration of a variety of necessary workflow steps involved in cellular analysis, such as selection, navigation, positioning and lysis as well as separation of cellular analytes (Roman and Kennedy 2007; Sims and Allbritton 2007; Roman et al. 2007; Chao and Ros 2008). Furthermore, microfluidic volume control further allows the combination of sensitive protein detection via fluorescence methods with cellular manipulation in microenvironments close to the

intrinsic volume of a single cell, thus advantageously preventing dilution in sampling steps.

A recent example is the work of Dittrich and coworkers reporting a microfluidic platform (Eyer et al. 2012) coupled with enzyme-linked immunosorbent assays (ELISA) suitable for analysis of proteins and metabolites in single mammal cells (Eyer et al. 2013). They further downscaled the device for probing intracellular enzymes in single bacteria as shown in Figure 1-2 (Stratz et al. 2014). They developed a cell trap with a ring valve integrated for trapping a single *Escherichia coli* bacterium. The target enzyme from the *Escherichia coli* bacterial lysate was captured by antibodies immobilized on the surface for further detection. Another example is related to droplet-based (digital) microfluidics which has recently been applied to MALDI MS (matrix assisted laser desorption ionization mass spectrometry) analysis. Multiple sample manipulation steps can be integrated in one device including sample preparation, matrix deposition as well as purification (Wheeler et al. 2005; Nelson et al. 2010; Moon et al. 2006; Chatterjee et al. 2010). Compartmentalization of single cells from droplets allows the analysis of proteins released from cells, thereby overcoming the major limitations of traditional flow cytometry. Mazutis et al. detailed a binding assay for detecting antibodies from single mouse hybridoma cells as depicted in Figure 1-3. Only 15 min was needed for antibody detection after co-compartmentalizing single mouse hybridoma cells (Mazutis et al. 2013). However, digital microfluidic platforms require sophisticated designs and electrode integration.

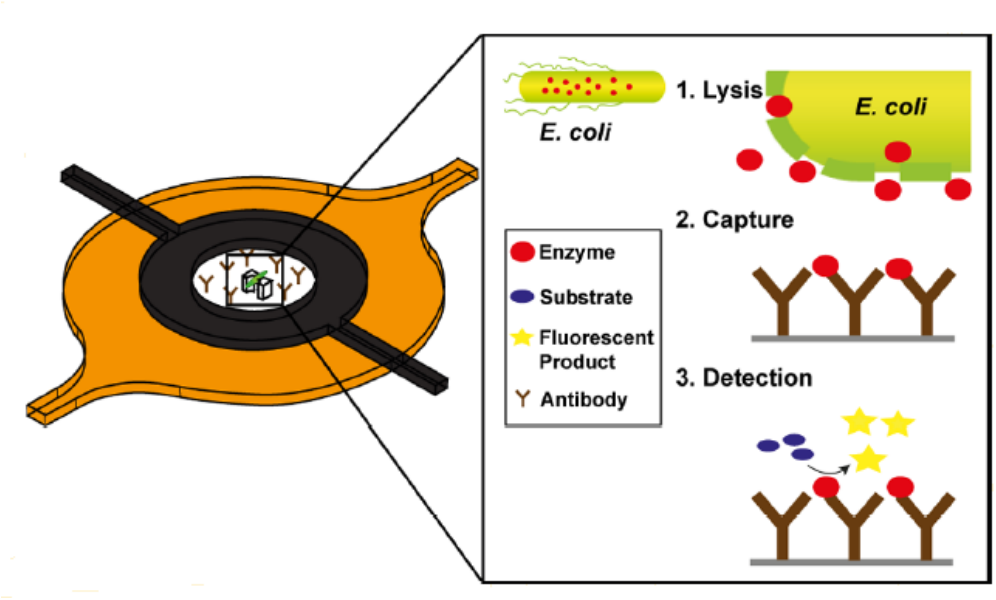

Figure 1-2: Workflow of β-galactosidase analysis in a single Escherichia coli bacterial. The ring shaped valve is designed for isolation of a single Escherichia coli bacterial. A single Escherichia coli bacterial expressing β-galactosidase is trapped, isolated and finally lysed. An immunoassay is performed on the surface to capture β-galactosidase. After a washing step, the enzyme (β-galactosidase) is detected by adding the β-galactosidase substrated FDG that is converted to highly fluorescent fluorescein. Adapted with permission from Stratz et al. (Stratz et al. 2014)

Furthermore, microfluidic technology can be combined with a variety of analytical detection schemes. The most widely used detection technique for protein quantification in single-cells is based on fluorescence measurements due to their high sensitivity such as laser-induced fluorescence (LIF) which can usually achieve detection limits in the pM range (Lee and Yeung 1992). Dovichi's group even achieved sub-attomole amino acid analysis by capillary zone electrophoresis combined with LIF (Cheng and Dovichi 1988). Recently, they pioneered the use of a sheath flow cuvette in a capillary electrophoresis-laser induced fluorescence (CE-LIF) system decreasing the limit of detection to less than 100 molecules (Dada, Huge, and Dovichi 2012). Besides, they published several articles for analyzing chemical contents of individual cells by two-

dimensional capillary electrophoresis (Harwood et al. 2007; Sobhani et al. 2007).

Nevertheless, high throughput analysis has not been realized in CE-LIF.

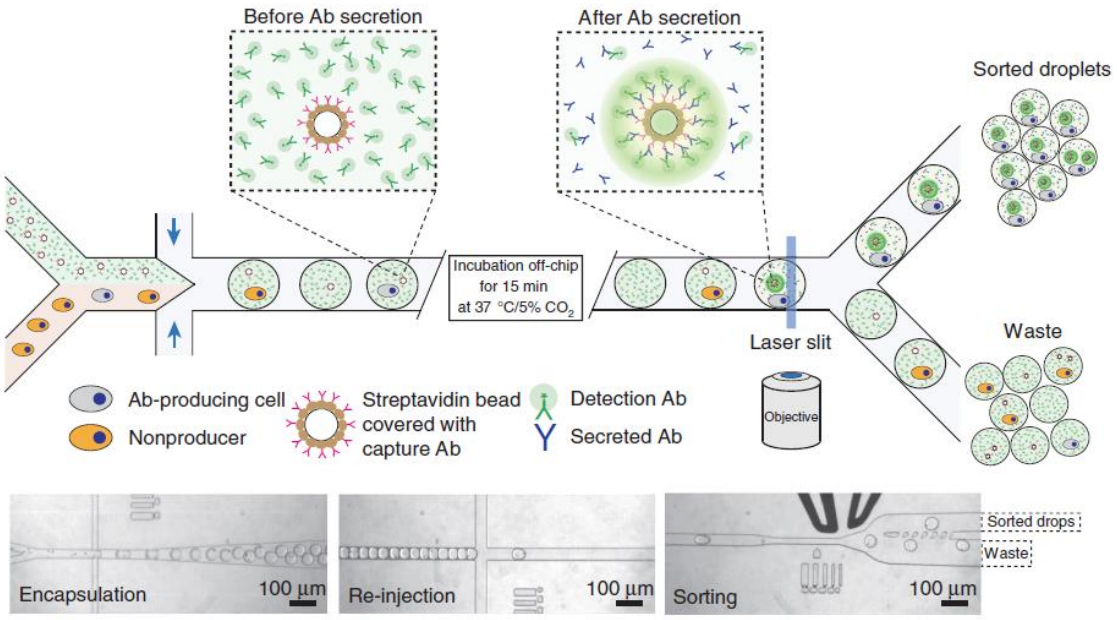

Figure 1-3: Antibody detection from single mouse hybridoma cells. Two types of cells are introduced with a bead suspension. The bead suspension contains goat detection antibodies which are labeled with green fluorescent dyes and the beads are coated with goat anti-mouse-Fc capture antibodies. One cell type produces mouse antibodies (grey) and the other (orange) does not. The droplets are generated by flow focusing with fluorinated oil containing fluorosurfactant. The cell suspension and the bead suspension can only mix inside the droplets due to laminar flow. Then the droplets are collected off-chip at 4° C. After incubation for 15min at 37° C and 5% CO_2, those beads which were encapsulated with an antibody-producing cell are highly fluorescent. The droplets are then introduced into a second microfluidic device and sorted using a fluorescent activated droplet sorter. Three microscope images below show the coencapsulation of cells with beads (left), droplets introducing to the second microfluidic device (middle), and droplet sorting (right). Adapted with permission from Mazutis et al. (Mazutis et al. 2013)

Flow cytometry with fluorescence activated cell sorting (FACS) is a potent highthroughput technique for single cells analysis. In this approach, fluorescence signals from fluorescent antibodies which are attached to the cell membrane antigens can be

monitored. A typical FACS workflow is shown in Figure 1-4 (Pedreira et al. 2013). This fluorescence signal from the detector is converted to an electrical signal, trigging the cell sorting in FACS. For example, it has been employed for the detection of mammalian β-glucuronidase activity at the single cell level (Lorincz et al. 1999). Furthermore, FACS can be used to analyze multiple proteins simultaneously in single cells due to the development of highly specific antibodies. Freer et al. detected 18 different colors of fluorescent antibodies in peripheral blood mononuclear cells, making it the only immunological technique allowing simultaneous determination of antigen-specific T cell function and phenotype (Freer and Rindi 2013). The Nolan group reported simultaneous measurement of the activation states of kinases within single cells by using a FACS-based strategy (Perez and Nolan 2002). They used multiparameter flow cytometry to monitor phospho-protein responses at the single cell level (Irish et al. 2004). However, since the number of fluorescent dyes suitable for FACS experiments is limited, the number of proteins that can be studied by this approach is quite restricted.

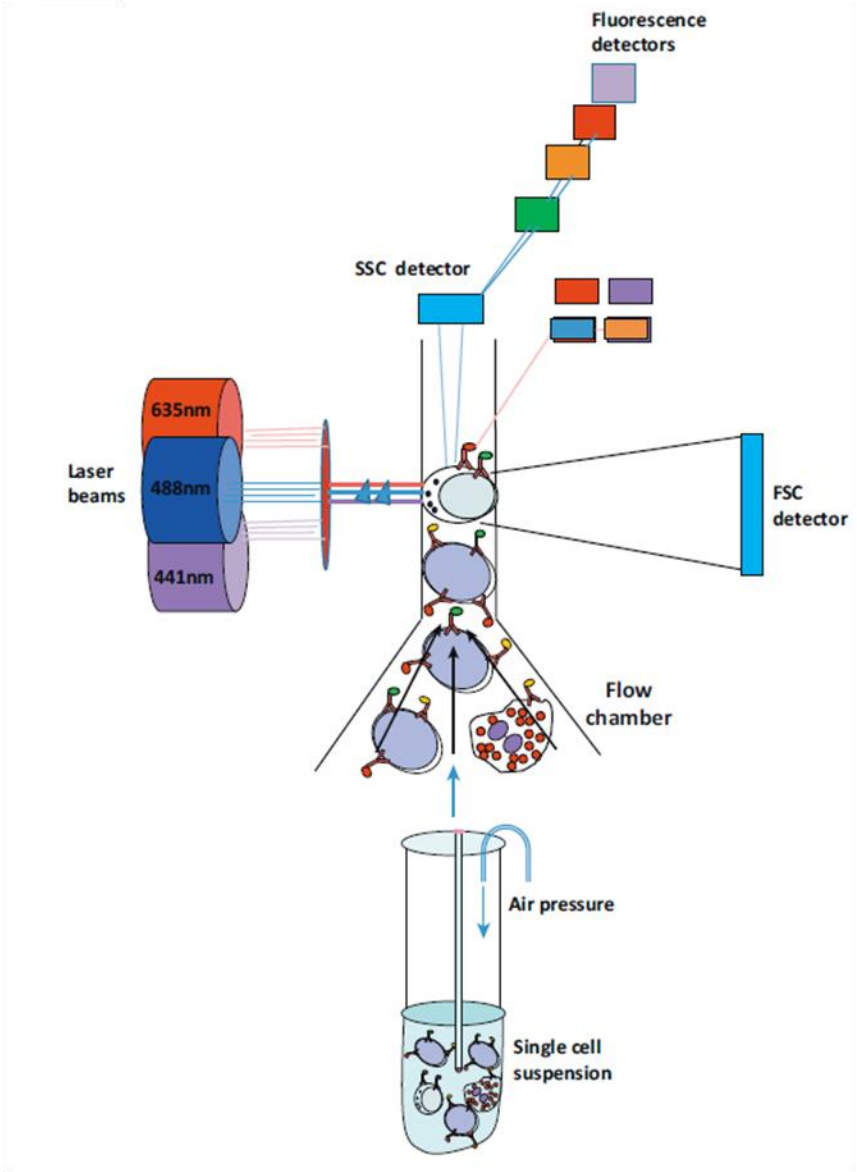

Figure 1-4: Workflow of FACS. Individual cells are forced to pass a small tube one-by one. Three different detectors (FSC: forward light scatter for collecting light at low angles; SSC: sideward light scatter and fluorescence detector to collect light and fluorescence) are placed into different positions. Adapted with permission from Pedreira et al. (Pedreira et al. 2013).

In comparison to fluorescence detection, mass spectrometry based single-cell analysis can potentially provide label-free analysis of a single cell. Sweedler's group developed a sensitive and robust capillary electrophoresis-electrospray ionization mass

spectrometry (CE-ESI MS) system suitable for investigation of metabolites at the single cell level (Nemes et al. 2011, 2012). Matrix assisted laser desorption and ionization- time of flight (MALDI-TOF) mass spectrometry is a powerful technique which has been widely used in the field of biomarker discovery (Calligaris, Villard, and Lafitte 2011; Chao, Hansmeier, and Halden 2010; Lu et al. 2012). Excellent sensitivity of this method has been demonstrated not only for metabolites (Amantonico et al. 2008; Miura et al. 2010) but also for peptides (Nordhoff, Lehrach, and Gobom 2007; Dong et al. 2010) and even proteins (Hanke et al. 2008). The matching of apparent protein copy numbers with the detection sensitivity of mass spectrometers has stimulated attempts to analyze single cells with both electron spray ionization (ESI) (Hofstadler et al. 1996; Cao and Stults 1999) as well as matrix assisted laser desorption/ionization (MALDI) (Rubakhin et al. 2006; Jo et al. 2007; Li, Golding, and Whittal 1996). Furthermore, it permits identification and characterization of the analyte and moreover provides quantitative information on the level of peptides formed by the cleavage and digestion of target proteins. Bai et al. found that the MALDI MS/MS spectra provided sufficient information for the identification of the studied peptides by analyzing the intensity of the fragment ions (Bai, Romanova, and Sweedler 2011).

Moreover, iTRAQ (isobaric tag for relative and absolute quantitation) tags have been implemented widely as a quantitative MALDI MS technology especially in discovery-based proteomics (Noirel et al. 2011) utilizing isobaric reagents with different stable isotope compositions (Ross et al. 2004; Merali et al. 2014; Treumann and Thiede 2010). This technology has been successfully adapted for the relative quantification of peptides from individual *A. californica* neurons (Rubakhin and Sweedler 2008) .

However, acquiring quantitative information of proteins from single cells by iTRAQ strategies has not been reported.

In this thesis, a label free detection and high throughput method was developed, combining the advantages of a sensitive mass analyzer (MALDI-TOF) and microfluidic technology. This combined approach may eventually allow the identification and quantificaton proteins from single cells in parallel thus improving our capability in understanding the protein functions, drug design and cancer diagnostics in early stages.

1.4 Dissertation Objective

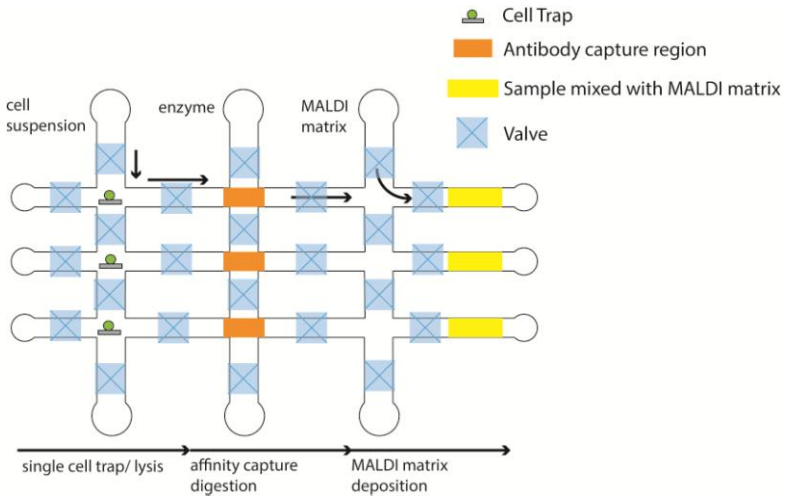

Figure 1-5: Scheme of entire microfluidic platform for single cell analysis. Fluidic channels (white channels enframed by black lines) in PDMS layer 1 are employed for single cell trapping, cell lysis, delivery of enzyme for enzymatic digestion and MALDI matrix deposition. Pneumatic valves (Blue squares) are in PDMS layer 2 for separating fluidic channels into separate regions. The black arrows indicate the workflow direction.

The objective of this dissertation is to develop a novel approach for single cell protein analysis based on the coupling of a multilayer microfluidic device with MALDI mass spectrometry. This approach will eventually allow resolving protein heterogeneity

at the single-cell level and thus potentially improving our current status in understanding the protein functions, drug design and cancer diagnostics.

The entire microfluidic platform is shown in Figure 1-5 for trapping a single cell and analyzing target proteins from cell lysate. This thesis mainly focuses on lysing the cells and analyzing target proteins from the cell lysate. Specifically, affinity capture regions are integrated for capturing proteins of interest from cell lysate. Enzymatic digestion is performed for protein identification and quantification on the level of peptides formed by the cleavage and digestion of target proteins. The last step is MALDI matrix deposition prior to MALDI MS analysis.

As discussed in Section 1.2, the complexity of the proteome requires powerful separation steps prior to analysis. This complexity can influence the subsequent MALDI MS detection of target proteins. Thus in this device, we take advantage of specific immunoreactions capturing the proteins of interest from cell lysate. MALDI-TOF MS is chosen as the detection technique to provide label-free detection. The sensitivity of MALDI MS is suitable for single cell analysis (Amantonico et al. 2008). In addition, absolute protein quantification can be realized by MALDI-TOF detection on the level of peptides formed by digestion of target proteins, allowing the study of protein expression levels in single cells. Moreover, this microfluidic device enables integration of necessary process steps involved in single cell analysis prior to MS analysis and thus simplifies tedious single cell handling techniques. It can confine samples in the necessary small area effectively preventing dilution and making the whole approach suitable for single cell analysis. More importantly, compared to capillary-based approaches, more parallel channels can be integrated, allowing high throughput analysis.

Background and theory are discussed in chapter 2. Hyphenation of a microfluidic platform and MALDI-TOF detection is demonstrated in chapter 3. Protein identification and quantification by two different methods are discussed in chapter 4 and 5. Analysis of proteins in MCF-7 cells with the proposed approach is described in chapter 6.

CHAPTER 2

FUNDERMENTALS AND THEORY

2.1 Immunoassays

An immunoassay represents a purification method to measure the presence of biomolecules (typically a protein) in complex samples by using their antibodies (Ab) also known as immunoglobulins. The molecule recognized by an antibody is called an antigen (Ag). There are five isotypes of antibody in mammals: IgA, IgD, IgE, IgG and IgM. IgG provides the majority of immune reactions towards invading pathogens. IgG is a Y-shaped protein containing two light chains and two heavy chains (Figure 2-1). Each light chain has a molecular weight of ~ 25,000 Da and consists of two domains, one constant domain and one variable domain. Each heavy chain has a molecular weight of ~50,000 Da and contains either three or four constant domains and one variable domain. An IgG can be cleaved by the enzyme papain into two antigen-binding fragments (F_{ab}) and one crystallizable fragment (F_c). The F_{ab} region contains variable sections that can determine the type of the target that the IgG can bind. In contrast, the F_c region is constant for all antibodies within the same animal class. A specific region on the antibody is called paratope. A particular region called epitope on an antigen is always specific to the paratope on the antibody, allowing the binding of these two structures precisely. The interaction between antibody and antigen is through a specific interaction including electrostatic interactions, hydrogen bonds, Van der Waals forces and hydrophobic interactions. Each antibody binds specifically to only one antigen. The specificity originates from the unique amino acid sequence in the antibody (paratope) and the

epitope on the antigen. The binding process for antigen and antibody is a dynamic equilibrium (Eq. 2-1):

$$[A_g] + [A_b] \rightleftharpoons [A_gA_b] \qquad (2\text{-}1)$$

Where A_b represents antibody , A_g represents antigen and A_gA_b represents antigen-antibody complex.

Understanding the specificity and the affinity strength of antibody-antigen binding are fundamental for studying the activity of these proteins. The binding constant K_a (Eq. 2-2) and the dissociation constant K_d (Eq. 2-3) are often used to characterize the affinity of antibody-antigen interaction. Apparently, they have reverse relationship. The smaller the K_d (the larger the K_a), the stronger the binding between the antibody and antigen. K_d typically ranges from 10^{-9} to 10^{-11} which means that the binding complex dominates in the immunoreactions.

$$K_a = \frac{[A_gA_b]}{[A_g][A_b]} \qquad (2\text{-}2)$$

$$K_d = \frac{[A_b][A_g]}{[A_bA_g]} \qquad (2\text{-}3)$$

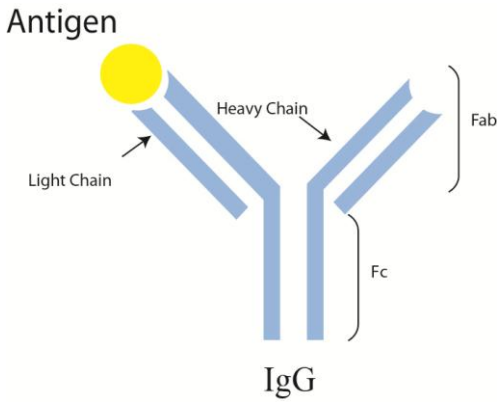

Figure 2-1: Scheme of antibody- antigen interaction. The IgG is a Y-shaped protein which has two light chains and two heavy chains. The positions binding to the antigen are on the tips of the antibody.

In the immunoassay, antibodies are often required to be immobilized on the surface with proper orientations allowing the high antigen-antibody binding efficiencies (Lee et al. 2013). Random orientation of antibodies can result in the loss of binding ability. For IgG, the ideal orientation is that the antibody is immobilized vertically to the surface which the paratopes (antigen binding sites) are exposed to the antigens. There are a wide variety of protein immobilization methods that have been reported (Kim and Herr 2013). A particular antibody immobilization method is chosen depending on various factors including the immobilization surface, antigen property, buffer components and the requirements of the assay such as sensitivity, selectivity and reproducibility. Antibody immobilization is often realized based on three binding mechanisms including physical adsorption, bioaffinity interaction, covalent bonding.

The simplest approach to immobilize antibodies on a surface is through physical adsorption. The antibodies can be attached to various surfaces via intermolecular forces such as electrostatic, hydrophobic, van der Waals forces. Generally, incubation of antibodies in solution contacting the immobilization surface or continuous flow of the antibody solution can attach the antibodies on the surface. Physical adsorption is often weak since there are no covalent bonds linking the antibody to the antigen.

The antibody immobilization based on bioaffinity interaction exploits specific binding phenomena existing in nature. Bioaffinity interactions are often used in conjunction with the other two immobilization mechanisms (physical adsorption and covalent bonding). The surface and the antibody are linked via a bioaffinity agent which is used as the intermediate. Avidin/streptavidin-biotin can be used as the bioaffinity agent

to immobilize antibodies. Streptavidin/avidin binds strongly with biotin acting as small ligands through coordination. The dissociation constant for avidin-biotin system is on the order of 10^{-15} M while the dissociation constant for streptavidin-biotin is on the order of 10^{-14} M (McMahon 2008). Wang et al. reported a bead-based immunoassay which was employed to detect proteins (Wang and Han 2008). Biotinylated GFP (green fluorescent protein) and R-PE (R-phycoerythrin) antibodies were attached to commercial streptavidin-coated beads to preconcentrate the biotinylated GFP and R-PE proteins. 50 pM to 10 fM detection limit was observed for both proteins.

Covalent bonds are frequently used to immobilize antibodies on the surface. The surface is activated by a specific chemical reagent, forming irreversible binding with antibodies. One of the most commonly used covalent linking agents is N-hydroxysuccinime (NHS) ester which can react with amines on proteins (Rusmini, Zhong, and Feijen 2007). Delamarche et al. reported antibody immobilization by NHS ester in microfluidic device (Delamarche et al. 1997). The surface of the glass or the silicon wafer was coated with aminosilane. The amine functional groups of the aminosilane were linked to the NHS ester for antibody immobilization. Epoxide is another functional group in covalent linking agents used for antibody immobilization. It can form covalent bonds with primary amines on proteins. One example is that the commercial HER2 antibody which was attached to the surface via epoxide group of the allyl glycidyl ether (AEG) polymer, allowing the subsequent capture of circulating tumor cells (CTCs) (Thierry et al. 2010).

The antibodies that bind to the antigens or proteins directly are called primary antibodies while the ones that bind to the primary antibodies are secondary antibodies.

Secondary antibodies are used to assist in detection of the target antigens and they are very efficient in immunolabeling. Secondary antibody binds to the primary antibody via its F_{ab} domain (Figure 2-1) to the F_c domain (Figure 2-1) of primary antibody. In the same animal class, the F_c domain is constant. Thus, one type of secondary antibodies can bind to many types of primary antibodies. In this way, instead of labeling many types of primary antibodies, only one type of secondary antibody is required, which reduces the cost and simplifies the labeling procedures.

Antibodies are used throughout various types of assays including western blot, enzyme-linked immunosorbent assay (ELISA), flow cytometry and immunohistochemistry. In terms of different detection methods, immunoassays are performed in different formats. There are many different detectable labels that can be used in the immunoassays. One major type of the labels is the enzyme. This type of immunoassay employing enzymes is the ELISA. The enzyme can catalyze a certain reaction, producing a color change to detect the presence of a substance. The enzymatic reactions provide signal amplification which can increase the detection limit and sensitivity. The ELISA has been used as a diagnostic tool (such as HIV test). A second major type of detectable label is fluorophore. With fluorescence emission, the distribution of antigens can be revealed using optical microscopy. A third major type of detectable label is radioactive isotopes. Radioactive isotopes can go through radioactive decay, emitting alpha, beta or gamma rays which can be revealed by autoradiography.

Immunoassays have been used in single cell proteome analysis (Eyer et al. 2013; Casey et al. 2010; Zhang and Jin 2006). An example (Stratz et al. 2014) is mentioned in Chapter 1.4 (Figure 1-2) demonstrating the integration of ELISA (enzyme-linked

immunosorbent assay) to capture the β-galactosidase from a single *Escherichia coli* bacterium. Choi et al. reported an improved immunoassay for the detection of cytokines released from human peripheral mononuclear cells. The detection sensitivity was enhanced by 200 fold by detecting the cytokines antibodies with covalently attached fluorescent oligomers (Choi et al. 2011).

2.2 MALDI Mass Spectrometry

MALDI mass spectrometry was invented in late 1980s (Karas et al. 1987). The introduction of MALDI mass spectrometry is a milestone in the history of mass spectrometry. It can provide soft desorption and ionization for sample molecules which is important for analysis of biomolecules. The key part of MALDI to be successful is the application of matrix which can assist the intact desorption and ionization of biomolecules.

In MALDI, matrix molecules are usually organic, aromatic and conjugated compounds. The sample molecules are dissolved into the matrix solution and they co-crystallize in the drying process. In this co-crystallization process, sample molecules are incorporated into the matrix crystals. A specific laser wavelength is used so that photons can only be absorbed by the matrix molecules while the sample molecules have little absorption. After the absorption of the laser photons, the matrix molecules become very hot (>1000K) and expand. The whole process is accomplished in a short time (~ps) which results in supersonic explosion (velocity reaches at km/s) (Chou, Nelson, and Williams 2009). The explosion of the matrix crystals carries sample molecules into the gas phase. The sample molecules are desolvated during this process. The supersonic expansion has a cooling effect on the sample molecules preventing fragmentation. The

ionization mechanism is believed to be associated with proton transfer. Under the high temperature after photon absorption, free protons are dissociated from matrix molecules (weak acid). The basic groups in the sample molecules tend to associate with the free protons to become ionized. Figure 2-2 shows a typical process of laser desorption and ionization (For illustration purposes, the figure is not drawn to scale, the laser beam is usually ~100 μm which is much bigger than sample molecules)

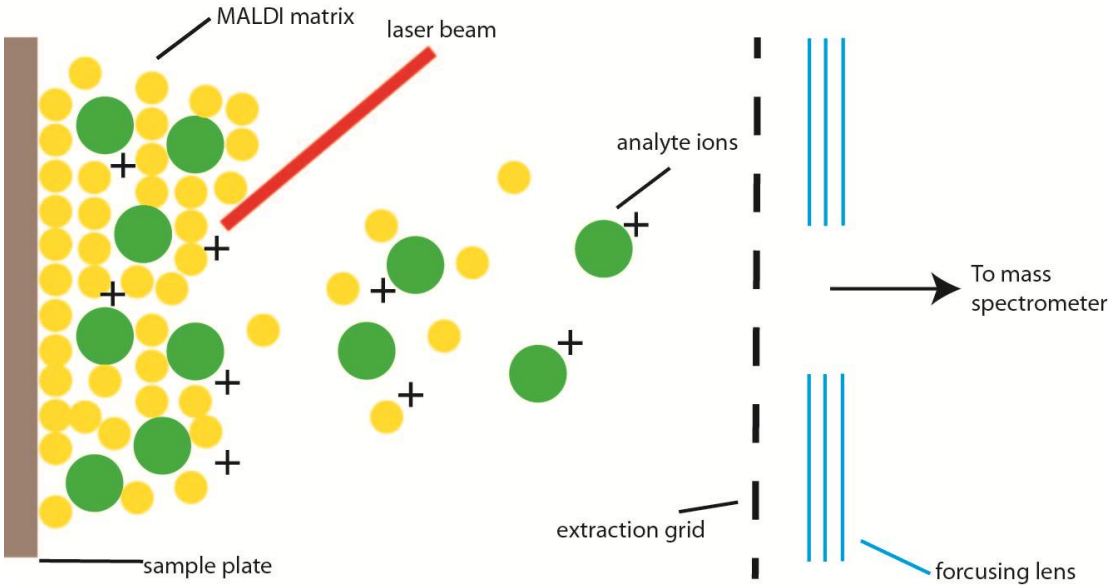

Figure 2-2: General principle of MALDI. Sample molecules are co-crystallized with matrix molecules. Desorption and ionization of sample molecules occurs after the matrix molecules absorb the laser photon. Sample ions are extracted by the extraction electric field into the mass spectrometer. For illustration purpose, the size of laser beam (~100 μm) is much smaller than it should be compared with sample or matrix molecules.

MALDI is usually coupled with a time of flight mass analyzer (e.g. TOF: time of flight), depicted as Figure 2-3. Ions leaving the sample surface are extracted by a static electric field (several kVs) into the field free drift zone. Ions with same number of charges will have the same total kinetic energy entering the drift zone. But due to the difference in the mass to charge ratio, their flight velocities are different. Ions with larger

m/Z have smaller velocity, thus needing a longer time to arrive the detector (equation 2-4, 2-5, 2-6). Based on their flight times, the corresponding m/Z can be calculated.

$$\text{Kinetic Energy} = \mathrm{E} \times \mathrm{e} = \frac{1}{2}\mathrm{mv}^2 \tag{2-4}$$

$$\mathrm{v} = \sqrt{\frac{2\mathrm{Ee}}{\mathrm{m}}} \tag{2-5}$$

$$\text{Flight Time} = \frac{\mathrm{L}}{\mathrm{v}} = \mathrm{L} \times \sqrt{\frac{\mathrm{m}}{2\mathrm{Ee}}} = \mathrm{L} \times \sqrt{\frac{\mathrm{m/Z}}{2\mathrm{Ee}}} \tag{2-6}$$

Where *E* is the static acceleration electric field strength; *e* is the number of charges carried by the ion; *m* is the mass of the ion; *v* is the velocity of ion flying in the TOF; *L* is the flight length in the TOF; m/Z is the mass to charge ratio of the ion.

In sophisticated MALDI-TOF instruments, reflectrons are used to minimize the initial energy spread due to the sample desorption, improving the mass resolution (Figure 2-3). Ions with bigger initial energy will fly through a longer pathway in the reflectron resulting in longer flight time. The MALDI-TOF detection system usually uses a micro-channel plate. For heavier ion detection, post-acceleration is usually required in order for ions to have enough energy producing secondary electrons after hitting the channel plate surface. Secondary electrons are extracted and amplified through the microchannel. The amplified electric signals are detected by the electronics system and are counted as counts of ions.

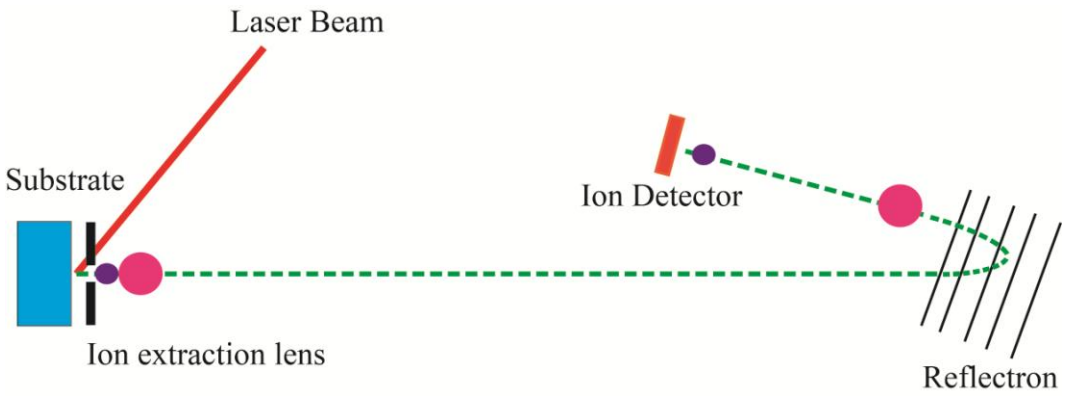

Figure 2-3: Scheme of MALDI-TOF mass spectrometer. After shooting the sample surface with laser beam, molecular ions are desorbed and extracted into the mass spectrometer. After entering into the time of flight tube (drift zone), the ions start flying with velocities corresponding to its mass to charge ratio. Reflectron is used to minimize the initial energy spread of ions coming out the sample surface. Heaver ions with bigger mass to charge ratio arrive at the detector later than the light ions. According to the ions' flight time arriving at the detector, their mass to charge ratios can be calculated.

MALDI is also employed in tandem mass spectrometry (also known as MS/MS) such as a MALDI TOF/TOF system. In tandem mass spectrometry, there are two mass analyzing stages involved and a fragmentation process occurs between these two stages. In the first stage (MS1), samples are ionized and desorbed in the ionization source (e.g. MALDI). And the ion species are separated according to their mass to charge ratios by the first mass analyzer (e.g. TOF). Ions with a specific mass to charge ratio are selected as the precursor ions. These precursor ions are further fragmented and the fragment ions (product ions) are created which will be separated by the second mass analyzer (e.g. TOF). Afterwards, the product ions are detected by the detector (e.g. microchannel plates). The workflow about MALDI TOF/TOF detection is shown in Figure 2-4. From the peaks of product ions in MS/MS spectrum, the structure and composition of the precursor molecules are obtained.

There are three commonly used methods for precursor ions fragmentation in tandem mass spectrometry. The first one is called collision-induced dissociation (CID). In this method, a gas collision cell is usually added to the ion drifting pathway. When the ions fly through the gas collision cells, the ions collide with the gas molecules and become fragmented. Another method is post-source decay (PSD). Ions with internal energy leaving the sample surface can self-fragment in the flying process generating fragment ions. This method does not require additional instrumentation and is therefore used in this thesis. The third method is through photon absorption which can induce the dissociation reaction.

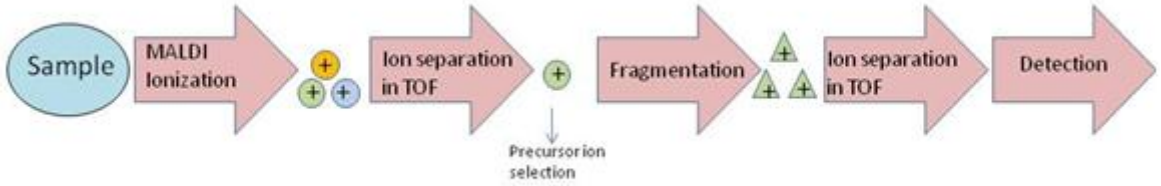

Figure 2-4: Workflow for the sample in MALDI TOF/TOF instrument. Sample is ionized and separated in the first TOF analyzer. Ions with a certain mass to charge ratio are selected as the precursor ions which are subsequently fragmented into small ions. These small ions are separated in the second mass analyzer and finally detected.

As mentioned, MALDI is a very powerful technique for detection of biomolecules due to the ability of desorption and ionization of intact molecules. MALDI imaging is one of the most popular imaging mass spectrometry methods. It has been used widely for lipids, peptides and proteins imaging in disease diagnosis. Caprioli et al. used MALDI imaging to image hundreds of proteins from a human breast carcinoma section (Seeley and Caprioli 2008), as shown in Figure 2-5. Three different proteins (Histone H2A, Calgizzarin and Thymosin β4) were found to have correlation to each different stage of

cancer. Histone H2A, Calgizzarin and Thymosin β4 were found to concentrate in the ductal carcinoma in situ region, invasive ductal carcinoma and stroma specifically. Nevertheless, since the imaging resolution of MALDI (~100 μm) is bigger than the size of human cells, MALDI imaging has poor application ina single cell. It has been reported that the sensitivity of MALDI MS detection is typically on the level of Pmole and attomole sensitivity is also possbile (Nordhoff, Lehrach, and Gobom 2007). By coupling with microfluidics, MALDI is applicable for single cell protein analysis, which is used in this thesis.

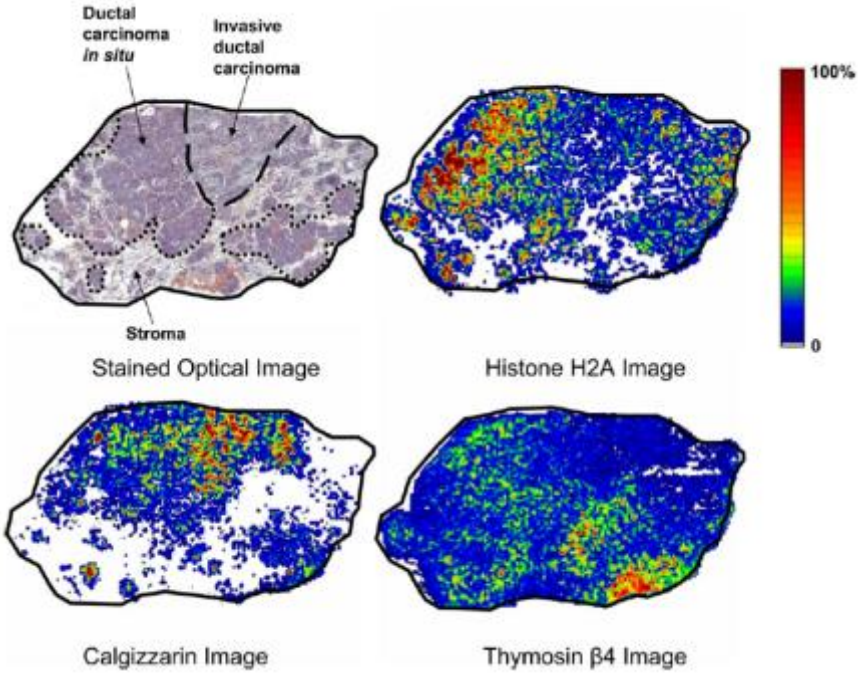

Figure 2-5: Application of MALDI imaging on a human breast carcinoma section. The scare bar shows the normalized amount of the proteins (red to white means 100% to 0%). H&E (Hematoxylin and eosin stain) stained section shows the areas of invasive ductal carcinoma, ductal carcinoma in situ (DCIS) and stroma. Protein histone H2A shows the highest signal in DCIS. Calgizzarin shows the highest intensity in inv asive ductal carcinoma and Thymosin β4 in stroma. Adapted from caprioli et al. (Seeley and Caprioli 2008)

2.3 Quantitative Proteome Analysis by MALDI MS

The goal of single cell proteome analysis is to demonstrate the changes of cell phenotypes induced by various environmental factors on the level of proteins. The proteome has been described as the quantitative image of a whole set of proteins in cells under defined conditions (Lottspeich 1999). Thus, acquisition of quantitative information about protein expression in single cells is a key subject in single cell proteome analysis.

In MALDI MS analysis, cocrystallization of MALDI matrix and analyte is required for the desorption and ionization, but on the other hand is the major reason limiting quantitative analysis with MALDI MS. As the major issue of non-homogeneous distribution of the analyte originates from the cocrystallizaition process, strong detection intensities can be probed at some points whereas no analyte signals can be found at other points. This leads to poor reproducibility even at different locations on one sample spot. Besides, different molecules usually have different ionization efficiencies which are not predictable. The ionization efficiency of a specific molecule is dependent on the physical and chemical properties of the molecule itself (e.g interaction with MALDI matrix, chemical bonds, hydrophobicity, and volatility) and the environment (matrix effect). Additionally, secondary ion reactions after ionization and ion suppression effect in complex samples (e.g cell lysate) further hamper the use of MALDI MS for quantitative purposes.

Despite these impeding factors, MALDI MS quantification can still be achieved via multiple strategies: (i) improvement of sample homogeneity by either modifying the matrix or solvent. (ii) isotope labeling (e.g: iTRAQ labeling, stable isotope labeling by amino acids in cell culture (SILAC)) or (iii) an isotope labeled standard.

As discussed above, inhomogeneous distribution of sample in the sample-matrix co-crystals is a key factor limiting the quantitative MALDI analysis. Approaches for improving the sample homogeneity have been reported previously. One of the most commonly used methods is using ionic liquid matrices (ILM) as the MALDI matrix. Unlike the traditional MALDI matrix such as α-cyano-4-hydroxyl-cinnamic acid (CHCA) or sinapic acid, ionic liquid matrices form a highly viscous layer on the MALDI target plate (Armstrong et al. 2001). Thus, the sample can form a more homogenous distribution in this liquid layer. ILMs have been successfully applied for analyzing amino acids(Zabet-Moghaddam, Heinzle, and Tholey 2004), phospholipids (Li, Gross, and Hsu 2005) and proteins (Armstrong et al. 2001). Relative quantification can be achieved in this analysis with applying suitable calibration standards. Moreover, it allows absolute quantification even without the use of the standards in a narrow dynamic range and under a specific matrix to analyte ratio (Tholey, Zabet-Moghaddam, and Heinzle 2006).

Stable isotope labels introduced in a sample allow the quantitative MALDI MS analysis. The earliest possible way for introducing a stable isotope into proteins is by metabolic labeling. Nowadays, one popular strategy for incorporation of stable isotopes is SILAC. In SILAC, the cell medium often contains $^{13}C_6$-arginine and $^{13}C_6$-lysin. This can guarantee that all the products from tryptic digestion have at least one isotope labeled peptide, resulting in a mass increase over the non-labeled samples. Relative quantification is performed based on comparing the intensities of heavy species and light species. The advantage of this approach is to label proteins at the level of intact cells, which excludes all error sources coming from the mass spectrometric procedures

(Bantscheff et al. 2007). However, maintaining this system is expensive and time consuming.

iTRAQ labeling is another method introducing stable isotopes into proteins. iTRAQ tags are a set of tags which have the same masses but different isotope compositions (Ross et al. 2004). The chemical structures of all tags are the same (drawn in Figure 2-6 A), eliminating the differences in ionization efficiencies. The complete molecule consists of a report group (N-methylpiperazine), a balance group (carbonyl), and a peptide-reactive group, a N-hydroxy succinimide). When the tag reacts with a peptide, the peptide-reactive group forms an amide linkage with all peptide amines (either N-terminal or amino group of side lysine). Figure 2-6 B shows an example of four iTRAQ tags with reporter groups ranging in mass from 114.1 to 117.1 Da while the balance groups range in mass from 28 to 31 Da. Due to a constant molar mass, the peptides labeled with each of the tags have the same peak (m/Z $[M+H]^+$ 145.1) in the MS spectrum. In the following MS/MS detection, the chemical bond linking the reporter group and the balance group breaks and the four reporter group ions appear as distinct masses (114-117 Da). The relative concentration of the peptides is thus obtained from the relative areas of the corresponding reporter ion peaks (Figure 2-6 C). Absolute quantification can be realized when the peptide amount is known in one sample. One potential disadvantage of this approach is that MS/MS analysis is a prerequisite, requiring more analysis time and additional instrumentation. But the ability to identify and quantify a protein without the need of peptide/protein sequence and complicated labeling process compared with in vivo labeling (SILAC) considerably outweighs this disadvantage.

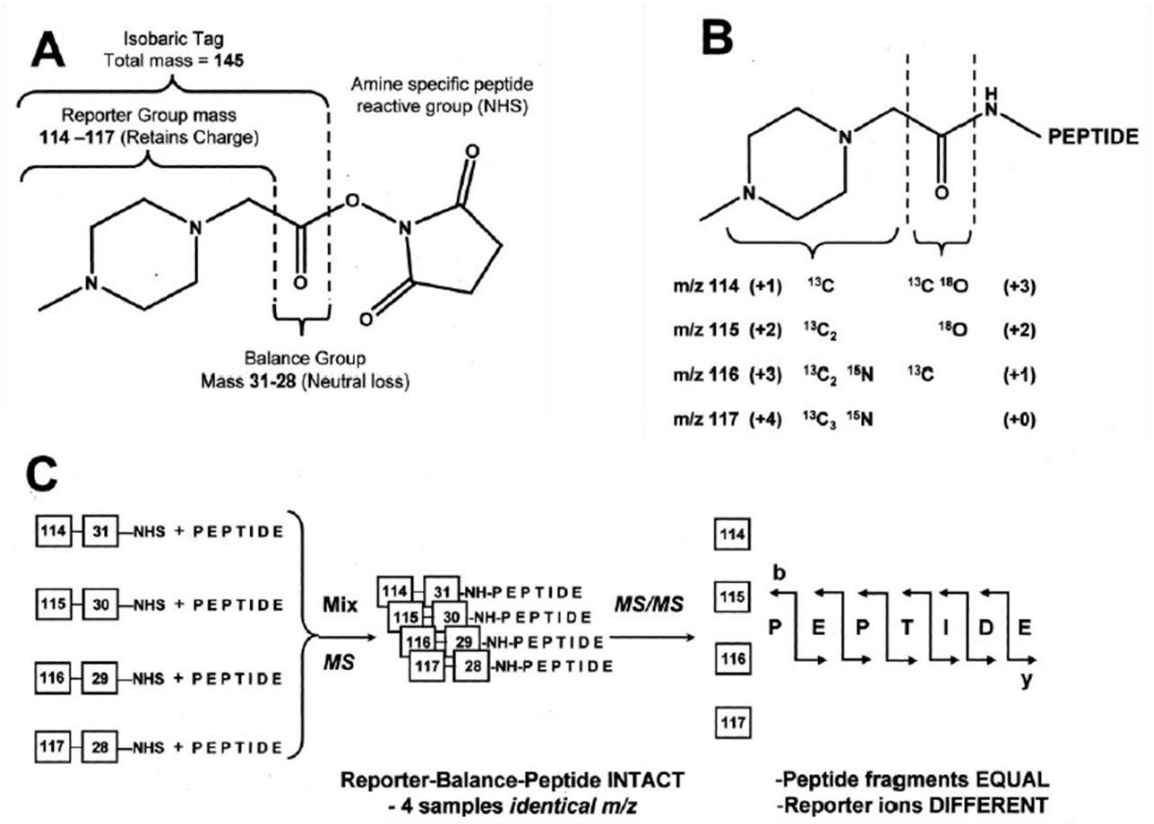

Figure 2-6: A diagram showing the multiplexed iTRAQ tagging strategy. (A) Chemical structure of iTRAQ tags. (B) the overall mass of tag molecule is kept constant using different isotope enrichment with 13C, 15N and 18O atoms. (C) Illustration of isotopic tagging and quantification process. A kind of peptide from four samples is labeled with four different iTRAQ tags with four different reporter group masses. They are mixed and detected by MS/MS. The report groups can be distinguished in the MS/MS detection. Adapted from Ross e.t al. (Ross et al. 2004).

Absolute quantification can also be achieved by applying internal standards (often known as isotope labeled synthetic standards). This method is now becoming more widely used and known as AQUA (absolute quantification of proteins). In this method, a known quantity of a stable isotope-labeled standard peptide is added to a protein digest. The comparison of internal standard signal and the sample peptide signal in MS spectrum allows the absolute quantification of the protein. This method has been used in clinics such as in the analysis and validation of potential biomarkers in a large quantity of

clinical samples (Pan et al. 2005). Unlike the metabolic labeling and iTRAQ labeling which can provide quantitative information for large numbers of proteins at the same time, the addition of isotope labeled peptide usually focuses on one or a few particular target proteins in the sample (Pan et al. 2005). In addition, the choice of the synthetic peptide is important as there are likely several isobaric peptides present in the target protein mixture. Despite these limits, the advantages of this method such as fast analysis, not requiring tedious instrumentation and expensive materials are still attractive.

CHAPTER 3

DIRECT DETECTION OF PEPTIDES AND PROTEINS REACHING SINGLE CELL SENSITIVITY

3.1 Introduction

It is well known that individual cells even having the same genotypes are different from each other (discussed in section 1.1). This kind of cellular heterogeneity cannot be revealed in the averaged bulk measurements. Understanding the heterogeneity between single cells is of enormous biological and clinical relevance. Single cell analysis gained a lot of interest in the past few years, capable of resolving the heterogeneity in single cells. However, new approaches with single cell sensitivity and label free detection are still needed.

MALDI-TOF is a very powerful technique which has been widely used in the field of disease biomarker discovery due to its high sensitivity, speed and accuracy (Calligaris, Villard, and Lafitte 2011; Chao, Hansmeier, and Halden 2010; Petricoin et al. 2002). However, in order to fully capitalize on these attributes, means of sample handling and manipulation techniques are needed that compatibly match the performance metrics of MALDI-TOF. This need is particularly acute when considering the analysis of a single cell where only an extremely low amount of analyte exists. Thus, technologies are necessary allowing sampling in the nano to pico liter range - ultimately reaching the volume of a single cell. Microfluidic devices have the potential to fulfill this requirement. It is suitable to handle picoliter single cell analyte with minimal dilutions. Moreover, proteome-relevant separation techniques such as immunoarrays, gel electrophoresis and

isoelectric focusing can be transferred to microfluidic devices, capable of reducing the sample complexity prior to MALDI-TOF analysis.

In this chapter, I report first evidence that a combined microfluidic and mass spectrometric approach allows the detection of targeted proteins. From our results, the detection limit was found to be as few as 300 molecules at the peptide level, and ~ 10^6 to 10^7 molecules at the protein level. Moreover, an immunoassay was integrated in the microfluidic device with subsequent MALDI-TOF-MS analysis. As it is known that for MALDI MS, lower molecular weight projectile has higher sputtering yield, narrower isotope distribution and thus higher detection sensitivity. Here, insulin was used as a target protein due to its low molecular weight compared with other proteins (>10kDa). This would result in an increased intensity in MALDI MS, making it a good model analyte as proof-of-principle. Based on the results of our study, we estimated detection limit on an anti-insulin immobilized surface (~0.05 mm^2) of 10^6 insulin molecules. This microfluidic-based method, therefore, approaches the sample-handling and sensitivity requirements for MS-based single-cell analysis of proteins and peptides.

3.2 Materials and Methods

3.2.1 Materials

PDMS was purchased from Dow Corning Corporation. Acetonitrile, alpha-cyano-4-hydroxycinnamic acid (α-CHCA), 3,5-dimethoxy-4-hydroxycinnamic acid, sinapic acid, recombinant human insulin, bovine serum albumin (BSA) and chicken anti-insulin antibody were obtained from Sigma-Aldrich. Alexa Fluor 488 chicken anti-rabbit IgG was purchased from Invitrogen. Peptide calibration mixture (bradykinin 904.4681 m/Z

$[M+H]^+$, angiotensin I 1296.6853 m/Z $[M+H]^+$, qlu-fibrinopeptide [1570.6774 m/Z $[M+H]^+$, neurotensin 1672.9175 m/Z $[M+H]^+$) was purchased from AB SCIEX. Protein calibration mixture (insulin 5734.51 m/Z $[M+H]^+$, ubiquitin 8565.76 m/Z $[M+H]^+$, cytochrome C12360.97 m/Z $[M+H]^+$, myoglobin 16952.30 m/Z $[M+H]^+$) was obtained from Bruker Daltonics. ITO slides (100 ohm/sq) were purchased from NANOCS and Cr was obtained from SPI Supplies. Tridecafluoro-1, 1, 2, 2-tetra-trichlorosilane (TTTS) was obtained from Gelest. Isopropanol and acetone were obtained from VWR. SU-8 organic resin solution and SU-8 2075 developer were purchased from MicroChem.

3.2.2 Microchip Fabrication

PDMS microfluidic channels were fabricated via soft lithography using printed polymer masks (Fineline Imaging, USA), depicted as Figure 3-1. SU-8 2075 photoresist was spin coated onto a silicon wafer, which was then exposed to UV light with a mask aligner (System 3A, HTG, USA) for 32 seconds through the film photomask. After a post bake of 2 min at 65℃ and then 7 min at 95℃, the silicon wafer was immersed in SU-8 developer for 4 minutes followed by 15 min hard bake at 150℃.

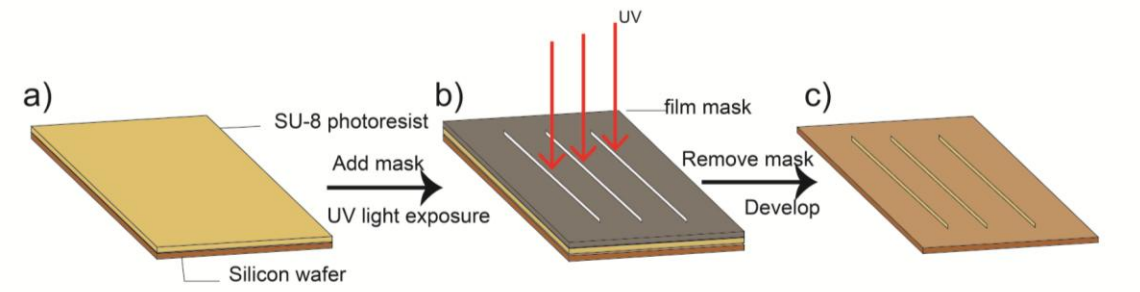

Figure 3-1: Workflow of photolithography. a) SU-8 negative photoresist is spin-coated on silicon wafer substrate. b) UV light exposure of SU-8 photoresist through a film mask to transfer the feature on the mask to the wafer. c) Mask removal and dissolvation of unexposed SU-8 photoresist in developing step. Exposed SU-8 photoresist remain on the wafer.

The chip was made through the procedures shown in Figure 3-2. The resulting silicon master was then silanized under vacuum with TTTS. Afterwards, PDMS was poured over the master and cured at 80℃ for 4 h, removed from the master and cut in suitable pieces. Reservoir holes were punched manually with a biopsy punch (Fray Products, USA) to create the final PDMS manifolds. Then the PDMS manifolds were exposed to oxygen plasma with a Harrick plasma cleaner (PDC-001, Harrick, USA) for 60 seconds under medium power settings. To ensure a reversible bonding between the PDMS and the ITO slides, the plasma treated PDMS slab was incubated in an oven at 80℃ before chip assembly. ITO coated glass slides (NANOCS, USA) were used as substrate for the PDMS manifolds. In order to allow better contrast for visual inspection during MALDI-TOF measurements the back of these slides was coated with a 25 nm thick layer of Cr with an Evaporator (308R, Cressington, UK). ITO slides were reused 5-8 times after washing with acetone and isopropanol.

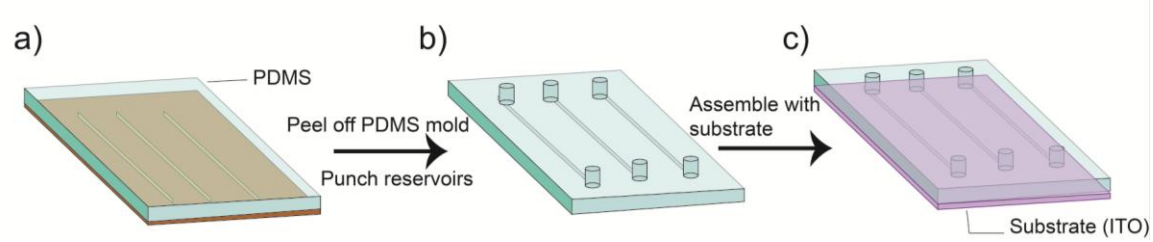

Figure 3-2: Workflow of making a chip. a) PDMS is poured to the master wafer. b) Holes are punched at the ends of channels. c) The chip is assembled after plasma treatment of the PDMS slab.

3.2.3 Protein Digestion

BSA was digested as reported earlier (Chao, Hansmeier, and Halden 2010) with minor modification. In short, to 100 µg of BSA in 500 mM triethylammonium carbonate buffer (pH 8.5) was mixed with 1 µl of a 2% SDS stock solution and reduced with 2 µL of 0.5 M Tris(2-carboxyethyl)phosphine at 60℃ for 1 h. The resulting peptides were then alkylated by the addition of 2 µL of 200 mM methylmethanethiosulfonate in isopropanol and incubated for 15 min in the dark. Subsequently, 10 µL of a 1 mg/mL sequencing grade trypsin stock solution (Promega, USA) was added to the protein mixture and incubated at 37℃ overnight. The digest sample was cleaned with a C_{18} cleanup tip (Varian, USA) and the peptides were eluted with 0.1% TFA / 70% acetonitrile.

3.2.4 Chip Loading and Manifold Removal

Protein and peptide samples were diluted to different concentrations with water. Insulin was dissolved in 0.1 % v/v trifluoroacetic acid (TFA) and also diluted with water to the final concentration. 3 µL of the respective sample was mixed with either 3 µL of saturated α-CHCA in 60% v/v acetonitrile and 0.1% v/v TFA (for peptides) or 3 µL of a

saturated solution of sinapic acid in 40% v/v acetonitrile and 0.1% v/v TFA (for proteins). The mixture was then pipetted into the reservoir and the channels were filled by capillary action. After 3 h drying at room temperature the PDMS manifold was peeled off and the ITO slide was used as a target for MALDI-TOF-MS. For immunocapture experiments with insulin, 5 µL of a saturated solution of sinapic acid in 30% v/v acetonitrile and 0.1% v/v TFA were filled in a reservoir and channels filled by capillary action. When the channel volume was completely dried (after ~3 h), the PDMS manifold was removed manually and the remaining ITO slide was used as target for MALDI-TOF-MS.

3.2.5 MS Analysis

MALDI-TOF-MS was performed using a Bruker Ultraflex III MALDI-TOF/TOF instrument. Peptide spectra were acquired in reflectron mode, whereas intact BSA and insulin were measured in linear mode. Calibration was performed with bradykinin, angiotensin, glu-fibrinopeptide and neurotensin in the low-MW range and with insulin, ubiquitin, cytochrome C and myoglobin for the higher MW-range. For a peptide spectrum 300 laser shots were summed while for intact BSA and insulin, 500 laser shots were summed. Variable laser intensities were used during each experiment to optimize the signal. The digested BSA-spectrum was searched against the Swissprot database ('The Uniprot Consortium' 2012) with the MASCOT algorithm (Perkins et al. 1999) for identity validation.

3.2.6 Immobilization of IgG and Insulin Immunoassay

Covalent IgG immobilization on ITO slides was performed as previously reported by Ng et al. (Ng et al. 2002). All protein solutions were prepared in phosphate buffer (20mM sodium phosphate dibasic, pH 8.0). Accordingly, 5 µL anti-insulin IgG solution (0.05mg/mL) was pipetted in the reservoir of an assembled chip and the microfluidic channels filled by capillary action. The chip was then kept in a humidity chamber at room temperature for 2 h. Subsequently, the protein solution was removed and the channel was washed three times with 20 mM phosphate buffer (pH=8.0) by vacuum action. This was followed by filling the channels with 1% (w/v) BSA solution by capillary action. The chip was then incubated in a humidity chamber at room temperature for 1h, the solution was removed and the channels were washed three times with phosphate buffer. Next, 5 µL insulin solution (2 µM in 20mM phosphate buffer) was filled in the channels by capillary action followed by 1 h incubation in a humidity chamber at room temperature. Last, the insulin solution was removed and phosphate buffer was used to wash the channels thrice. After the phosphate buffer was removed, 5 µL of a saturated solution of sinapic acid in 40% v/v acetonitrile, 0.1% v/v TFA in water filled the channels by capillary action. The chip was subsequently allowed to dry and MALDI-TOF-MS performed.

3.3 Results and Discussion

3.3.1 Hyphenation of a Microfluidic Device with MALDI-TOF Instrument

The goal of this study is to explore approaches with which an integrated device allowing immunocapture and subsequent mass-spectrometric quantification of proteins

with single-cell resolution can be realized. Our approach is based on a removable microfluidic platform on which analytes dissolved in suitable matrix solution are deposited in specific areas defined by the microfluidic platform, ultimately reaching the volume of a single cell. The top part of the microfluidic device consists of a PDMS manifold with a 0.5 cm long channel exhibiting a cross section of 50 µm x 60 µm fabricated by standard photo and soft-lithographic techniques. An ITO coated glass slide is used as reversible sealing during fluid handling steps and as the conductive MALDI target after matrix deposition. Moreover, this surface allows the covalent immobilization of immunocapture proteins and is fully transparent enabling the microscopic analysis of all sample and pre-treatment steps.

To ensure a reversible bonding between the PDMS and the ITO slides, PDMS manifolds are exposed to oxygen plasma for 60 sec under medium power settings while the ITO slide is not treated. During the oxygen plasma treatment, the surface of the PDMS is oxidized and hydroxyl groups were generated, forming a strong covalent bond with an ITO slide. The plasma treated PDMS slab is incubated in an oven at 80 ℃ for half an hour before chip assembly. This possibly help reduce the strength of the bond due to the hydrophobic recovery of PDMS surface. In this way, reversible assembling can be achieved. To find out this best protocol enabling reversible binding and capillary action, multiple conditions were attempted (data not shown).

The PDMS platform is removed after all liquid handling steps, with the remaining analyte-matrix co-crystallized on the spatially defined ITO surface. The microfluidic manifold thereby created micrometer sized patterns that were analyzed with MALDI-TOF-MS. This approach is schematically depicted in Figure 3-3.

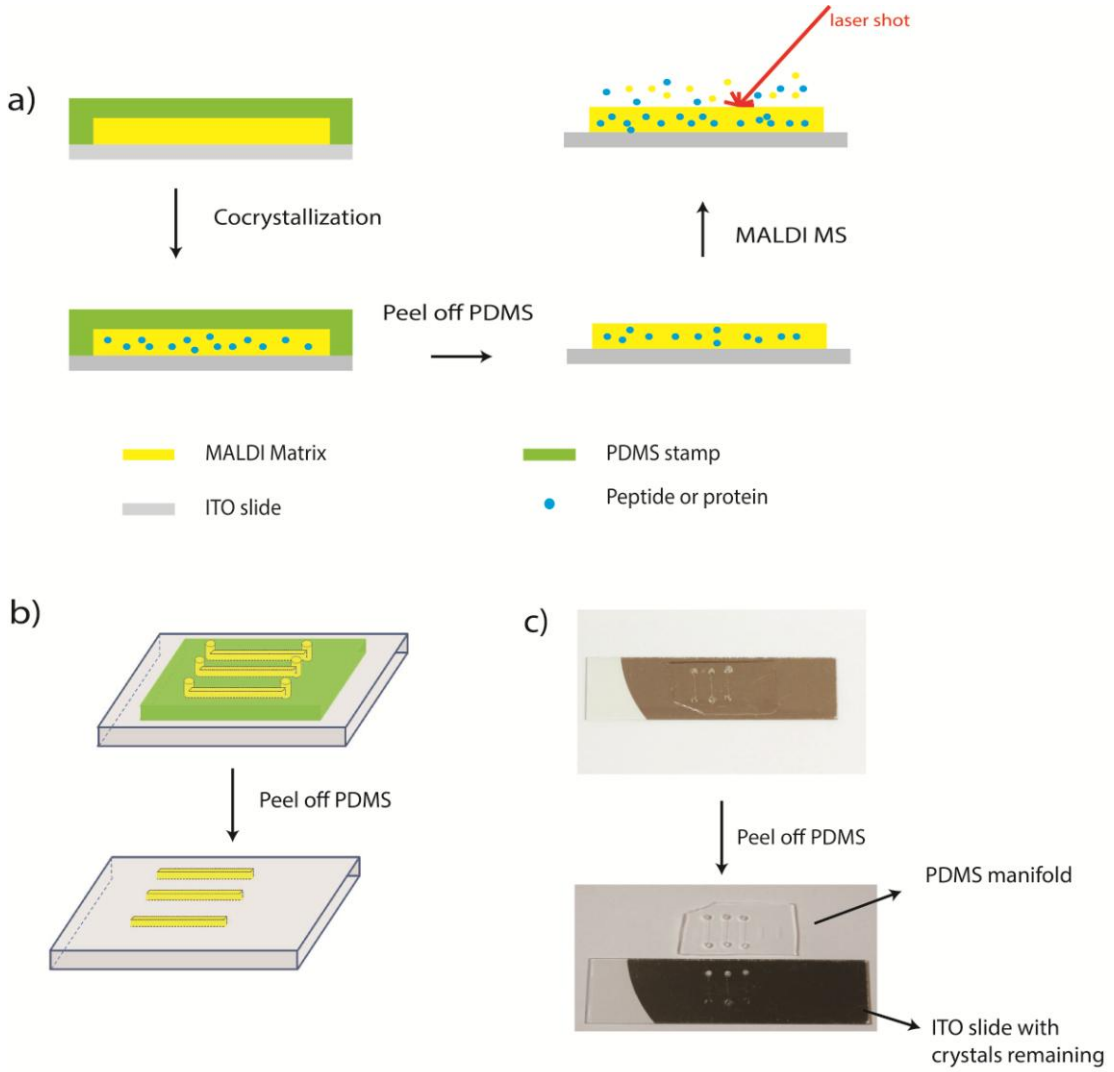

Figure 3-3: a) Schematic workflow of microfluidic-based MALDI-TOF-MS analysis. Cross section of a channel manifold containing several microchannels is fabricated using the elastomer PDMS (Note: only one channels cross sections is shown). A microfluidic channel is filled with a mixture containing either peptides or proteins and a suitable MALDI matrix. After the cocrystallization of the sample and matrix, the top PDMS manifold is removed and the remaining crystals are probed by MALDI-TOF-MS subsequently. b) Schematic of the 3D peel-off procedure for three channels. c) Photographs of the assembled microchip (top) and showing deposited co-crystals on the ITO surface (bottom) after peel-off (Note: the backside of the ITO slide is coated with a 25 nm thick layer of Cr).

3.3.2 Detection and Identification of Peptides and Proteins

Using optimized assembly conditions (as reported in section 3.3.1) we studied the sensitivity of the proposed combined MALDI MS and microfluidic technique for the detection and identification of proteins and peptides. To assess the detection limit for proteins, we used BSA, BSA digest and insulin, whereas the peptide calibration mixture was used as a peptide sample.

Samples were premixed with matrix solution before loaded into the microdevice. After they co-crystallized at ambient temperature, areas both resulting from the reservoir and channel regions defined by the microfluidic manifold were analyzed. Since highly purified calibration peptides generally provide excellent S/N ratios we first investigated the detection limit with a dilution series of a peptide mixture consisting of angiotensin, bradykinin, neurotensin and Glu-fibrinopeptide within our microdevice. We measured within the reservoir as well as regions defined by the microfluidic manifold (Figure 3-4 a) and b)). The lowest limit of detection was achieved for angiotensin with a loaded concentration of 1.3 pM and a S/N of 7.7 from a microchannel region (Figure 3-4 b)). The resulting S/N ratio at this concentration in the reservoir was 2.7. The other peptides could still be detected at concentrations of 130 pM with S/N ranging from 1.6 to 10.8 in the reservoir and from 3.2 to 14.0 in microchannels (data not shown).

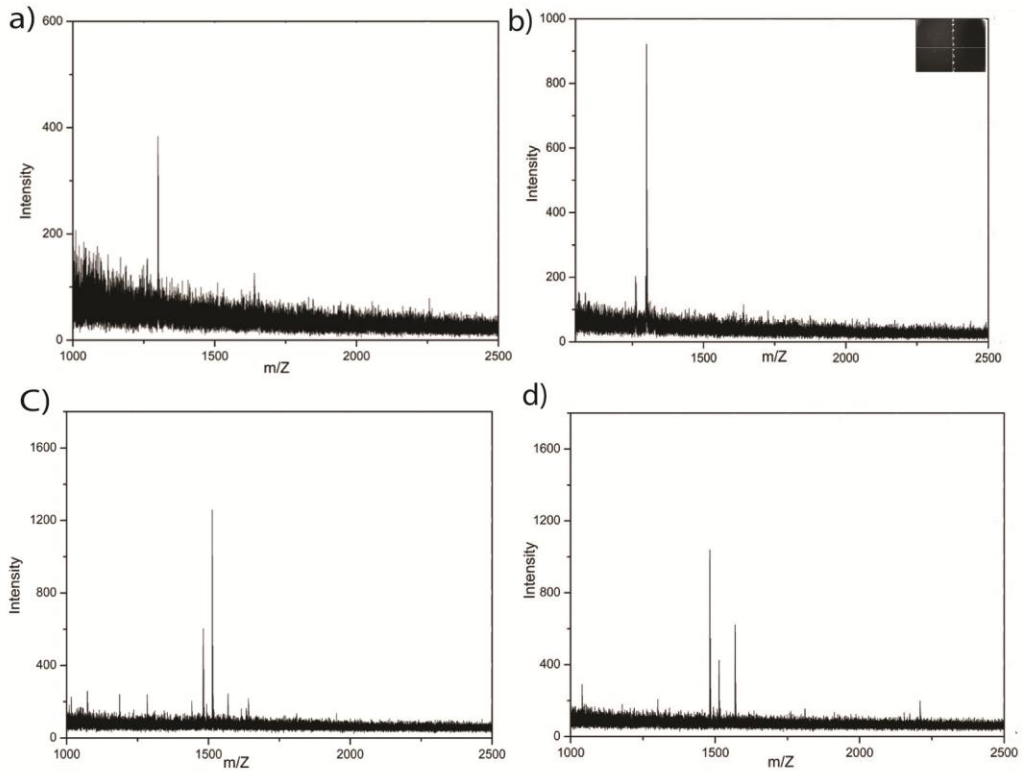

Figure 3-4: MALDI-TOF-MS spectra of peptides and protein digest obtained from the combined microfluidic and MALDI-MS approach: Angiotensin spectra obtained from a) reservoir and b) microchannel at a concentration of 1.3 pM (resulting in ~300 molecules probed). Spectra of a trypsin BSA digest obtained from c) reservoir and d) microchannel at a concentration of 6.0×10-9M corresponding to 1.1×106 molecules.

Since the analytes are distributed evenly along the length of the channel and throughout the reservoirs, we estimated the number of molecules detectable in any given channel segment by assuming a laser diameter of 100 µm hitting the surface. Thus, a surface area fo 50 µm x 100 µm was tested corresponding to a volume of 300 pL (note that the cross section of the microchannel is 50 µm x 60 µm). We further assume that the complete amount of proteins or peptides in this given volume contributed to the final signal. Using angiotensin as example, we calculate that 3.9×10^{-22} mol (0.4 zmol) angiotensin were detected. This corresponds to only ~ 300 molecules. This indicates that

a peptide could be detected in copy numbers relevant for single cell analyses (Beck et al. 2011).

For proteins such as BSA a higher detection limit is expected. Accordingly, we were able to detect BSA with S/N of 2.5 with an initial concentration of 5.0×10^{-7} M from surface regions defined by a microfluidic channel (see Figure 3-5 a) and b)). For insulin, we could obtain a spectrum with S/N of 4.3 with concentration of 5×10^{-8}M in a microfluidic channel (see Figure 3-5 c) and d)). Using the above mentioned considerations, this corresponds to about 9×10^{7} BSA molecules or 9×10^{6} insulin molecules contributing to the displayed spectrum.

These detection limits are at the higher abundance limit of protein content suitable for single-cell- based assays. Note that Beck et al. (Beck et al. 2011) recently reported protein abundance spanning seven orders of magnitude within a range of 10.000 to 20 million in single human cells. Considering the large range in abundance we decided to test whether a protein digest would improve the protein detection limit. As an additional benefit this approach also allows the identification of the protein using the resulting fragment peptide spectra in a peptide mass fingerprinting approach, which provides more information on the measured protein than the average mass alone.

Thus, we loaded varying concentrations of trypsin-digested BSA with matrix solution into the microdevice and performed MALDI-TOF-MS (Figure 3-4 c) and d)). The number of detectable peaks declined with decreasing concentration of the digest within the channel. However, even at a concentration of 6×10^{-9} M, 7 peaks were detected with S/N ratios ranging from 2.6 to 17.3 from a region defined by the microchannel. Moreover, the identified peptides covered 18% of the protein and allowed the

identification of BSA with a significant score of 117 in UniprotKB human protein database . Assuming the same laser beam diameter and channel volume probed as mentioned above and with a BSA concentration of 6.0×10^{-9}M, we estimate 1.8×10^{-19} mol corresponding to 1.1×10^{6} molecules. These results are encouraging and indicate that in principle even without pre-concentration the detection of as few as 3.1×10^{-22} mol peptides and 1.8×10^{-19}mol proteins is possible.

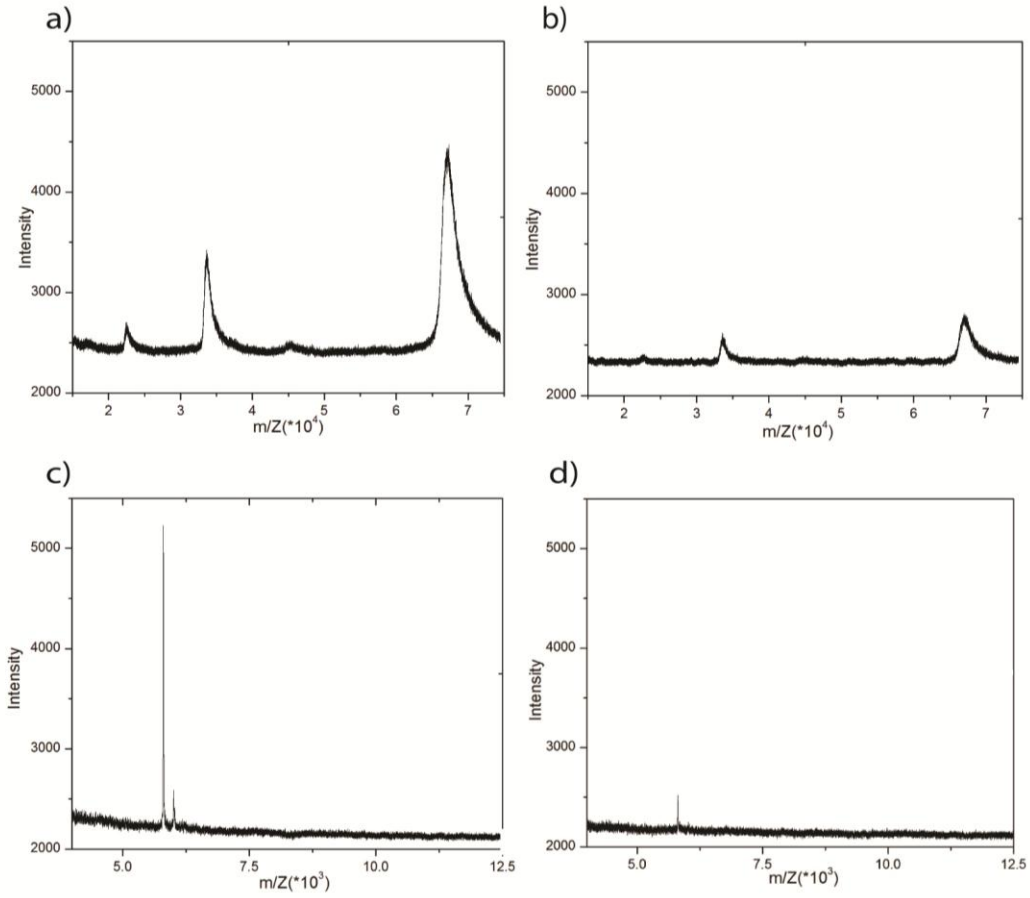

Figure 3-5: MALDI-TOF-MS spectra of proteins obtained from the combined microfluidic and MALDI-MS approach: Intact BSA spectra obtained from c) reservoir and d) microchannel at a concentration of $5.0*10^{-7}$ M corresponding to ~$9*10^{7}$ molcules probed. Intact insulin spectra obtained from a) reservoir and b) channel at a concentration of $5*10^{-8}$M corresponding to ~ $9*10^{6}$ molecules probed.

3.3.3 Affinity Capture and MS Detection in a Microfluidic Channel

After establishing a method to detect proteins and peptides with MALDI-TOF-MS in a microfluidic system, we developed a simple method to allow specific immunoreaction of analytes of interest within the microfluidic device. For this purpose, we chose anti-insulin IgG to capture and subsequently detect human insulin within from surface areas previously defined by the microfluidic manifold.

Covalent IgG immobilization on ITO slides was performed as previously reported (Ng et al. 2002). To ensure optimal coverage of the ITO surface with IgGs, we determined the saturation concentration with fluorescently labelled IgGs. The saturated concentration of IgG for the immobilization on ITO slides was determined by fluorescence microscopy. Fluor 488 chicken anti-rabbit IgG was dissolved in water and diluted in a series of concentrations ranging from 2×10^{-4} mg/mL to 0.1mg/mL. 5 μL of IgG solution with varying concentrations were pipetted into different reservoirs on an ITO surface and incubated in a humidity chamber at room temperature for 2 h. These reservoirs were subsequently washed with 20 mM phosphate buffer for three times. Fluorescence intensity of each reservoir was recorded on a fluorescence microscope (Olympus IX71, Olympus, USA) using a CCD camera (Photometrics, AZ). The intensity of each reservoir was obtained by averaging the intensity of five images and the result is shown in Figure 3-6. At a concentration of 0.05 mg/mL we observed no further increase in fluorescence indicating the saturation of surface coverage. We thus employed this concentration for all further IgG immobilization steps.

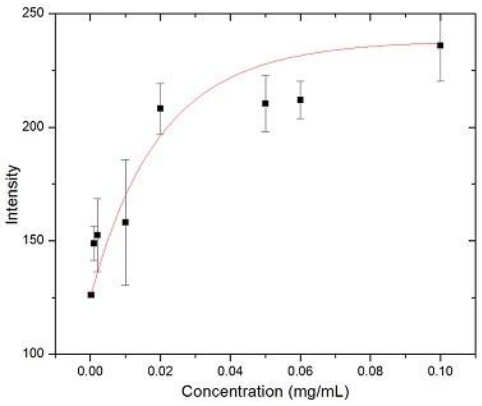

Figure 3-6: Fluorescence intensity of fluorescently labeled IgG for various incubation concentrations immobilized on ITO slides.

In order to ascertain specificity in our immunoassay we first performed a series of experiments on the ITO surface without the PDMS manifold. We treated the ITO surface with a 5 µL droplet of an anti-insulin IgG at a concentration of 0.05 mg/mL. To block free binding sites on the ITO slide we then incubated the slides with a 10 mg/mL BSA solution. After washing with phosphate buffer, we incubated the slide with a 2 µM insulin solution for 1 h to allow binding to the antibodies. Following removal of unbound insulin through an additional washing step, we added matrix solution and performed MALDI-TOF-MS.

The resulting MS spectra allowed the detection of insulin peaks with an average m/Z of 5808.05 corresponding to the expected mass of insulin with $[M+H^+]$ ($[5808.57]^+$), see Figure 3-7 a). In addition, we found additional peaks with an average m/Z of 8536.45 that we were not able to assign to any of the used components. Subsequent analyses revealed that it is most likely a contaminant found in the commercial BSA batch. Due to its m/Z we were not able to detect the contaminant in the assay for the intact BSA, nor in the digest.

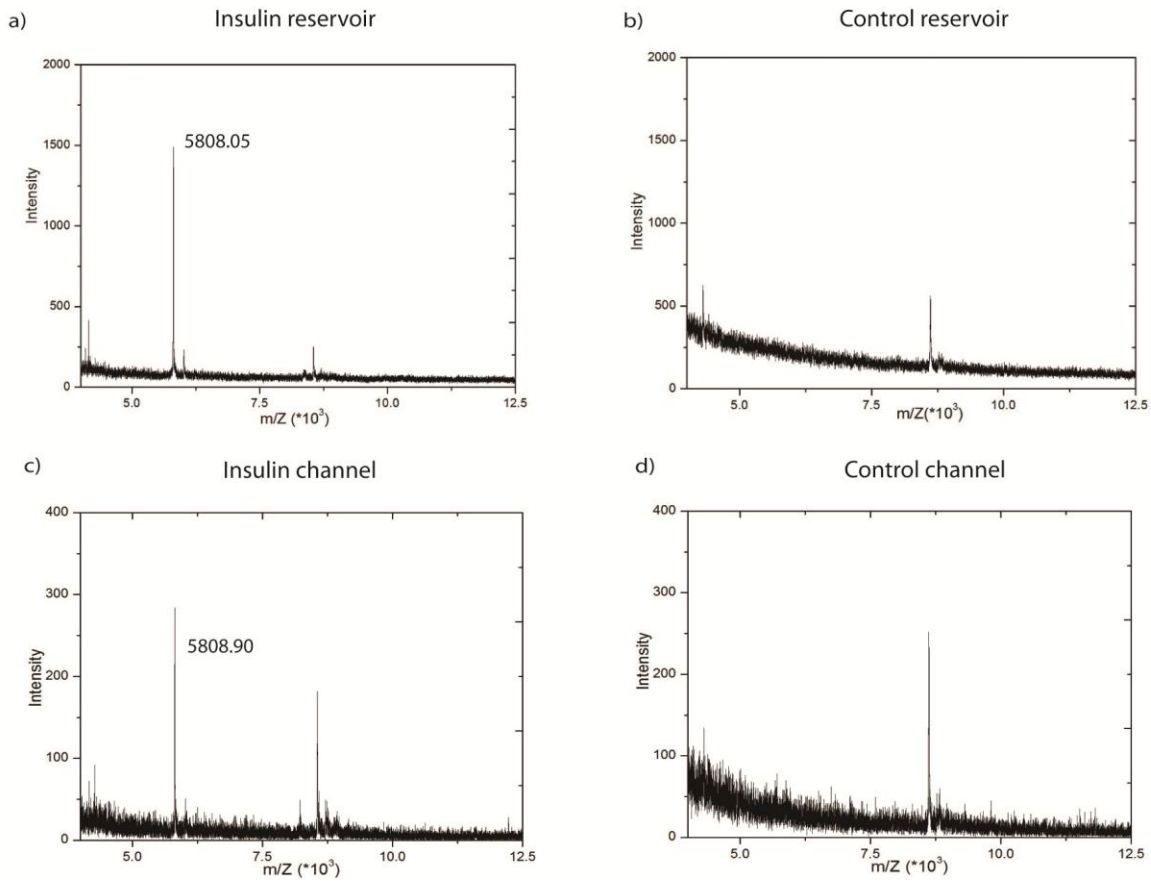

Figure 3-7: MALDI-TOF-MS analysis of anti-insulin immunoassays: a) Representative spectrum obtained with anti-insulin IgG from a reservoir, b) representative spectrum obtained with non-binding IgG from a reservoir, c) Representative spectrum obtained with anti-insulin IgG from single probed spot defined by the microchannel, d) Representative spectrum obtained with non-binding IgG from single probed spot defined by the microchannel.

As a control for the specificity of the binding reaction we performed the same experiment but replaced the anti-insulin antibody with IgG directed against rabbit-IgG (see Figure 3-7 b)). From 9 independent experiments we were not able to detect spectra corresponding to insulin, indicating that the binding of insulin occurred specifically to the corresponding IgG and blocking steps of the ITO surface were sufficient.

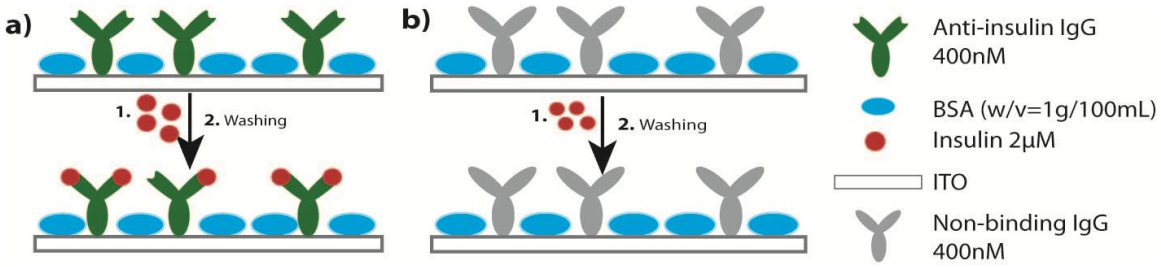

Figure 3-8: Schematics of the Insulin immunoassay performed on an ITO surface within a microfluidic channel: a) with insulin binding specific anti-insulin IgG, b) with non-binding IgG.

Next, we performed the same assay in the complete microdevice (shown in Figure 3-8). The same concentrations and incubation times as for the slide assay were used and after the final washing step matrix solution was introduced by capillary action. The resulting mass spectra are shown in Figure 3-7 c) and Figure 3-7 d). For the insulin-binding IgG, a peak at m/Z 5808.90 demonstrated again the specific capture of insulin. Correspondingly, the insulin signal did not appear for the non-specific anti-body assay. Finally, we estimated the number of molecules of immobilized anti-insulin IgG per surface area and deducted the number of molecules of insulin probed by this assay. As we performed IgG incubations at the saturation concentration, we estimate that a monolayer of IgG molecules was formed. This monolayer is probed by a laser of ~100 µm diameter. With an estimated area of 5 nm×10 nm (50 nm^2) one immobilized IgG molecule covers, we conclude that roughly 10^8 IgG molecules were probed by the MALDI laser on the area defined as the intersection of laser spot and ITO surface defined by the microfluidic channel. We further estimate that only 5 % of the immobilized IgG molecules are active and that each IgG binds one insulin molecule. This results in roughly 5×10^6 molecules that were probed in this assay in a microchannel.

Our study thus demonstrated that affinity capture of insulin on a single anti-insulin IgG coated surface layer is possible. We emphasize that this is the first example – to the best of our knowledge - realized on an ITO surface and with an immunoassay specific for insulin. Although other immunocapture assays on gold surfaces have been demonstrated with various analytes by others (Kim et al. 2012) and us (Nelson et al. 1999; Nelson and Krone 1999; Nelson, Nedelkov, and Tubbs 2000), this work furthermore demonstrates the coupling of microfluidic pre-treatment steps and consequently a high spatial resolution (~50 µm). Moreover, the number of molecules probed with our approach originating from a surface area of of 0.05 mm^2 approaches the detection sensitivity of proteins for single cell analysis. We emphasize on the fact that the probed area can easily be decreased by reduction of the microfluidic pattern. Using standard photolithography, such patterns can be created as small as a few µm and the possibility of nanostructuring could further reduces this limit. Coupling integrated fluidic handling tools such as valves and pumps additionally provide the advantage of automizing and parallelizing this technology for high throughput applications coupled to minute sample amounts down to single cell.

3.4 Section Conclusions

In this work we investigated a suitable condition to create a microfluidic device that allows direct coupling of immunocapture with following MALDI-MS analysis with a spatial resolution of 50 µm. The key aspect of this approach is that the microfluidic manifold can be removed readily from the MADLI-MS target after immunocapture for subsequent analysis. Detection sensitivity for peptides and proteins has been

demonstrated with this approach. We were able to infer the detection of as low as 300 molecules (0.4 zmol) of the peptide angiotensin. As expected from the generally higher detection sensitivity for MALDI-MS of proteins we obtained mass spectra originating from defined areas in a microfluidic channel amounting in roughly 108 molecules of BSA and 10^7 insulin. Not unexpectedly, the mass fingerprinting of a BSA-digest resulted in two orders of magnitude better sensitivity. Besides, a simple insulin immunoassays on ITO surfaces within areas of ~0.05 mm^2 was successfully coupled in this microfluidic device and the MALDI MS Spectra indicated that the insulin was specifically captured by anti-insulin on the ITO surfaced confined by microfluidic channels. More importantly, the observed detection limits are close to the requirements of analyzing proteins and peptides originating from single or few cells. We envision that this inexpensive microfluidic system holds the potential to perform bioanalytical investigations with single cell resolution.

CHAPTER 4

A MICROFLUIDIC PLATFORM FOR PROTEIN IDENTIFICATION AND PROTEIN QUANTIFICATION

4.1 Introduction

Gain of quantitative information about protein expression in single cells is essential to understand biological processes such as those involved in cell apoptosis, cancer, biomarker discovery, disease diagnostics, pathology or therapy. Most of the quantification approaches in single cell analysis are based on fluorescence measurements which are limited due to restricted range of fluorescent dyes. Analysis of cellular compounds in single cells using MALDI MS has been reported suitable for characterization of proteins in single cells such as single mammal cells (Li, Golding, and Whittal 1996) and single yeast cell (Amantonico et al. 2008). However, quantitative information is not provided and lack of proper compartmentalization approach leads to extremely low throughput.

In this chapter, I report on our efforts to develop a quantitative mass spectrometric approach combined with microfluidic technology for protein identification and quantification. Analysis multiplexing was realized by a series of chambers and valves in a microfluidic platform, ensuring a set of defined wells for absolute quantification of targeted proteins. To this aim, isotopic labeling strategies were applied by employing iTRAQ-labels to an on-chip protocol. Simultaneous protein digestion and labeling was performed on the microfluidic platform, making the labeling strategy compatible with all necessary manipulation steps on-chip, including the matrix delivery for MALDI-TOF

analysis. We demonstrated this approach with the apoptosis related protein Bcl-2 and quantitatively assess the number of Bcl-2 molecules detected.

4.2 Materials and Methods

4.2.1 Materials

iTRAQ reagents multi-plex kit was obtained from AB Sciex (USA). Trypsin was obtained from Promega Corporation (USA). Isopropanol and acetone were from VWR (USA). SU-8 2075 photoresist and SU-8 developer were from MicroChem (USA). PDMS was purchased from Dow Corning Corporation (USA). Acetonitrile, alpha-cyano-4-hydroxycinnamic acid (α-CHCA), Bcl-2 active human, Anti-Bcl-2 antibody and bovine serum albumin (BSA) were from Sigma-Aldrich (USA). Alexa Fluor 488 chicken anti-rabbit IgG was purchased from Invitrogen (USA). Peptide calibration mixture (angiotensin II 1046.5418 m/Z $[M+H]^+$, angiotensin I 1296.6848 m/Z [M+H]+, substance P [1347.7354 m/Z $[M+H]^+$, bombesin 1619.8223 m/Z $[M+H]^+$, ACTH clip 1-17 2093.0862 m/Z $[M+H]^+$, ACTH clip 18-39 2465.1983 m/Z [M+H]+, somtostatin-28 3147.4710 m/Z $[M+H]^+$) was purchased from Bruker Daltonics Inc (USA). ITO slides (100 ohm/sq) were obtained from NANOCS and Cr was obtained from SPI Supplies (USA). Tridecafluoro-1, 1, 2, 2-tetra-trichlorosilane (TTTS) was purchased from Gelest (USA).

4.2.2 Microchip Fabrication

All polydimethylsiloxane (PDMS) channels were fabricated via soft lithography using printed polymer masks. For proof of principle, three straight channels were used for Bcl-2 immunoassay, on-chip digestion and iTRAQ tagging experiments. The chip was assembled reversibly with the method reported previously (Yang et al. 2012).

Standard procedures of PDMS-based multi-layer soft lithography were also used to fabricate microfluidic devices with normally closed valves (called ladder-like device in the following text) (Unger et al. 2000). The structure of the ladder-like device is shown in Figure 4-1 a. This two layer device included a fluidic layer (filled with colors) composed of ten separated wells and a control layer (red) with microchannels actuated by negative pressure. PDMS microchannels on both layers were molded from patterns of 43 μm thick negative photoresist SU-8 2075. The photoresist was spin-coated onto a silicon wafer followed by a soft baking procedure for 3 min at 65℃, and 9 min at 95℃. The wafer was exposed to UV light for 45 seconds through the film photomask with a mask aligner (System 3A, HTG, USA). After a post baking for 2 min at 65℃ and 7 min at 95℃, the silicon wafer was soaked in SU-8 developer for 5 min followed by 20 min hard baking at 150℃. The silicon master was then silanized with TTTS to avoid adhesion between PDMS and the silicon wafer. For the control layer, 48 g of a 6:1 w/w ratio of PDMS to curing agent solution was poured onto the silicon master. For the fluidic layer, 16 g of a 15:1 w/w ratio of PDMS to curing agent solution was spin-coated on the silicon master for 30 sec at 1300 rpm, yielding a thickness of 75 μm thin layer (Zhang and Ferguson 2004). Both layers were cured at 65℃ for about 40 min. After curing, the control layer was cut from the silicon master and manually aligned with the fluidic layer which was

still on the silicon wafer using a stereomicroscope (FB-220U, Olympus, USA). The whole device was cured again at 65℃ overnight for tight bonding. Afterwards, the two-layer PDMS mold was peeled off from the silicon master and holes were punched manually with a 2 mm biopsy punch (Fray Products, USA).

The PDMS manifold was treated with oxygen plasma in a Harrick plasma cleaner (PDC-001, Harrick, USA) for 90 sec under medium power settings before chip assembly. ITO coated glass slides (100ohm/sq, NANOCS, USA) were used as the substrate. The backside of ITO slides was coated with a 25 nm thick layer of Cr with an Evaporator (308R, Cressington, UK), allowing visual inspection during MALDI-TOF measurements. ITO slides were reused 5-8 times after cleaning with acetone and isopropanol.

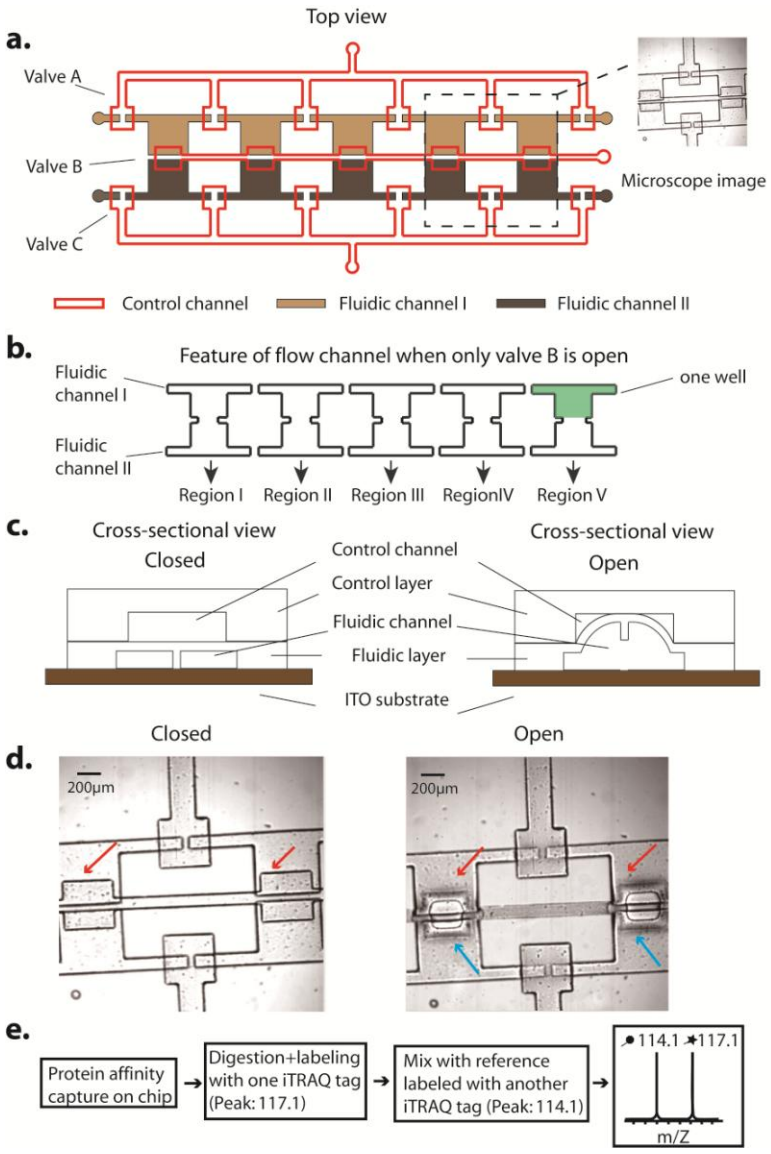

Figure 4-1: a) Top view of the ladder-like microfluidic device with pneumatic valves. Red lines indicate the channels in the actuation layer and rectangles the position of the pneumatic valves. Channels filled with brown and yellow color indicate the fluidic layer containing the incubation and mixing wells (not to scale). Right: bright field image of two chambers (at left and right of image). b) Feature of the flow channel when valve B is open and valve A and C are closed. Five regions (I-V) are available for MALDI-TOF-MS after the PDMS manifold is peeled off. Each region is composed of two opposed wells with each well (filled with green color) amounting in a volume of ~15 nL. c) Cross-sectional views of the pneumatic valve in closed (left) and open (right) state. d) Optical images of the valve in closed and open state. e) Workflow of on-chip protein quantification by iTRAQ tags.

4.2.3 Bcl-2 Immunoassay, Digestion and iTRAQ Tagging

Proof-of-principle experiments for the iTRAQ labeling and digestion procedure were performed in a straight channel with a dimensions of 50 μm×60 μm×1 cm. Anti-Bcl-2 antibody was immobilized covalently on ITO slides as reported by Ng et al.(Ng et al. 2002) Protein solutions were prepared in phosphate buffer (20 mM sodium phosphate dibasic) if not stated otherwise. 5 μL anti-Bcl-2 IgG solution (0.05 mg/mL) was pipetted into the reservoir and capillary flow filled the channel within a few seconds. After 2 h incubation in a humidity chamber at room temperature, IgG solution was removed and the microchannel was washed three times with 20 mM phosphate buffer by vacuum suction. Then, the channel was filled with 1%(w/v) BSA and incubated for an hour in order to block the unspecific binding positions. The BSA was removed followed by washing with phosphate buffer for three times. Subsequently, 5 μL Bcl-2 solution (0.037 mg/mL) was filled in the channels by capillary action. After 1 h incubation in a humidity chamber at room temperature, Bcl-2 solution was removed by vacuum and the channel was washed three times by 100 mM ammonium bicarbonate buffer. Afterwards, the channel was filled with 5 μL trypsin solution (0.1 μg/μL, dissolved in 100 mM ammonium bicarbonate buffer) and incubated in a humidity chamber at 37 ℃ overnight. When the channel was completely dried, the channels were filled with 5 μL matrix solution (saturated α-cyano-4-hydroxycinnamic acid (CHCA) in 40% v/v acetonitrile, 0.1% v/v TFA in water solution) by capillary action. After the matrix solution in the channel was completely crystallized, the PDMS mold was peeled off and the remaining ITO slide with crystals was used as target for MALDI-TOF-MS.

In the tagging experiment, initial steps were the same as above except adding trypsin solution mixed with one iTRAQ tag. After the Bcl-2 solution was removed and the channel was washed three times by iTRAQ dissolution buffer (iTRAQ™ reagent kit, AB SCIEX, USA), a mixture composed of 4 μL trypsin solution (0.1mg/mL) and 5 μL iTRAQ tag solution (obtained by adding 70 μL ethanol to one tube of 117 tag) filled the channel simultaneously followed by 4 h incubation in a humidity chamber at 37 ℃. When the channel was completely dried, 5 μL CHCA matrix solution was added and the same steps were repeated for the MALDI measurement.

4.2.4 Bcl-2 Quantification in the Ladder-Like Device

In preparation of internal standard sample, Bcl-2 was digested and labeled with one iTRAQ tag off chip. First, Bcl-2 was cleaned by a centrifugal filter (Amicon-0.5mL 3K, Millipore, USA) to get rid of glycerol which would affect the digestion. Concentration of cleaned Bcl-2 solution was determined by Bradford protein assay (Bradford assay, Bio-Rad, USA). 2 μL cleaned Bcl-2 was mixed with 8 μL iTRAQ dissolution buffer, 2 μL trypsin solution (0.1mg/mL) and 8 μL iTRAQ tag solution (obtained by adding 70 μL ethanol to one tube of 114 tag). This solution was incubated at 37 ℃ overnight and used as the internal standard for on-chip Bcl-2 quantification.

Bcl-2 quantification experiment on chip was carried out with pneumatic valves integrated (Figure 4-1 a). Negative pressure of ~100 mbar was applied through a MFCSTM-EZ system (Fluigent Inc, USA) to open and close the valves (Figure 4-1 c and d) for fluidic manipulation steps. Stainless steel pins (Idex corporation, USA) were cut to 1.5 cm each for connecting the chip with the MFCSTM-EZ system. The workflow is

shown in Figure 4-1 e. First, Bcl-2 immunoassay, digestion and iTRAQ tagging steps were repeated in the fluidic channel I. In this step, valve A was open while valve B and C were closed for all of chip loading steps. Valve A, B and C were closed for all of the incubation steps. Next, in fluidic channel II, valve C was open while valve A and B were closed. 5 μL internal standard solution filled the fluidic channel II by negative pressure. Afterwards, valve A and C were closed while valve B was open and closed repeatedly for 2 min in order to mix the sample and the internal standard solution. The chip was placed at ambient atmosphere overnight until channels were completely dried. Last, valve B was closed while valve A and C were open. 5 μL of CHCA matrix solution filled the fluidic channel I and II. After the solution in the channel was completely crystallized, the two-layer PDMS manifold was peeled off and MALDI-TOF-MS was performed on the ITO slide with crystals.

4.2.5 MS Analysis

MALDI-TOF-MS was performed using a Bruker Ultraflex III MALDI-TOF/TOF instrument. Peptide spectra were acquired in reflectron mode and 1000 laser shots were summed. Calibration was performed with angiotensin II, angiotensin I, substance P, bombesin, ACTH clip 1-17, ACTH clip 18-39, somtostatin 28. The digested Bcl-2 spectrum was searched with the MASCOT algorithm for identity validation. Experiments with iTRAQ tags were performed by using MALDI-TOF MS/MS. MS/MS spectra were acquired with 1000 shots for each examined spot. The whole detection region (as shown in Figure 4-1 b) was manually scanned in order to capture signal from all crystals in the well area. Thus, around 35 spots were examined in each detection region. The position of

each well in the device was identified via the crystal rim formed by co-crystallization of MALDI matrix and sample with the camera in the MALDI TOF instrument. The spectrum of Bcl-2 digest was searched against the Swissprot database with the MASCOT algorithm for identity validation. Due to a narrow isotope distribution of the peak, the peak area and peak height are nearly the same in this analysis. The peak area was chosen here for quantification purposes. Peak areas of report groups in MS/MS spectra were analyzed using OriginPro software.

4.3 Results and Discussion

This section is divided into three parts. First, a novel microfluidic device was described for quantification of proteins combined with MALDI-MS analysis. Second, we report on the adaptation of enzymatic digestion and iTRAQ labeling necessary for the combined microfluidic-MS approach. In the last part, we report the quantitative detection of the apoptosis marker Bcl-2 with the combined microfluidic-MS approach and discuss the impact for future single cell analysis.

4.3.1 Chip Fabrication and Valve Actuation

The aim of our study is to achieve protein affinity capture, protein identification and quantification by a combined microfluidic and mass spectrometric method. Ultimately, this method should allow studies on small cell ensembles or single cells. To this aim, we developed a reversible bonding procedure between an ITO substrate and a PDMS manifold allowing the PDMS to be peeled off and thus exposing matrix crystals on the ITO substrate for MALDI-TOF analysis. Improvement of microfluidic devices

(Figure 4-1 a) over our precious study (Yang et al. 2012) was realized by integration of membrane valves actuated by negative pressure. This approach has the advantage that first, regions formed by closed valves have a fixed surface area and volume, allowing for absolute quantification; second, the novel approach allows adding matrix solution in a control channel preventing dilution or washing out sample when internal standard was added; third, it allows active mixing of an internal standard with the sample by actuating valves. A PDMS membrane valve (Figure 4-1 c) was selected due to its compatibility with the necessary reversible binding condition. Positive pressure actuated valves (Unger et al. 2000) were not considered to avoid fluid leaking due to the reversible bonding of PDMS manifold and ITO substrate (data not shown).

Figure 4-1 c shows the cross sectional view of this valve. This valve includes a control layer with ~3 mm height and a fluidic layer with ~100 μm height. Both the control channel which is in the control layer and the fluidic channel which is in the fluidic layer resulted in a thickness of 43 μm. The thin membrane, also serving as the ceiling of the fluidic channel was ~30 μm thick (Zhang, Ferguson, and Tatic-Lucic 2004) and the valve stop attached to the thin membrane had a height of 43 μm to stop the flow in the fluidic channel. To actuate the valve, negative pressure was applied in the control channel to lift the valve stop. A key factor determining the actuation pressure was the adhesion forces between the valve stop and the ITO surface (Mohan et al. 2011). Optical microscopy was employed to verify the open and closed states of the valve (Figure 4-1 d). The oval-shaped area indicated by blue arrows in the state indicated that the membrane was lifted off and touched the roof of the control channel.

4.3.2 Affinity Capture and Identification of Bcl-2 in Microfluidic Channels

In order to adapt the proposed methodology to a larger protein with suitable sensitivity, we first developed an enzymatic digestion step succeeding an affinity capture step on-chip (see Figure 4-2). Herein, a larger protein Bcl-2 was chosen for this approach. Bcl-2 is known to play a critical role in apoptosis regulation (Czabotar et al. 2014). In order to test the incubation and digestion procedure, we first carried out experiments in a straight microfluidic channel without integrated valves. It was previously demonstrated that biomolecules including antibodies and antigens, attached covalently, spontaneously, and robustly onto the ITO surface (Ng et al. 2002). The saturation concentration for antibodies on ITO was determined with fluorescently labeled IgGs as previously reported (Yang et al. 2012). We followed this strategy and the ITO surface was treated within the microchannel with an anti-Bcl-2 antibody at a saturated concentration of 0.05mg/mL. A BSA treatment step followed in order to block the non specific binding sites. After the BSA was removed by washing with phosphate buffer, the channel was filled with Bcl-2 solution and then incubated to allow the binding with anti-Bcl-2 antibody. After renewed washing, trypsin was added and the channel was incubated in a humidity chamber at 37 ℃ overnight for complete protein digestion. Last, matrix solution was added to facilitate MALDI-TOF-MS. The detailed incubation and washing steps for this protocol are outlined in the Section 4.2.3.

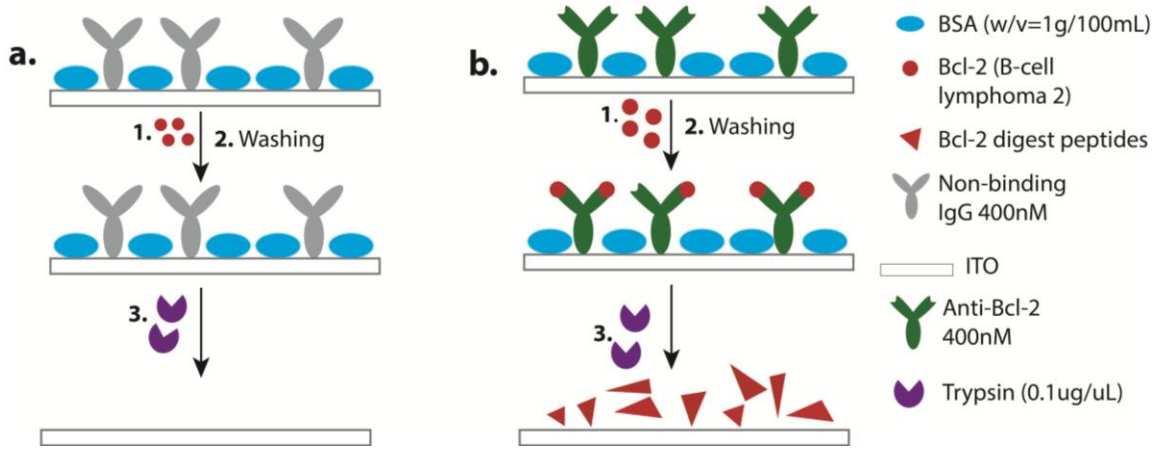

Figure 4-2: Schematics of the Bcl-2 immunoassay and tryptic digestion performed on an ITO surface within a microfluidic channel: a) with insulin binding specific anti-insulin IgG, b) with non-binding IgG (anti-rabbit IgG).

As shown in Figure 4-3 a, the MALDI-TOF spectrum in which six peptide peaks (1210.6 m/Z $[M+H]^+$, 1950.8 m/Z $[M+H]^+$, 1994.8 m/Z $[M+H]^+$, 2295.1 m/Z $[M+H]^+$, 2886.6 m/Z $[M+H]^+$, 3596.8 m/Z $[M+H]^+$) labeled with red triangles were identified corresponding to expected masses from a tryptic Bcl-2 digest (See Table 4-1). These peaks showed a sequence coverage of 50% with a significance score of 104 in a SwissProt data base search successfully identifying the protein Bcl-2. Additional peaks from BSA, anti-Bcl-2 IgG and trypsin fragments were also found in the spectra.

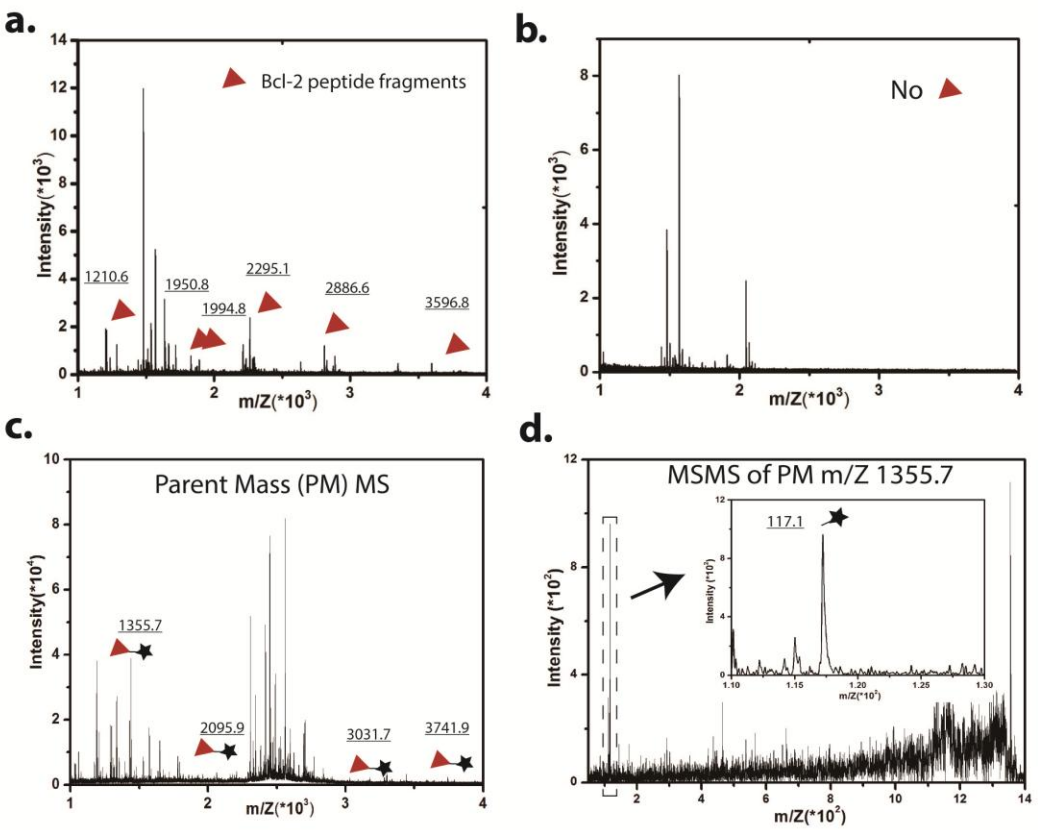

Figure 4-3: a-b) MALDI-TOF-MS analysis of an anti-Bcl-2 immunoassay followed by Bcl-2 on-chip tryptic digestion: a) Representative spectrum obtained with anti-Bcl-2 IgG. b) Similar to a) but with non-binding IgG. c-d) MALDI-TOF-MS analysis employing an immunoassay on chip followed by iTRAQ labeling during digestion: c) simultaneous on-chip tryptic digestion and iTRAQ labeling after an anti-Bcl-2 immunoassay. d) MS/MS spectrum of parent mass ([M+H]+ m/Z=1355.7) selected from the spectrum shown in c) (inset: low mass range spectrum showing the report ion used for quantification).

Mass In the spectrum	Peptide Position	Peptide Sequence
1210.6	130-139	FATVVEELFR
1950.8	111-127	DFAEMSSQLHLTPFTAR
1994.8	130-146	FATVVEELFRDGVNWGR
2295.1	165-183	EMSPLVDNIALWMTEYLNR
2286.6	69-98	TSPLQTPAAPGAAAGPALSPVPPVVHLTLR
3596.8	27-63	GYEWDAGDVGAAPPGAAPAPGIFSSQPGHTPHPAASR

Table 4-1: Identification of peaks from 1.4 μM in the spectrum

A control experiment was performed employing the same protocol but using chicken anti-rabbit IgG to verify the specificity of the immunoassay. As shown in Figure 4-3 b, m/Z peaks corresponding to the Bcl-2 digestion could not be found in the spectra, indicating that Bcl-2 was specifically captured by the binding IgG, but not in the control experiment. Moreover, BSA blocking and washing steps on the ITO surface were sufficient to remove nonspecific binding of Bcl-2.

This MS-based on chip immunoassay can now be compared with previous work. Our previous study demonstrated that the affinity capture of insulin on a single anti-insulin IgG coated ITO surface layer was achieved by detection of intact insulin (Yang et al. 2012). Here, with the additional on-chip digestion approach, we were able to detect the larger 26 kDa protein Bcl-2. We thus extended the combined microchip-MS approach to the identification of proteins on the level of peptides formed by digestion of target proteins via peptide mass fingerprinting. Our previous results showed that detection of a protein digest would improve the protein detection limit by two orders of magnitude (Yang et al. 2012). This is another benefit of performing on-chip enzymatic digestion

allowing the analysis of larger proteins in small amounts of cells even down to a single cell.

4.3.3 iTRAQ Tagging of Bcl-2

Due to lower limit of peptide detection, we further quantitatively investigated the number of Bcl-2 proteins detected employing the microchip digestion procedure. In our previous approach (Yang et al. 2012) without enzymatic digestion, we estimated that roughly 5×10^6 molecules were probed. This amount is in the range of high abundant proteins in single cells ($\sim 10^6$ protein molecules) (Xie et al. 2008) however is limited to small proteins and peptides, lacked the possibility of multiplexing and is potentially subject to washing and dilution losses. Here, we improved our previous approach by adapting the protocol for two iTRAQ tags allowing for true quantification. In this approach, the on-chip immunoassay was followed by a digestion step in which peptides were labeled with one iTRAQ tag. A protein digest with a known concentration as an internal standard was labeled with the second iTRAQ tag and mixed with the first digest on chip for quantification, which was achieved based on the peak area ratio of these two tags after MS/MS analysis.

A typical iTRAQ protocol as suggested by the supplier is not possible in this chip-assay, since two independent steps of digestion and iTRAQ labeling will not allow quantitative results. Renewed filling steps would simply wash sample out of the microfluidic channel. Thus, in order to avoid this problem, we developed a protocol allowing for simultaneous digestion and labeling in one step (see section 4.2.3). An experiment of simultaneous digestion and iTRAQ labeling of captured Bcl-2 digest was

carried out in a straight channel to verify that the iTRAQ labeling process could be applied in the proposed microfluidic platform (as outlined in Figure 4-1e). Instead of adding the trypsin solution alone, we added a mixture composed of trypsin and iTRAQ tag simultaneously, followed by an incubation at 37 ℃. MALDI matrix was added and the co-crystallized sample was analyzed by MALDI MS.

The resulting MS spectrum (Figure 4-3 c) shows four Bcl-2 digest peaks (1210.6 m/Z $[M+H]^+$, 1950.8 m/Z $[M+H]^+$, 2886.6 m/Z $[M+H]^+$, 3596.8 m/Z $[M+H]^+$) shifted to larger masses (1355.7 m/Z $[M+H]^+$, 2095.9 m/Z $[M+H]^+$, 3031.7 m/Z $[M+H]^+$, 3741.9 m/Z $[M+H]^+$) due to addition of the iTRAQ tag (145.1 m/Z $[M+H]^+$). The corresponding MS/MS spectrum of one selected mass 1355.7 m/Z $[M+H]^+$ is shown in Figure 4-3 d and the reporter group 117.1 m/Z $[M+H]^+$ of the tag is apparently observed. Figure 4-3 c and Figure 4-3 d indicate that the simultaneous digestion and iTRAQ labeling was successfully developed.

To examine whether iTRAQ labeling approach is proper for single cell analysis, we tested the lowest concentration of Bcl-2 which could be quantified by iTRAQ strategy was determined. 1.4×10^{-5}M of Bcl-2 was digested and separately labeled with 114 tag and 117 tag by using the procedures described in the above section. The stock concentration of tagged Bcl-2 digest was 1.4×10^{-6} M. A dilution series of this solution (either 114 tagged or 117 tagged) was made from 1.4×10^{-6} M to 1.4×10^{-9} M. The two tags were mixed in 1:1 ratio. Results are shown below (Table 4-2). We further note that the typical concentration of protein in the cell lysate is ~1 μM calculated via the copy number (10^6) of a high abundant protein in about 1 pL cell volume. The iTRAQ strategy is successful down to a concentration of 14 nM, suitable for quantifying the proteins in

single cells. We further tested the sensitivity of the method in regards to the Bcl-2 concentrations and the iTRAQ labeling ratio (see Appendix A 1-2), which are in good agreement with previous studies on iTRAQ labeling strategies (Wiese et al. 2007).

Concentration	114/117 ratio
1.4×10^{-6}M	0.75 ±0.26
1.4×10^{-7}M	1.08 ±0.44
1.4×10^{-8}M	1.21 ±0.46
1.4×10^{-9}M	No peak identified

Table 4-2: Dilution series for iTRAQ quantification on Bcl-2. The theoretical ratio of two tags was 1:1.

4.3.4 Quantification of Bcl-2 in the Ladder-Like Device

The next challenge consisted in reproducible and metered delivery of the second iTRAQ label for the intended quantification. For this purpose, a microfluidic platform was developed capable of on-chip iTRAQ tagging of target protein captured in an immunoassay and delivering reference iTRAQ label in known amounts with integrated mixing of the sample and reference peptide. This procedure is outlined schematically in Figure 4-1 e. In fluidic channel I (Figure 4-1 a), Bcl-2 immunoassay, digestion and iTRAQ tagging steps were performed when valves A are open and valves B and C were closed. In the opposed fluidic channel II (Figure 4-1 a), an internal standard solution originating from 1.4×10^{-7} M reference digest was loaded when valve C was open and valve A and B were closed. Subsequently, the contents in opposite wells were mixed by actuating valve B while valve A and C were closed.

This procedure allows for mixing of the iTRAQ peptides from the chip digest with a reference digest containing the reference protein at a known concentration labeled

with the second iTRAQ tag. Five regions could be manipulated simultaneously allowing for five parallel experiments. The valves formed defined surface area and volume in each well allowing for absolute quantification. Repeatedly actuating valve B allowed active mixing of an internal standard in fluidic channel II with the sample in fluidic channel I. Thorough mixing of these two solutions was required in this protocol since Bcl-2 was quantified based on the peak area ratio of two tags from two fluidic channels.

To assure that the digested sample and the internal standard were mixed sufficiently and the signal was homogeneous in one detection area, a control experiment was performed with a fluorophore in the above ladder-like device (Figure 4-1 a). We repeated the mixing procedure in our quantification experiment by using 100mM sodium fluorescein. Fluidic channel I was filled with sodium fluorescein while the opposing fluidic channel II was filled with water when valve B was closed. Then, valve B was repeatedly opened and closed to mix dye and water. Averaged fluorescence intensities for each well were calculated at each time point. We found that fluorescence intensities on both fluidic wells reached the same value at 2 min indicating the homogeneity of the fluorescence in one detection region (see Figure 4-4).

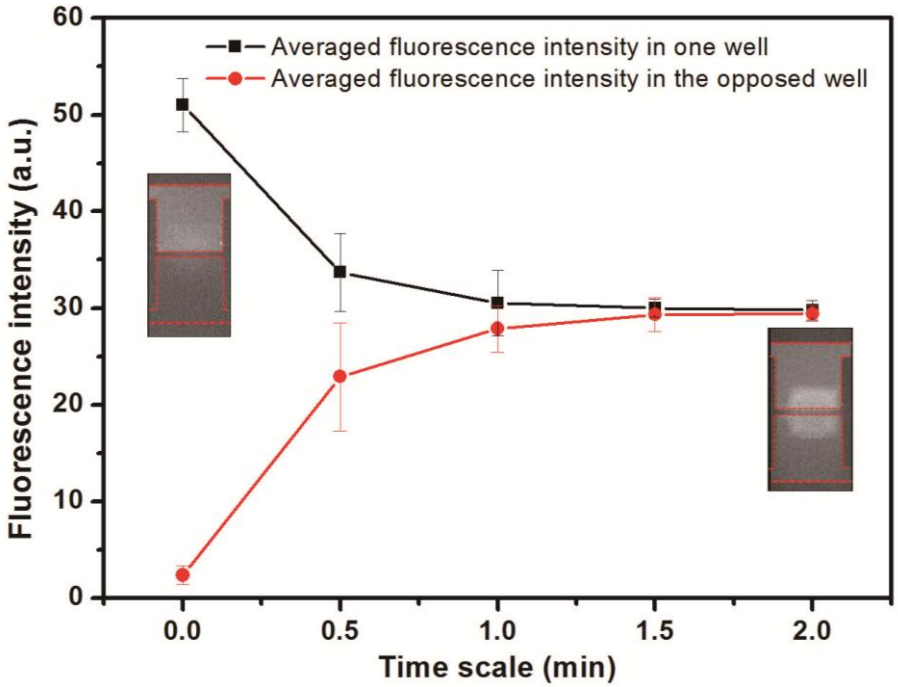

Figure 4-4: Averaged fluorescence intensity in one well in fluidic channel I and the opposed well in fluidic channel II when valve B is repeatedly opened and closed. Errors are the standard deviations of fluorescence intensities recorded in each well (insert: fluorescent images showing the opposite wells before mixing (left) and 2 min after mixing (right). The brighter area in the middle of the right image indicates the region where the valve is open).

Next, this improved platform was tested in the complete MALDI MS assay. For this purpose, MALDI matrix was loaded in both fluidic channel I and fluidic channel II after affinity capture of Bcl-2, digestion, iTRAQ tagging and mixing with the reference iTRAQ tag was accomplished. Finally, the PDMS manifold was removed after co-crystallization on chip and MALDI-TOF analysis was performed. The parent mass (1355.7 m/Z [M+H]+) was selected to perform MS/MS analysis and one example spectrum is shown in Figure 4-5, showing both the sample and reference iTRAQ mass. The MS/MS spectrum in Figure 4-5 indicates that this approach was successfully applied for quantitative MALDI MS analysis. Moreover, five regions shown in Figure 4-1 b (I-V)

from four chips were analyzed with an average peak area ratio of 2.9 (±0.45) corresponding to the ratio of 114.1 m/Z [M+H]+ to 117.1 m/Z [M+H]+. We note that the addition of matrix to channels I and II can potentially lead to dissolution of peptides during the filling process and a peptide concentration gradient along the wells. Assessing each well in all devices tested has however not revealed a gradient of the peptide intensities (data not shown). The matrix introduction procedure was necessary to assure matrix/sample co-crystallization, since filling of the matrix through channel I alone did not result in crystals. Further improvement of the valving system can improve this situation as well as a careful study of the matrix composition.

The quantitative analysis of the peak ratios now allows the calculation of the number of Bcl-2 molecules detected. One well as shown in Figure 4-1 b comprises a volume of ~15 nL. Thus, with an internal standard sample at a concentration of 1.4×10^{-7} M, we conclude that ~ 4.4×10^{8} Bcl-2 molecules were captured in each well. Moreover, one well results in a surface area of $(3.5\pm0.2)\times10^{5}$ μm^2 from which we calculate a surface coverage of Bcl-2 of $(2.1\pm0.4)\times10^{-21} mol/\mu m^2$. In this calculation, we assume that labeling efficiencies of both reactions are the same since the same iTRAQ procedures are applied for the sample and the internal standard. Thus, the labeling efficiency can be neglected in the ratiometric determination of peptide concentrations.

Previously, we estimated roughly 5×10^{6} molecules that were probed in a similar assay with insulin where the laser laser shot area amounted in 5×10^{4} μm^2 in a microchannel (Yang et al. 2012). This resulted in a surface coverage of $1.7\times10^{-21} mol/\mu m^2$ which is comparable to the result obtained by the here presented iTRAQ quantification.

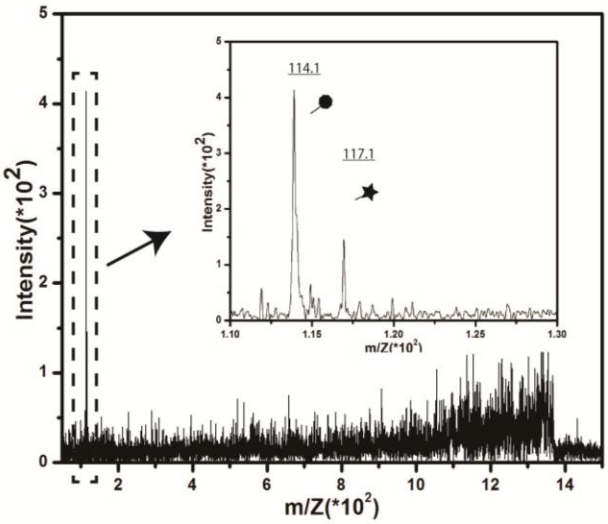

Figure 4-5: Representative MS/MS spectrum of the two iTRAQ labels from a Bcl-2 on-chip quantification with an anti-Bcl-2 immunoassay. MS/MS spectrum was assayed from parent mass [M+H]+ m/Z=1355.7 (insert: low mass range showing the report ions used for quantification).

It is commonly assumed that copy numbers of proteins in single cells vary from low abundant (several ten copies) to high abundant (a few million copies) (Xie et al. 2008). Assuming 10^6 protein molecules of one kind, the current surface area of the detection well could capture protein from a maximum of ~440 cells. Note that a well with area of ~800 μm^2 would be required for detecting high abundant proteins (10^6 molecules) from one single cell. It is well known that using standard photolithography technology, the area of a well can be made as small as 800 μm^2. The here presented approach advantageously performs all incubation steps in a defined volume – the well on the chip – avoiding the problem of dilution.

4.4 Section Conclusions

We investigated suitable experimental conditions for simultaneous tryptic digestion and iTRAQ labeling for on-chip protein identification and quantification. Moreover, we integrated this workflow in a microfluidic device capable of five simultaneous assays followed by MALDI MS/MS analysis. The new device allowed assay steps to be performed independently with subsequent on chip delivery of iTRAQ labels for absolute protein quantification. This approach allowed the analysis of the number of molecules detected in each individual well through iTRAQ labeling. This study indicates that in order to reach single cell sensitivity, i.e. assessing a protein copy number of 10^6 molecules from a single cell, a microfluidic well downscaled to a minimum surface area of ~800 μm^2 is required. The presented microfluidic approach could thus be adapted to capture one cell per well and would allow the quantification of high abundant proteins from single cells. The downscaling of the well geometry will further increase the throughput whereas the current soft lithography and fluidic mixing approaches are suited for a larger scale integration. Our future work is dedicated to the integration of cell loading and cell lysis steps with the here presented approach and we envision that it can be applied to quantitative proteomics in single cells in the future.

CHAPTER 5

IMPROVEMENT OF ABSOLUTE PROTEIN QUANTIFICATION BY AN ISOTOPICALLY LABLED PEPTIDE

5.1 Introduction

Accurate measurement of a specific protein amount that a cell produces is essential for investigating basic biological processes. And the assessment of this quantitative information will ultimately lead to significant progresses in drug design and development, cancer diagnostics and treatment. Single cell proteomic analysis has attracted more and more interest in the past few decades (Janicki et al. 2004). However, there is an urgent need for technologies that permit the direct quantification of proteins from single cells.

Traditional quantitative assays measuring relative or absolute protein amounts such as western blots or immunoblots typically start with the separation of large amount of cells (Renart, Reiser, and Stark 1979; Verbeek et al. 1996). The detection limits are often picomole at the best, making them limited for single cell analysis. The conventional method for single cell protein analysis is fluorescence-based approaches due to the high sensitivity. For example, FACS (fluorescence-activated cell sorting) uses fluorescently labeled antibodies to label the target proteins from single cells. Currently there are a maximum of 18 proteins from single cells that can be measured and quantified simultaneously by multi-color flow cytometry (Freer and Rindi 2013). Despite of these recent developments, fluorescence-based approaches reply on molecular probes that need to be preselected. And the species that can be detected by the fluorescence analysis are also limited due to the limited range of fluorescent dyes.

We reported a novel microfluidic device for absolute quantification of proteins by using two iTRAQ tags previously (discussed in chapter 4). This method could potentially be used for single cell protein analysis. However, there are some drawbacks for this approach. MS/MS spectra must be obtained for distinguishing iTRAQ tags, requiring more analysis time and additional instrumentation. Besides, technical issues of applying this iTRAQ technology to our approach still exist. In the iTRAQ quantification experiment, mixing the MALDI matrix with the iTRAQ internal standard beforehand would not lead to co-crystallization. Consequently, the MALDI matrix solution filled after the sample was dried in both fluidic channels. The renewed filling of MALDI matrix would lead to dissolution of peptides and sample washing out. In this chapter, we improve our quantification approach by applying an isotope labeled peptide as the internal standard. Adding the isotope labeled peptide with the MALDI matrix can avoid the problem of peptides dissolution and transport. Thus five completely independent experiments can be performed in parallel in our device. Without the need of MS/MS analysis, quantification by using isotope labeled peptide can simplify the quantification process and holds the potential to quantify Bcl-2 from single cells.

5.2 Materials and Methods

5.2.1 Materials

PDMS was purchased from Dow Corning Corporation (USA). Acetonitrile, alpha-cyano-4-hydroxycinnamic acid (α-CHCA), Bcl-2 active human was from Sigma-Aldrich (USA). Peptide calibration mixture (angiotensin II 1046.5418 m/Z $[M+H]^+$, angiotensin I 1296.6848 m/Z $[M+H]^+$, substance P [1347.7354 m/Z $[M+H]^+$, bombesin

1619.8223 m/Z $[M+H]^+$, ACTH clip 1-17 2093.0862 m/Z $[M+H]^+$, ACTH clip 18-39 2465.1983 m/Z $[M+H]^+$, somtostatin-28 3147.4710 m/Z $[M+H]^+$) were purchased from Bruker Daltonics Inc (USA). Trypsin was obtained from Promega Corporation (USA). ITO slides (100 ohm/sq) were obtained from NANOCS and Cr was obtained from SPI Supplies (USA). Tridecafluoro-1, 1, 2, 2-tetra-trichlorosilane (TTTS) was purchased from Gelest (USA). Isopropanol and acetone were from VWR (USA). SU-8 2075 photoresist and SU-8 developer were from MicroChem (USA). Isotope labeled peptide (FATVVEELeu(d10)FR) was from GenScript USA Inc.

5.2.2 Digestion Efficiency Test of Bcl-2 in Solution

5 μL of 1.4×10^{-5} M was diluted with 45 μL of 50 mM NH_4HCO_3 and then was mixed with 10 μL of 0.1 μg/μL trypsin (dissolved in 50 mM NH_4HCO_3). The mixture was divided into five parts which were incubated separately for 4 h, 6 h, 12 h, 24 h, 36 h at 37 ℃. Subsequently, 1.5 μL of 1.1×10^{-5} M internal standard peptide was added to each sample and the vials were vortexed. 5 μL matrix solution (saturated α-cyano-4-hydroxycinnamic acid (CHCA) in 40% v/v acetonitrile, 0.1% v/v TFA in water solution) was added. The samples were pipetted and spotted on an ITO slide followed by MALDI-TOF-MS analysis.

5.2.3 Absolute Protein Quantification by Using an Isotope Labeled Peptide

The Bcl-2 quantification experiment by using isotope labeled peptide as an internal standard was carried out in the ladder-like device (Figure 4-1a). First, Bcl-2 immunoassay and digestion steps were repeated in fluidic channel I as described in

Section 4.2.3. In this step, valve A was open while B and C were closed for all chip loading steps. Valve A, B and C were closed for all of the incubation steps. Next, 5 μL of 100nM isotope labeled peptide with a sequence of FATVVEELeud10FR was mixed with 5 μL matrix solution. This mixture filled the fluidic channel II by applying negative pressure when valve A and B were closed and valve C was open. Afterwards, valve A and C were closed while valve B was open and closed repeatedly for 2 min in order to mix the sample and the internal standard solution. The chip was placed in air overnight at room temperature until channels were completely dried. After the solution in the channel was completely crystallized, the two-layer PDMS manifold was peeled off and MALDI-TOF-MS was performed on the ITO slide with crystals.

5.3 Results and Discussion

In our approach, the peptide with sequence of FATVVEELFR and m/Z $[M+H]^+$ 1210.6 is chosen as the sample peptide in the Bcl-2 digest since this peptide usually has the highest S/N in Bcl-2 digest MS spectrum An isotope labeled peptide with the same sequence as the sample peptide but containing stable isotopes is used as an internal standard (reference peptide). In comparison to the sample peptide which originates from Bcl-2 digest, the reference peptide with sequence of FATVVEELeu(d10)FR has a 10 Da shift m/Z $[M+H^+]$ 1220.6 due to deuterium labeling. Therefore, the MS analysis allows the detection of both the sample peptide from the Bcl-2 digest and the isotope labeled peptide. By comparison of the peak area intensities between the reference peptide and the sample peptide, the number of the sample peptide from the Bcl-2 digest is determined.

5.3.1 Solution Digestion Efficiency

Our ultimate goal is to apply this quantification method in single cell protein analysis which requires high sensitivity detection. To find out the optimum incubation time in the digestion protocol, the efficiency of in solution digestion was tested. Bcl-2 with known amount (1.4×10^{-11} mol) was digested by trypsin in a vial for various incubation times (4h, 6h, 12h, 24h, 36h). 1.7×10^{-11} mol of reference peptide was added in the digest for quantification purpose. One example spectrum is shown in Figure 5-1. The average peak area ratio of peak $[M+H]^+$ m/Z 1220.6 and peak $[M+H]^+$ m/Z 1210.6 was 1.6 ± 0.12 obtained from three repeated trials. With the amount of 1.7×10^{-11} mol reference peptide, the number of the sample peptide was calculated as $(1.1\pm0.08)\times10^{-11}$ mol. Since the starting Bcl-2 amount was 1.4×10^{-11} mol, we calculated that the digestion efficiency was 78.6% in this case. By using the same approach, the digestion efficiencies for 4 h, 6 h, 12 h, 24 h, 36 h were calculated accordingly. As shown in Figure 5-2, the digestion efficiency reached the maximum at 12 h incubation. Thus, for all digestion experiments, 12h incubation was used and 78.6% digestion efficiency was used for correlation of the sample peptide and the corresponding Bcl-2 amount.

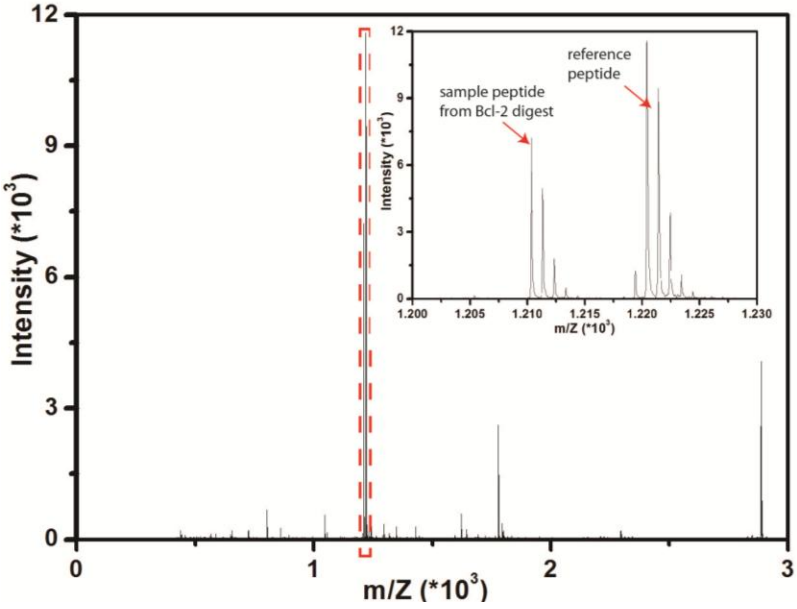

Figure 5-1: Representative MS spectrum of Bcl-2 in solution digestion with 12h incubation. (insert: zoom in picture of the red rectangular region showing the sample peptide and reference peptide peaks used for quantification).

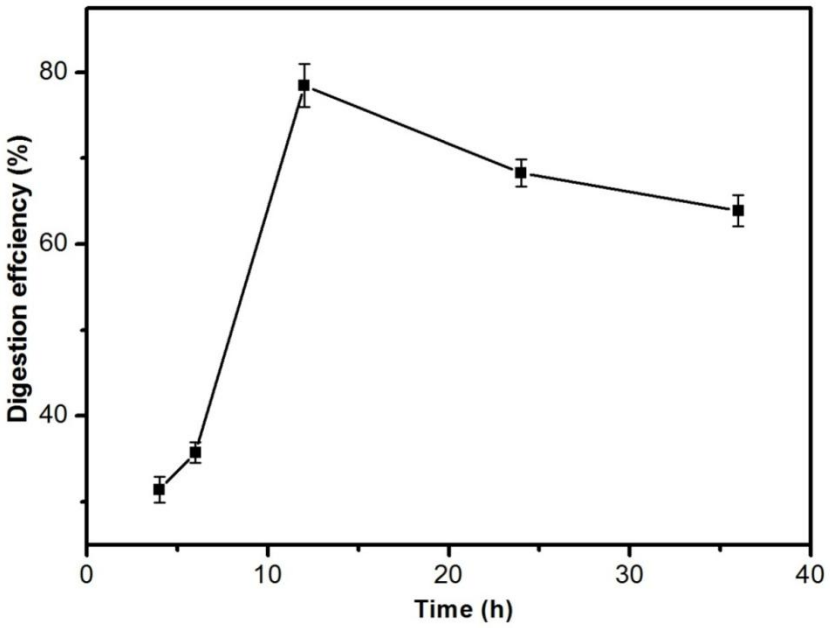

Figure 5-2: Digestion efficiencies for various incubation times ranging from 4h to 36h.

5.3.2 Bcl-2 Quantification On-chip by Using an Isotope Labeled Peptide

In our previous study with iTRAQ tags for quantification (Section 4.3.4), one problem we encountered was that the MALDI matrix could not be added together with the iTRAQ internal standard from the opposite channel as the sample and MALDI matrix would not cocrystallize. Thus, we filled the MALDI matrix from both channel I and channel II after the whole chip was completely dried. This procedure might lead to dissolution of peptides during the filling process and a peptide concentration gradient along the wells. To further verify the quantification results and avoid the problem of not being able to cocrystalize, a quantification experiment was performed in the ladder-like device (Figure 4-1a) by applying an isotope labeled peptide as the internal standard.

Similarly, Bcl-2 affinity capture and digestion were performed in fluidic channel I. In comparison to the iTRAQ quantification experiment, the major difference was that the MALDI matrix was mixed with internal standard beforehand. This mixture loaded in fluidic channel II by applying negative pressure and was then mixed with contents in channel I by actuating valve B. In this way, the internal standard loading step and MALDI matrix loading step were combined without the need of filling the matrix separately to the channel where samples were dried. Therefore compared with the iTRAQ quantification experiment, the problem of peptides dissolution and transport along the five detected regions can be avoided. Last, after co-crystallization, the PDMS manifold was removed and subsequent MS analysis was performed. The peaks of sample peptide and reference peptide were distinguished in MS spectrum and the peak area ratio of two peptides indicated their concentration ratio.

One example MS spectrum from these five regions is shown in Figure 5-3. Both the sample peptide (m/Z $[M+H]^+$ 1210.6) and the isotope labeled peptide (m/Z $[M+H]^+$ 1220.6) are shown in the spectrum (red arrows), allowing the quantitative analysis of Bcl-2 captured on chip. Five regions shown in Figure 4-1b (I-V) from four chips were analyzed with an average peak area ratio of 17.7 ± 1.19 corresponding to the ratio of 1210.6 m/Z $[M+H]^+$ to 1220.6m/Z $[M+H]^+$. As the isotope labeled peptide concentration was 100 nM and the volume of a well was ~15 nL, we calculated that around 8.5×10^{-17} mol of Bcl-2 sample peptide was in each well. Thus, the number of Bcl-2 captured in each well was ~7.0×10^{7} mol corrected with the 78.6% digestion efficiency.

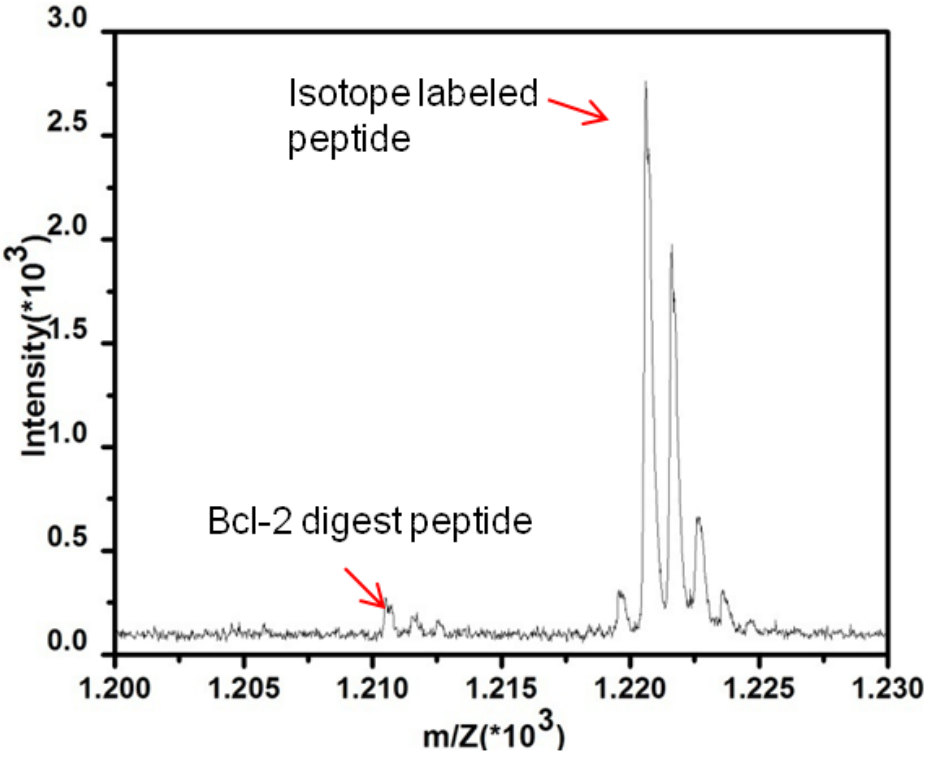

Figure 5-3: Representative MS spectrum of sample peptide from Bcl-2 digest and the internal standard peptide.

Based on quantification by using iTRAQ tags discussed in chapter 4, 4.4×10^{8} Bcl-2 molecules are detected in each well. By using an isotope labeled peptide, we conclude that 7.0×10^{7} is detected in each well which is around six times lower than the detected Bcl-2 number obtained from iTRAQ quantification approach.

Errors might exist in both quantification approaches. For iTRAQ quantification experiment, possible errors are related to the labeling efficiency and digestion efficiency. The prerequisite of using iTRAQ labeled peptide as the internal standard is that the ways of labeling sample and internal standard should be kept the same. In spite of applying the same simultaneous digestion and labeling protocol for both sample and internal standard, the labeling and digestion efficiencies on chip (for the sample) and in solution (for the reference peptide) might be different.

For quantification by an isotope labeled peptide, a possible error related to the determination of digestion efficiency might also exist. Digestion efficiency is calculated for solution digestion whereas the Bcl-2 is captured and digested on the surface in the quantification experiment. In the calculation of the absolute number of Bcl-2 molecules, the solution digestion efficiency is used to correlate the sample peptide with the corresponding Bcl-2. It has been shown that the enzymatic cleavage of an antigen-antibody complex is reduced, especially at the region where the protein contacts with the antibody (Doucette, Craft, and Li 2003). Considering a smaller digestion efficiency for proteins bound to the antibodies on chip, the corresponding Bcl-2 amount calculated will be larger than 7.0×10^{7} molecules per well.

Besides, the variation of Bcl-2 peptide intensities along five detection regions was examined for both approaches by looking at the relative standard deviation of signals in

different detection regions. For quantification by isotope labeled peptide, the relative standard deviation (RSD) of five detection regions was found to be 7% while 20% RSD is determined in iTRAQ experiments. As discussed in Section 4.3.4, the MALDI matrix must be loaded separately with internal standard in the iTRAQ approach since mixing the MALDI matrix with the internal standard beforehand could not lead to sample co-crystallization. The renewed MALDI matrix loading step could possibly result in the dissolution of peptides and transport of the samples along the channel. Thus, the iTRAQ tag quantification expectedly has a higher variation of peptide intensities along the five detection regions.

5.4 Section Conclusions

In this chapter, we investigated the optimum condition for Bcl-2 tryptic digestion and found that 12h incubation could result in best digestion efficiency. 76.8% digestion efficiency for 12h digestion incubation was determined by using an isotope labeled peptide as the internal standard. The quantitative analysis of proteins was improved by applying an isotope labeled peptide for on-chip Bcl-2 quantification. The internal standard (isotope labeled peptide) could be introduced with MALDI matrix at one time from fluidic channel II, which would not lead to dissolution of peptides during the matrix filling process and thus keep the five detection regions separate. This can further enable a smaller variation of peptide intensities in five detection regions compared to the iTRAQ quantification experiment. Our study based on an isotope labeled peptide indicated that 7.0×10^7 Bcl-2 molecules were detected in each well. In order to assess a protein copy number of one million molecules from a single cell, the current device is required to be

further downscaled. Our future work is to couple this protein analysis method with cell loading and cell lysis on chip. We anticipate that this approach can be applied to quantify cancer biomarkers from single cells in the future.

CHAPTER 6

DETECTION AND QUANTIFICATION OF BCL-2 IN CANCER CELLS

6.1 Introduction

Single cancer cell detection provides a new powerful tool in understanding cancer evolution and the role of rare cells in the cancer development which is difficult to address with bulk tumor measurements. This new tool is especially useful in cancer early detection and monitoring. Cancer cells undergo dramatic changes compared with normal cells including and protein expression level (Weinberg 2013). The protein express level change can serve as an indicator of the cancerous cells. These indicators are termed biomarkers (Jain 2010). Biomarker discovery is a hot topic in the biomedical research area. Significant differences in single cells were found for the concentration of various proteins (Wu and Singh 2012; Ullal et al. 2014). This strong protein expression diversity within a cell population is associated with the diagnosis of various diseases such as cancer (Shapiro et al. 1995; Verbeek et al. 1996). Therefore, understanding the protein expression level in single cells is of high clinical and biological interest.

Spectroscopy approaches can give a snapshot of the cell content but is often incapable of detecting specific proteins. Analysis of cellular contents at the single-cell level using MALDI MS has been reported (Rubakhin and Sweedler 2008) . However, it lacks an efficient way for multiplexed analysis, resulting in low throughput. Thus, high throughput analysis with MALDI MS detection is needed. Cell isolation and the subsequent cell lysis based on microfluidics have been well established for single cell analysis such as the droplet microfluidics (Mazutis et al. 2013), mechanical microtraps (Stratz et al. 2014) and microwells (Xie et al. 2015). In addition, microfluidics can

provide high throughput analysis and an efficient way to integrate multiple sample manipulations steps, which is convenient for subsequent detection.

We achieved multiplexed and label free single cell protein analysis by using the ladder-like microfluidic device developed before (discussed in Chapter 4 and 5). Our previous work showed that protein identification and quantification could be realized in this device with MALDI-TOF MS detection. In this chapter, this work is extended to analyze proteins in single cancer cells. Several functions including single cell loading and lysis, sample pretreatment prior to MALDI MS can be integrated in this device. Bcl-2 is a key protein involved in cell apoptosis (Czabotar et al. 2014) and it has been reported that Bcl-2 is over expressed in various types of malignant cells compared to normal cells (Kandouz et al. 1996). It has an important biological and clinical relevance. Thus Bcl-2 is chosen as our target protein for proof of principle. We believe that our approach can be applied to analyze other proteins in single cells and thus provides a powerful way for single-cell proteomics.

6.2 Materials and Methods

6.2.1 Materials

PDMS was purchased from Dow Corning Corporation (USA). Acetonitrile, alpha-cyano-4-hydroxycinnamic acid (α-CHCA), Bcl-2 active human, Anti-Bcl-2 antibody and bovine serum albumin (BSA), bovine insulin were from Sigma-Aldrich (USA). Dulbecco's phosphate-buffered saline (DPBS) buffer and the Hausser scientific hemocytometer were purchased from Thermo Fisher Scientific (USA). Peptide calibration mixture (angiotensin II 1046.5418 m/Z $[M+H]^+$, angiotensin I 1296.6848 m/Z

$[M+H]^+$, substance P [1347.7354 m/Z $[M+H]^+$, bombesin 1619.8223 m/Z $[M+H]^+$, ACTH clip 1-17 2093.0862 m/Z $[M+H]^+$, ACTH clip 18-39 2465.1983 m/Z $[M+H]^+$, somtostatin-28 3147.4710 m/Z $[M+H]^+$) was purchased from Bruker Daltonics Inc (USA). ITO slides (100 ohm/sq) were obtained from NANOCS and Cr was obtained from SPI Supplies (USA). Tridecafluoro-1, 1, 2, 2-tetra-trichlorosilane (TTTS) was purchased from Gelest (USA). Isopropanol and acetone were from VWR (USA). SU-8 2075 photoresist and SU-8 developer were from MicroChem (USA). Isotope labeled peptide (FATVVEELeu(d10)FR) was from GenScript USA Inc. MCF-7 cells, Eagle's Minimum Essential Medium (EMEM), fetal bovine serum were obtained from ATCC (USA).

6.2.2 Cell Lysis

MCF-7 cells were cultured in a solution of Eagle's Minimum Essential Medium (EMEM) (ATCC, USA) with L-glutamine, 10% fetal bovine and 0.01 mg/mL of bovine insulin at 37 ℃ for five days. The flask with cells was placed in the sterilized fume hood. The EMEM medium was removed by vacuum from the flask which was then washed by 7mL Dulbecco's phosphate-buffered saline (DPBS) buffer (Thermal Fisher Scientific, USA). Then the DPBS buffer (thermal fisher scientific, USA) was sucked out and 2mL of cell stripper solution was added for stripping the cells from the surface of the petri dish. The flask was placed in 37 ℃ incubator for 10 min. Then 3 mL MCF-7 medium was added to the flask. The solution in the flask was transferred to a tube and centrifuged. The cell pellet was used for the following experiments.

The cell pellet was frozen in a -20 ℃ freezer for 5 min and then thawed at 37 ℃ for 5 min. This freezing and thawing cycle was repeated for 3 times to lyse the cells. Next, the glass hemocytometer and the coverslip were cleaned with alcohol before use. The coverslip was moistened with water and affixed to the hemocytometer. Last, 100 μL cell suspension was gently vortexed and applied to the hemocytometer. Live cells from five selected rectangular areas were counted before lysis and after lysis under the microscope (IX71, Olympus, US).

6.2.3 Detection of Spiked Bcl-2 in MCF-7 Cell Lysate

Bcl-2 was spiked and detected in MCF-7 cells with concentrations over five orders of magnitude from 5 cells/μL to 5×10^4 cells/μL to understand the influence of the sample complexity on Bcl-2 detection. MCF-7 cells were stripped from a Petri-dish and resuspended in 50 mM NH_4HCO_3 (digestion buffer). Cells were lysed by three freezing and thawing cycles and a dilution series was made ranging from 5 cells/μL to 5×10^4 cells/μL to 5 cells/μL. For 140nM Bcl-2 sample, 1 μL of 1.4×10^{-6} M Bcl-2 was added while for 14nM Bcl-2 sample, 1 μL of 1.4×10^{-7} M Bcl-2 was added to 8 μL cell lysate with various concentrations. 1 μL of 0.2 μg/μL trypsin were added in all sample solutions subsequently. All samples were probed by MALDI-TOF after 12 h incubation at 37 ℃.

6.2.4 Coupling Cell Loading, Lysis with Protein Affinity Capture, Identification and Quantification on Chip

This experiment was also performed in the device shown in Figure 6-1a. Likewise, in all procedures, valve A was open while valve B and C were closed for all chip loading

steps. Valve A, B and C were closed for all incubation steps unless otherwise stated. First, channel I was filled with anti-Bcl-2 IgG solution (0.05mg/mL) through capillary flow. After 2 h incubation, IgG solution was removed and the microchannel was washed three times with DPBS buffer. 1% BSA solution filled the channel I followed by 1 h incubation. BSA solution was removed by vacuum and the channel was washed again by DPBS buffer. Next, cell solution with Bcl-2 spiked in (3000 cells/μL in DPBS buffer) was loaded in fluidic channel I. Here, spiked Bcl-2 concentration was 10^{-8}M. The whole chip was repeatedly placed in the -20 ℃ freezer for 3 min and 37 ℃ oven for 3 min three times to lyse the cells. Subsequently, the chip was incubated for 1h at the room temperature and the solution was removed by vacuum. 0.1 μg/μL trypsin dissolved in 50 mM NH_4HCO_3 filled channel I and the chip was incubated at 37 ℃ for 12 h. A mixture composed of MALDI matrix and the isotope labeled peptide (10^{-8}M) was loaded in fluidic channel II. Solutions from fluidic channel I and channel II were mixed when valve A and C were closed while B was repeatedly opened and closed. Last, after channel I and channel II were completely dried to induce cocrystallization, the PDMS slab was removed. The sample on the ITO substrate was probed by MALDI MS. This experiment was repeated with three chips.

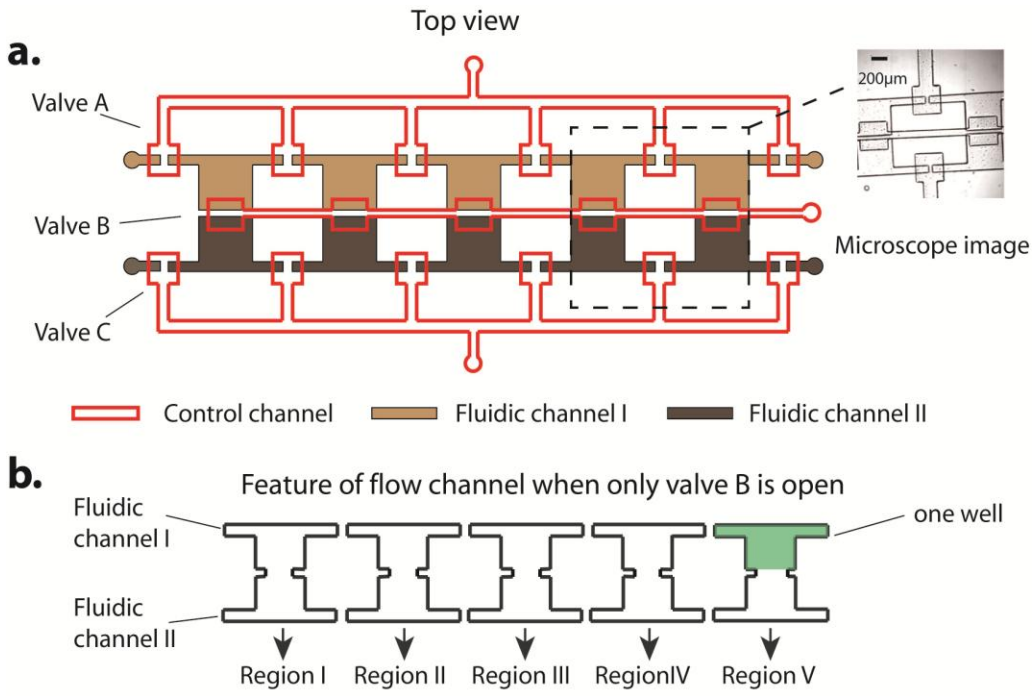

Figure 6-1: Structure of ladder-like device. a) Top view of the ladder-like device (Red line: control channels; Brown and Yellow filling: fluidic channels). b) Feature of the flow channel when valve B was open and valve A, C were closed. Five regions (I-V) were available for MALD-TOF MS detection after PDMS slab was peeled off.

6.3 Results and Discussion

6.3.1 MCF-7 Cell Lysis

Since we aim in detecting the proteins produced in single cells, a proper cell lysis approach is needed to release the proteins from the cells before the subsequent protein measurements. The lysis of single cells for downstream lab-on-a-chip devices can be achieved by a variety of means such as optical (Rau et al. 2004; Rau et al. 2006), acoustic (Zhang and Jin 2004), mechanical (Di Carlo, Jeong, and Lee 2003), electrical (Lu et al. 2006) or chemical lysis (Berezovski, Mak, and Krylov 2007; Ocvirk et al. 2004). Each has their strength and weakness. Selection of the appropriate lysis method is highly dependent on the particulars of the downstream analysis of cell lysate. In our approach,

after the cell lysis, proteins are expected to be captured by antibodies and subsequently digested by trypsin before MALDI MS detection. Chemical lysis is often performed with highly concentrated detergents which will interfere the downstream MALDI MS analysis. Electrical cell lysis has always been used widely in lab-on-a chip devices or in capillaries (Han et al. 2003; Nashimoto et al. 2007; Lu et al. 2006; Gabriel and Teissie 1999). However, in our case, potentials applied to a microchannel with buffer over ITO slides destroyed the ITO coating on the surface (data not shown). That might be due to electrochemical reactions occurring on the conductive ITO surface. In addition, the proteins from the cell lysate retain their ability to are preferred to be native which can actively bind with antibodies immobilized on the surface. Freezing and thawing has been reported to not denature the proteins as much as other methods (detergent-based, acoustic, mechanical lysis) (Qi, Sun, and Xiong 2015). Besides, it does not need complex and expensive instrumentation. Therefore, rapid freezing and thawing cycles were used as the cell lysis method in our work.

Our goal is to analyze proteins at the single cell level after they are released from single cells due to cell lysis. In order to release target proteins completely from single cells, the lysing method with high efficiency was required. The performance of cell lysis by freezing and thawing cycles was firstly tested in solution by a glass hemocytomer. 100 μL cell suspension filled chambers underneath the coverslip, allowing the cell suspension to spread out by capillary force. Under the bright field microscope (IX71, Olympus, USA), five areas in the grid were selected and live cells were counted. With on average of 108 live cells before lysis and 5 cells still alive after freezing and thawing cycles, a lysing efficiency of 95% was determined.

Next, the cell lysis was performed in microfluidic channels. Cell suspension loaded in straight channels by capillary action. After three freezing and thawing cycles, images of cells were taken by a bright field microscope. The example images of cells before lysis (Figure 6-2a) and after lysis (Figure 6-2b) are shown below.

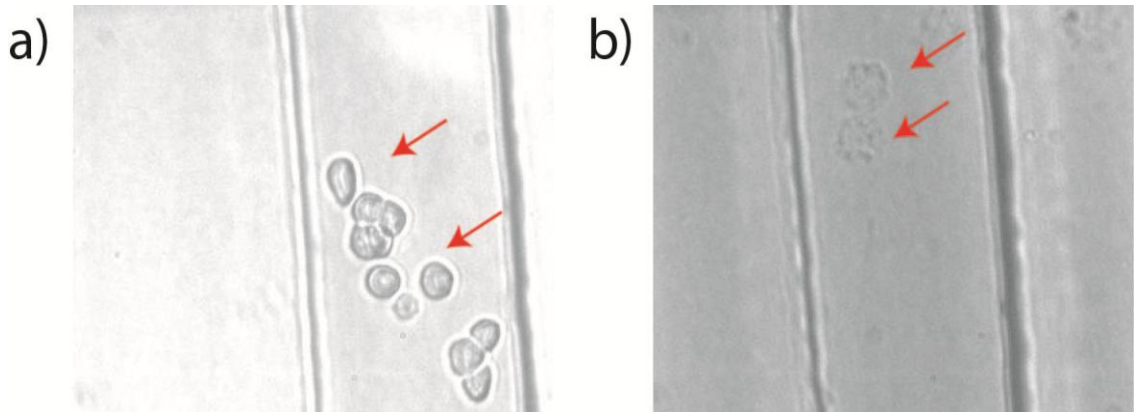

Figure 6-2: Bright field microscope images of cells resulting from in chip lysis experiments (channel width: 100 μm). a) Cells before lysis. b) Cells after lysis.

6.3.2 Influence of Sample Complexity on Detection of Bcl-2 in Cell Lysate

Bcl-2 is a key protein involved in control of cell apoptosis (Czabotar et al. 2014) and of great relevance in biological and clinical studies. Therefore, Bcl-2 was chosen as our target protein. Previous studies indicated that Bcl-2 expression was over expressed in breast cancer cell line MCF-7 (Kandouz et al. 1996). However, in our case, MALDI MS detection of tryptic digested MCF-7 cell lysate ranging from 5 cells/μL to 5×10^4 cells/μL did not show any peptide peaks from Bcl-2 digest (data not shown).

To investigate if sample complexity in MCF-7 lysate is a factor influencing Bcl-2 detection, pure Bcl-2 with known concentration (either 140 nM or 14 nM) was spiked in MCF-7 cells with various cell concentrations over five orders of magnitude from 5 cells/μL to 5×10^4 cells/μL. Results are shown in Figure 6-3 (with 140 nM spiked Bcl-2)

and Figure 6-4 (with 14nM spiked Bcl-2). Our previous study showed that the lowest concentration of pure Bcl-2 that could be probed was in the nM range (Appendix Figure A 2). However, none of Bcl-2 peptides can be probed in 5×10^4 cells/μL cell lysate for 140 nM Bcl-2 and none of Bcl-2 peptides can be probed in 5×10^3 cells/μL cell lysate for 14 nM Bcl-2. In both cases, signal to noise decreases when concentration of cells increases for most of Bcl-2 digest peptides, which further demonstrate that contents in the MCF-7 cell lysate reduce the intensity of Bcl-2 peptides. This might be the reason why Bcl-2 produced in MCF-7 cells is not detectable. It is interesting to note that not all peptides responded in the same way such as peptide m/Z 2295.1 which exhibites higher S/N at a cell concentration of 500 cells/μL than 5 cells/μL. A similar phenomenon was also reported in a previous study on peptide detection in complex samples (Albalat et al. 2013).

In addition, it is clearly seen that peptide m/Z 1210.6 always has the highest S/N for detection of 140 nM and 14 nM Bcl-2 in all of the cell concentrations. Thus in all Bcl-2 quantification experiments with using an isotope labeled peptide, this peptide (m/Z 1210.6) was chosen as the sample peptide from Bcl-2 digest.

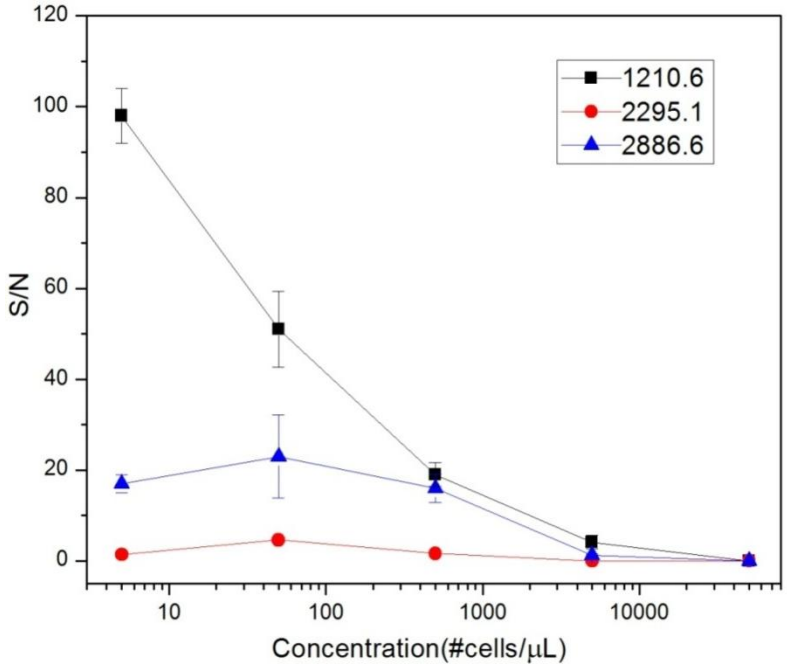

Figure 6-3: Signal to noise of Bcl-2 peptides in MCF-7 cell lysate with Bcl-2 (140nM) spiked. Three peptides are detected from Bcl-2 digest (Black square: peptide m/Z 1210.6; Blue triangle: peptide m/Z 2886.6; Red dot: peptide m/Z 2295.1).

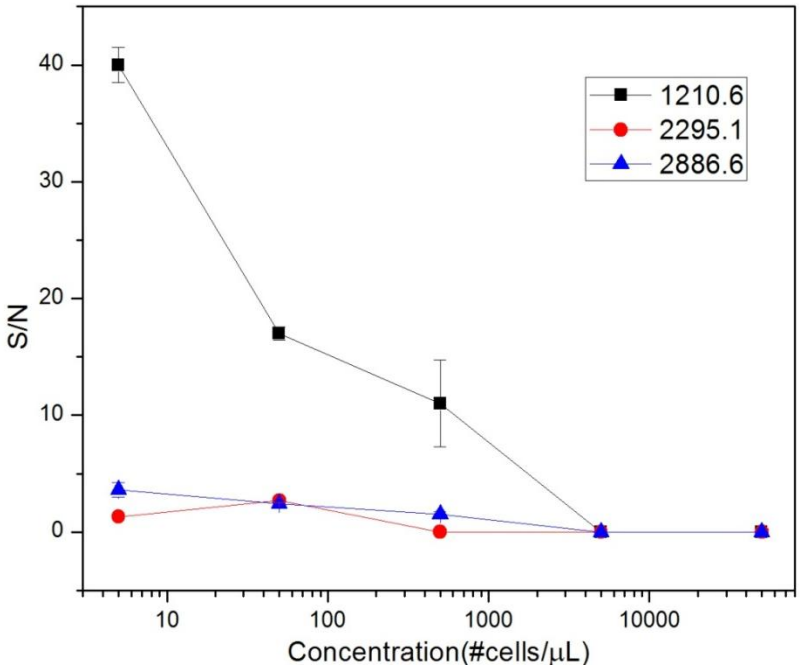

Figure 6-4: Signal to noise of Bcl-2 peptides in MCF-7 cell lysate with Bcl-2 (14nM) spiked. Three peptides are detected from bcl-2 digest (Black square: peptide m/Z 1210.6; Blue triangle: peptide m/Z 2886.6; Red dot: peptide m/Z 2295.1).

6.3.3 Bcl-2 Identification and Quantification in Single MCF-7 Cells

Previously, we designed a novel microfluidic device (ladder-like device) with valves for pure Bcl-2 affinity capture, identification by peptides from enzymatic digestion and quantification by isotopically labeled peptide. As mentioned above, the detection of tryptic digested MCF-7 cell lysate did not show any peptide peaks from Bcl-2 digest. For proof of principle, pure Bcl-2 with a detectable concentration (10^{-7} M) was spiked in MCF-7 cell lysate (3000 cells/μL). We used this ladder-like device (shown as Figure 6-1a) and extended our approach to analyze the spiked Bcl-2 in MCF-7 cell lysate. In our approach, cell loading and lysis, Bcl-2 affinity capture as well as enzymatic digestion were performed in fluidic channel I (details described in Section 6.2.3). A mixture composed of MALDI matrix solution and the reference peptide (an isotope labeled peptide) with known concentration filled fluidic channel II of the ladder-like device. Thorough mixing of contents in fluidic channel I and II was performed by actuating valve B. The Bcl-2 was quantified based on the peak area ratio of sample peptide (m/Z 1210.6) and the reference peptide (m/Z 1220.6).

Since the antibodies were immobilized on the surface when cells were lysed by freezing and thawing cycles, the antibodies might be denatured. A control experiment was performed in a reservoir to test the binding ability of antibodies after freezing and thawing cycles. Similar to the previous affinity capture experiment (described in Section 4.3.2), Anti-Bcl-2 antibody was immobilized in the reservoir and BSA was applied for blocking the unspecific binding positions. After removal of BSA from the channel, the reservoir was filled with pure Bcl-2. Next, the chip was placed in -20 ℃ for 3min and then 37 ℃ for 3min. This freezing and thawing cycle was repeated for 3 times.

Afterwards, the chip was incubated for 1h at room temperature, allowing the binding of anti-Bcl-2 and Bcl-2. MALDI matrix was applied to the reservoir before subsequent MALDI-TOF analysis. The resulting MS spectrum is shown in Figure 6-5. There are four peaks found from Bcl-2, indicating that antibodies can still bind with Bcl-2 after freezing and thawing. However, in comparison to the spectrum (Figure 4-3a) obtained in the affinity capture experiment but without additional freezing and thawing step, the peaks of two digest peptides disappear. This might indicate that the reactivity of anti-Bcl-2 antibodies is reduced due to freezing and thawing cycles and thus less Bcl-2 is captured in this case.

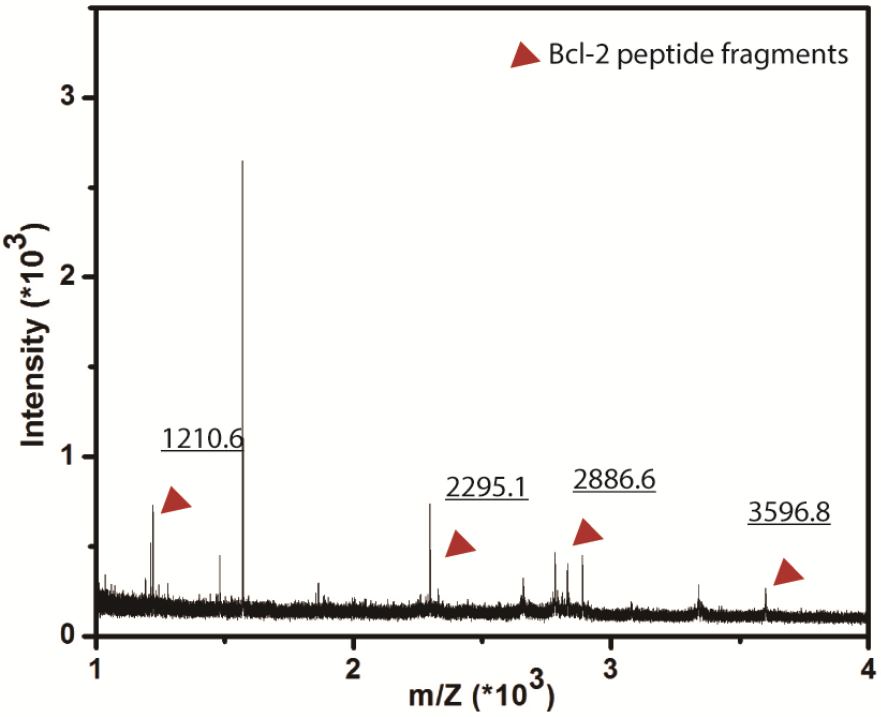

Figure 6-5: MALDI-TOF-MS analysis of an anti-Bcl-2 immunoassay with treating antibody by freezing and thawing cycles. Four peptides (red triangle) are found from Bcl-2 digest.

Next, we applied an isotope labeled peptide in our approach to quantify the spiked Bcl-2 in MCF-7 cell lysate. The ladder-like device was used in this experiment. 10^{-8} M isotope labeled peptide dissolved in MALDI matrix solution was loaded in fluidic channel II by vacuum pressure. Components from fluidic channel I and II were mixed by repeatedly opening and closing valve B. After the chip was completely dried, the PDMS slab was peeled off and the sample on the ITO slide was detected by MALDI-TOF MS. This procedure allows the mixing of spiked Bcl-2 digest and 10^{-8} M internal standard (isotope labeled peptide). The spiked Bcl-2 was quantified by the peak area ratio of sample peptide from Bcl-2 and the isotope labeled peptide.

Five detection regions (I-V) (shown in Figure 6-1b) in ladder-like devices are completely separated, enabling five independent experiments. Moreover, these five regions (I-V) from three chips were analyzed by MALDI MS. An example spectrum (Figure 6-6) shows both the sample peptide (m/Z [M+H] 1210.6) from Bcl-2 and the internal standard (m/Z $[M+H]^+$ 1220.6). The average peak area ratio of the internal standard and the sample peptide was 4.6 ($\pm$0.84). With the reference peptide concentration of 10^{-8} M and one well volume of 15 nL, we calculated that the number of spiked Bcl-2 was 9×10^7 molecules. However, according to the peak area ratio of 4.6 ($\pm$0.84), the number of spiked Bcl-2 detected in each well was 2.5 ($\pm$0.55)$\times10^7$ molecules, indicating that not all spiked Bcl-2 was captured on the anti-Bcl-2 antibody immobilized surface.

This might be attributed to several factors. First, the reactivity of anti-Bcl-2 antibodies is reduced due to freezing and thawing cycles and less Bcl-2 is captured in this

case (Figure 6-5). Second, cell lysate masks the Bcl-2 and anti-Bcl-2 binding sites, resulting in less Bcl-2 captured. More control experiments are needed to confirm these factors and improve the current approach to detect the proteins produced in a single cell. Nevertheless, our approach is still promising for single cell analysis since all cell handling steps including loading and lysis and the downstream protein analysis steps for identification and quantification are successfully coupled in one device.

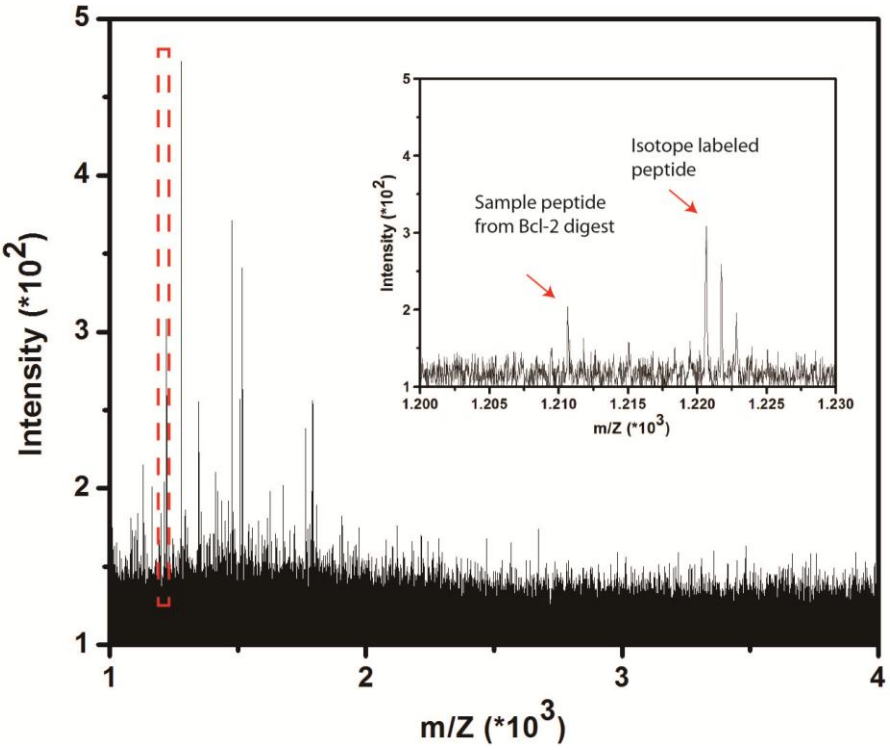

Figure 6-6: Representative MS spectrum of spiked Bcl-2 detection in MCF-7 cells. (insert: zoom in picture of the red rectangular region showing the sample peptide and internal standard peptide used for quantification).

6.4 Section Conclusions

In this chapter, we demonstrated cell lysis by freezing and thawing on chip, which was suitable for the downstream protein analysis. Furthermore, with the detection of spiked Bcl-2 in various concentrations of MCF-7 cells, we concluded that sample

complexity is a factor affecting the detection of Bcl-2 in a cell lysate. This might be the reason why Bcl-2 is not detectable in MCF-7 cells. Moreover, cell loading and cell lysis were successfully coupled with affinity capture, protein identification and quantification on chip. The quantification result showed that not all spiked Bcl-2 was captured by anti-Bcl-2 immobilized on the surface.

Our future work involves finding an approach to avoid the problem of Bcl-2 signal suppressing by other components in the cell lysate. That might be achieved by improving the Bcl-2 capturing performance of the immunoassays by applying an improved antibody immobilization method. Antibody immobilization with a higher surface coverage and more binding sites exposed to the antigen can improve the Bcl-2 capturing. We also expect to prevent antibody denaturation during the cell lysis by alternative methods to freezing and thawing. A possible solution might be adding an additional channel to separate the affinity capture and cell lysis step. Beyond that, further downscaling our current device is also required to analyze proteins from a single cell.

CHAPTER 7

CONCLUSION AND OUTLOOK

This work has demonstrated a novel approach for single cell protein analysis based on combining a microfluidic platform with MALDI-TOF mass spectrometry. Suitable conditions were found to remove the PDMS manifold from the MALDI-MS target (ITO slide), allowing the direct coupling of the microfluidic device with MALDI-TOF mass spectrometry. The detection sensitivity of this approach for peptides was found to be ~300 molecules and ~10^6 copies for proteins which is comparable to the amount of high abundant proteins in a single cell. In addition, an insulin assay was successfully coupled in the microfluidic device within areas of ~0.05 mm^2. Based on our estimation, the observed detection limit of insulin is close to the amount of high abundant proteins from a single cell or a small cell ensemble.

Similarly, by using the same approach, Bcl-2 was captured in the immunoassay on chip and then detected by MALDI-MS. We improved the detection limit two orders of magnitude by probing the peptides formed by the tryptic digestion of Bcl-2. Besides, in this way, Bcl-2 could be identified with the human protein database. Next, we presented an improved microfluidic device using a series of chambers and valves for absolute quantification of target proteins, here Bcl-2, realized by employing two iTRAQ tags. Suitable conditions for simultaneous tryptic digestion and iTRAQ labeling have been found to achieve iTRAQ quantification on chip. From the quantification results, we concluded that for the current immunoassay, a minimum surface area of ~800 μm^2 was required to capture a high abundant protein from a single cell.

The quantification approach was then improved by applying an isotope labeled peptide as the internal standard. The MALDI matrix solution could be loaded together with the internal standard in the microchannel. Thus, the sample was not washed out due to the renewed filling with the MALDI matrix. Compared with iTRAQ quantification, the approach employing an isotope labeled peptide was found to be more reliable due to less error sources and variations along the five detection regions.

Last, the whole approach was applied to analyze spiked Bcl-2 in MCF-7 cells. We found that the sample complexity in MCF-7 cells influenced the Bcl-2 detection. Furthermore, MCF-7 cell lysis, Bcl-2 affinity capture, Bcl-2 identification and quantification were successfully coupled in a microfluidic device to analyze the spiked Bcl-2 in MCF-7 cells. Based on the quantification by an isotope labeled peptide, we calculated that 2.5×10^7 Bcl-2 molecules in MCF-7 cell lysate were detected in each well. This quantification result showed that spiked Bcl-2 was not fully captured by anti-Bcl-2 antibodies immobilized in the channel.

Future work for improving the current approach can possibly be proceeded with the following aspects:

First, with the integrated immunoassay, we aim in capturing all protein molecules apparent in a single cell. This should ideally occur in a well with extremely small surface area to prevent dilution. Immobilizing antibodies with high active sites and high surface coverage is the key success factor for this purpose. It has been reported that antibodies immobilized on the surface often lose their binding ability since the antigen binding sites of antibodies may be partially blocked by the substrate surface (Cho et al. 2007). Antibodies immobilized with improper orientations can further decrease the binding

efficiencies. The ideal orientation is that the antibody is immobilized vertically to the surface with the paratopes (antigen binding sites) freely accessible for antigen binding to occur. This can be accomplished by using a protein linker which can be directly coupled to the surface and bind to the F_c fragment of the antibody.

For example, the streptavidin-biotin system can provide linkage between the solid surface and immunoglobulins (Lee et al. 2005). An antibody can be biotinylated randomly on lysine residues by NHS-activated biotin and then immobilized on a streptavidin-coated surface (Rowe et al. 2003). When the streptavidin-biotin interaction is used to orient the IgGs, the N-linked glycosylation sites on the F_c portion can be oxidized and selectively biotinylated by using the biotin-aminooxy compound such as N-(aminooxyacetyl)-N'-(D-biotinoyl)hydrazine (ARP). Thus, only these biotinylated sites can bind to the streptavidin-coated surface, making the F_{ab} region accessible to the antigen (Peluso et al. 2003). An alternative antibody (IgG) immobilization can be accomplished via protein A and protein G. They can specifically bind to the constant F_c region of IgGs. Thus the bound IgGs point away from the immobilization surface, leaving the antigen binding region accessible to bind to the antigen (Krenkova and Foret 2004).

Second, to enable the antibody immobilization at a higher surface coverage, three-dimensional materials and polymers can be applied which are expected to result in a higher capacity of antibody immobilization than that on two-dimensional surfaces (Perez-Almodovar and Carta 2009; Tanaka et al. 2009). Shen et al. synthesized a hyperbranched polymer (HBP) to improve the antibody immobilization (Figure 7-1). In their strategy, protein A reacted with the carboxyl groups of HBP and then the antibody could be

immobilized by linking with protein A. Since HBP was a three dimensional polymer which contained a high density of carboxyl groups, the amount of immobilized protein A was enhanced and thus the antibody binding sites per surface area were increased (Shen et al. 2011).

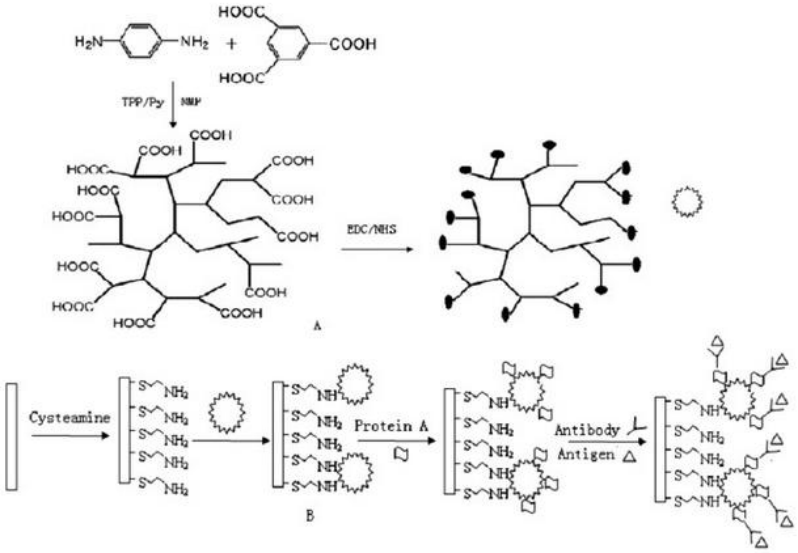

Figure 7-1: A. Synthesis of the hyperbranched polymer used for antibody immobilization. B. Procedure for the preparation of the immunosensor. Adapted with permission from Shen et al. (Shen et al. 2011).

Third, the matrix/sample cocrystallization conditions can be optimized to improve the detection limit of the target protein. One of the factors influencing the sensitivity and resolution of MALDI TOF MS analysis is the sample/matrix cocrystallization. Multiple stages in the sample preparation can be tuned: 1) The matrix/sample ratio can be optimized since the optimum matrix/sample ratios vary by analyte. 2) change the MALDI matrix solvent, for example mixing the two components (water and acetonitrile) in the right proportions. 3) use improved sample deposition approach such as spin-coated MALDI matrix, sprayed MALDI matrix in order to get better homogeneity of the

cocrystals. The above factors can be optimized in order to improve the sample/matrix cocrystallization and thus decrease the detection limit.

Fourth, we plan to modify the current device and make it suitable for single cell analysis. To prevent dilution, the size of each well needs to be further downscaled, comparable to the size of a single cell. In addition, hundreds of wells can be integrated on a microfluidic device, allowing for performing hundreds of individual experiments simultaneously. In this way, high throughput analysis of single cells can be achieved.

This novel combined microfluidic and MALDI-TOF mass spectrometric approach will eventually be employed for analysis of proteins in single cells. A possible proof-of principle could be performed with the analysis of tumor-associated QSOX1 protein on the single cell level. QSOX1 has been demonstrated to be over-expressed in pancreas and prostate tumor cells and thus represents an excellent target for our study. In addition, investigation of protein post-translational modifications is also of interest. For example, to study the phosphorylation of a protein, the antibody for the phosphorylated protein can be applied for capturing and the above discussed workflow applied to quantify phosphorylation on the single cell level. In summary, I predict that our approach will provide a novel diagnostic tool for analysis of limited sample amount and open a new era of single cell protein analysis.

REFERENCES

Albalat, Amaya, Angelique Stalmach, Vasiliki Bitsika, Justyna Siwy, Joost P. Schanstra, Alexandros D. Petropoulos, Antonia Vlahou, Joachim Jankowski, Frederik Persson, Peter Rossing, Thorsten W. Jaskolla, Harald Mischak, and Holger Husi. 2013. 'Improving peptide relative quantification in MALDI-TOF MS for biomarker assessment', *Proteomics*, 13: 2967-75.

Altschuler, Steven J., and Lani F. Wu. 2010. 'Cellular Heterogeneity: Do Differences Make a Difference?', *Cell*, 141: 559-63.

Amantonico, Andrea, Joo Yeon Oh, Jens Sobek, Matthias Heinemann, and Renato Zenobi. 2008. 'Mass spectrometric method for analyzing metabolites in yeast with single cell sensitivity', *Angewandte Chemie-International Edition*, 47: 5382-85.

Arcibal, Imee G., Michael F. Santillo, and Andrew G. Ewing. 2007. 'Recent advances in capillary electrophoretic analysis of individual cells', *Analytical and Bioanalytical Chemistry*, 387: 51-57.

Armstrong, D. W., L. K. Zhang, L. F. He, and M. L. Gross. 2001. 'Ionic liquids as matrixes for matrix-assisted laser desorption/ionization mass spectrometry', *Analytical Chemistry*, 73: 3679-86.

Bai, Lu, Elena V. Romanova, and Jonathan V. Sweedler. 2011. 'Distinguishing Endogenous D-Amino Acid-Containing Neuropeptides in Individual Neurons Using Tandem Mass Spectrometry', *Analytical Chemistry*, 83: 2794-800.

Bantscheff, Marcus, Markus Schirle, Gavain Sweetman, Jens Rick, and Bernhard Kuster. 2007. 'Quantitative mass spectrometry in proteomics: a critical review', *Analytical and Bioanalytical Chemistry*, 389: 1017-31.

Batchelor, Eric, Alexander Loewer, and Galit Lahav. 2009. 'The ups and downs of p53: understanding protein dynamics in single cells', *Nature Reviews Cancer*, 9: 371-77.

Beck, Martin, Alexander Schmidt, Johan Malmstroem, Manfred Claassen, Alessandro Ori, Anna Szymborska, Franz Herzog, Oliver Rinner, Jan Ellenberg, and Ruedi Aebersold. 2011. 'The quantitative proteome of a human cell line', *Molecular Systems Biology*, 7.

Berezovski, Maxim V., Tak W. Mak, and Sergey N. Krylov. 2007. 'Cell lysis inside the capillary facilitated by transverse diffusion of laminar flow profiles (TDLFP)', *Analytical and Bioanalytical Chemistry*, 387: 91-96.

Calligaris, David, Claude Villard, and Daniel Lafitte. 2011. 'Advances in top-down proteomics for disease biomarker discovery', *Journal of Proteomics*, 74: 920-34.

Cannon, D. M., N. Winograd, and A. G. Ewing. 2000. 'Quantitative chemical analysis of single cells', *Annual Review of Biophysics and Biomolecular Structure*, 29: 239-63.

Cao, P., and J. T. Stults. 1999. 'Phosphopeptide analysis by on-line immobilized metal-ion affinity chromatography-capillary electrophoresis-electrospray ionization mass spectrometry', *Journal of Chromatography A*, 853: 225-35.

Casey, Rosalyn, Deena Blumenkrantz, Kerry Millington, Damien Montamat-Sicotte, Onn Min Kon, Melissa Wickremasinghe, Samuel Bremang, Murphy Magtoto, Saranya Sridhar, David Connell, and Ajit Lalvani. 2010. 'Enumeration of Functional T-Cell Subsets by Fluorescence-Immunospot Defines Signatures of Pathogen Burden in Tuberculosis', *Plos One*, 5.

Chao, Tzu-Chiao, Nicole Hansmeier, and Rolf U. Halden. 2010. 'Towards proteome standards: The use of absolute quantitation in high-throughput biomarker discovery', *Journal of Proteomics*, 73: 1641-46.

Chao, Tzu-Chiao, and Alexandra Ros. 2008. 'Microfluidic single-cell analysis of intracellular compounds', *Journal of the Royal Society Interface*, 5: S139-S50.

Chatterjee, Debalina, A. Jimmy Ytterberg, Sang Uk Son, Joseph A. Loo, and Robin L. Garrell. 2010. 'Integration of Protein Processing Steps on a Droplet Microfluidics Platform for MALDI-MS Analysis', *Analytical Chemistry*, 82: 2095-101.

Cheng, Y. F., and N. J. Dovichi. 1988. ' Subattomole amino-acid analysis by capillary zone electrophoresis and laser-induced fluorescence', *Science*, 242: 562-64.

Cho, Il-Hoon, Eui-Hwan Paek, Haiwort Lee, Ji Yoon Kang, Tae Song Kim, and Se-Hwan Paek. 2007. 'Site-directed biotinylation of antibodies for controlled immobilization of solid surfaces', *Analytical Biochemistry*, 365: 14-23.

Choi, Jonghoon, Kerry Routenberg Love, Yuan Gong, Todd M. Gierahn, and J. Christopher Love. 2011. 'Immuno-Hybridization Chain Reaction for Enhancing Detection of Individual Cytokine-Secreting Human Peripheral Mononuclear Cells', *Analytical Chemistry*, 83: 6890-95.

Chou, Chau-Wen, Randall W. Nelson, and Peter Williams. 2009. 'Dependence of the ejection velocities of laser-ablated ions on the Laser wavelength and fluence', *European Journal of Mass Spectrometry*, 15: 305-14.

Clark, Andrew G., Michael B. Eisen, Douglas R. Smith, Casey M. Bergman, Brian Oliver, Therese A. Markow, Thomas C. Kaufman, Manolis Kellis, William Gelbart, Venky N. Iyer, Daniel A. Pollard, Timothy B. Sackton, Amanda M. Larracuente, Nadia D. Singh, Jose P. Abad, Dawn N. Abt, Boris Adryan, Montserrat Aguade, Hiroshi Akashi, Wyatt W. Anderson, Charles F. Aquadro, David H. Ardell, Roman Arguello, Carlo G. Artieri, Daniel A. Barbash, Daniel Barker, Paolo Barsanti, Phil Batterham, Serafim Batzoglou, Dave Begun, Arjun Bhutkar, Enrico Blanco, Stephanie A. Bosak, Robert K. Bradley, Adrianne D. Brand, Michael R. Brent, Angela N. Brooks, Randall H. Brown, Roger K. Butlin, Corrado Caggese, Brian R. Calvi, A. Bernardo de Carvalho, Anat Caspi, Sergio Castrezana, Susan E. Celniker, Jean L. Chang, Charles Chapple, Sourav Chatterji, Asif Chinwalla, Alberto Civetta, Sandra W. Clifton, Josep M. Comeron, James C. Costello, Jerry A. Coyne, Jennifer Daub, Robert G. David, Arthur L. Delcher, Kim Delehaunty, Chuong B. Do, Heather Ebling, Kevin Edwards, Thomas Eickbush, Jay D. Evans, Alan Filipski, Sven Findeiss, Eva Freyhult, Lucinda Fulton, Robert Fulton, Ana C. L. Garcia, Anastasia Gardiner, David A. Garfield, Barry E. Garvin, Greg Gibson, Don Gilbert, Sante Gnerre, Jennifer Godfrey, Robert Good, Valer Gotea, Brenton Gravely, Anthony J. Greenberg, Sam Griffiths-Jones, Samuel Gross, Roderic Guigo, Erik A. Gustafson, Wilfried Haerty, Matthew W. Hahn, Daniel L. Halligan, Aaron L. Halpern, Gillian M. Halter, Mira V. Han, Andreas Heger, LaDeana Hillier, Angie S. Hinrichs, Ian Holmes, Roger A. Hoskins, Melissa J. Hubisz, Dan Hultmark, Melanie A. Huntley, David B. Jaffe, Santosh Jagadeeshan, William R. Jeck, Justin Johnson, Corbin D. Jones, William C. Jordan, Gary H. Karpen, Eiko Kataoka, Peter D. Keightley, Pouya Kheradpour, Ewen F. Kirkness, Leonardo B. Koerich, Karsten Kristiansen, Dave Kudrna, Rob J. Kulathinal, Sudhir Kumar, Roberta Kwok, Eric Lander, Charles H. Langley, Richard Lapoint, Brian P. Lazzaro, So-Jeong Lee, Lisa Levesque, Ruiqiang Li, Chiao-Feng Lin, Michael F. Lin, Kerstin Lindblad-Toh, Ana Llopart, Manyuan Long, Lloyd Low, Elena Lozovsky, Jian Lu, Meizhong Luo, Carlos A. Machado, Wojciech Makalowski, Mar Marzo, Muneo Matsuda, Luciano Matzkin, Bryant McAllister, Carolyn S. McBride, Brendan McKernan, Kevin McKernan, Maria Mendez-Lago, Patrick Minx, Michael U. Mollenhauer, Kristi Montooth, Stephen M. Mount, Xu Mu, Eugene Myers, Barbara Negre, Stuart Newfeld, Rasmus Nielsen, Mohamed A. F. Noor, Patrick O'Grady, Lior Pachter, Montserrat Papaceit, Matthew J. Parisi, Michael Parisi, Leopold Parts, Jakob S. Pedersen, Graziano Pesole, Adam M.

Phillippy, Chris P. Ponting, Mihai Pop, Damiano Porcelli, Jeffrey R. Powell, Sonja Prohaska, Kim Pruitt, Marta Puig, Hadi Quesneville, Kristipati Ravi Ram, David Rand, Matthew D. Rasmussen, Laura K. Reed, Robert Reenan, Amy Reily, Karin A. Remington, Tania T. Rieger, Michael G. Ritchie, Charles Robin, Yu-Hui Rogers, Claudia Rohde, Julio Rozas, Marc J. Rubenfield, Alfredo Ruiz, Susan Russo, Steven L. Salzberg, Alejandro Sanchez-Gracia, David J. Saranga, Hajime Sato, Stephen W. Schaeffer, Michael C. Schatz, Todd Schlenke, Russell Schwartz, Carmen Segarra, Rama S. Singh, Laura Sirot, Marina Sirota, Nicholas B. Sisneros, Chris D. Smith, Temple F. Smith, John Spieth, Deborah E. Stage, Alexander Stark, Wolfgang Stephan, Robert L. Strausberg, Sebastian Strempel, David Sturgill, Granger Sutton, Granger G. Sutton, Wei Tao, Sarah Teichmann, Yoshiko N. Tobari, Yoshihiko Tomimura, Jason M. Tsolas, Vera L. S. Valente, Eli Venter, J. Craig Venter, Saverio Vicario, Filipe G. Vieira, Albert J. Vilella, Alfredo Villasante, Brian Walenz, Jun Wang, Marvin Wasserman, Thomas Watts, Derek Wilson, Richard K. Wilson, Rod A. Wing, Mariana F. Wolfner, Alex Wong, Gane Ka-Shu Wong, Chung- I. Wu, Gabriel Wu, Daisuke Yamamoto, Hsiao-Pei Yang, Shiaw-Pyng Yang, James A. Yorke, Kiyohito Yoshida, Evgeny Zdobnov, Peili Zhang, Yu Zhang, Aleksey V. Zimin, Jennifer Baldwin, Amr Abdouelleil, Jamal Abdulkadir, Adal Abebe, Brikti Abera, Justin Abreu, St Christophe Acer, Lynne Aftuck, Allen Alexander, Peter An, Erica Anderson, Scott Anderson, Harindra Arachi, Marc Azer, Pasang Bachantsang, Andrew Barry, Tashi Bayul, Aaron Berlin, Daniel Bessette, Toby Bloom, Jason Blye, Leonid Boguslavskiy, Claude Bonnet, Boris Boukhgalter, Imane Bourzgui, Adam Brown, Patrick Cahill, Sheridon Channer, Yama Cheshatsang, Lisa Chuda, Mieke Citroen, Alville Collymore, Patrick Cooke, Maura Costello, Katie D'Aco, Riza Daza, Georgius De Haan, Stuart DeGray, Christina DeMaso, Norbu Dhargay, Kimberly Dooley, Erin Dooley, Missole Doricent, Passang Dorje, Kunsang Dorjee, Alan Dupes, Richard Elong, Jill Falk, Abderrahim Farina, Susan Faro, Diallo Ferguson, Sheila Fisher, Chelsea D. Foley, Alicia Franke, Dennis Friedrich, Loryn Gadbois, Gary Gearin, Christina R. Gearin, Georgia Giannoukos, Tina Goode, Joseph Graham, Edward Grandbois, Sharleen Grewal, Kunsang Gyaltsen, Nabil Hafez, Birhane Hagos, Jennifer Hall, Charlotte Henson, Andrew Hollinger, Tracey Honan, Monika D. Huard, Leanne Hughes, Brian Hurhula, M. Erii Husby, Asha Kamat, Ben Kanga, Seva Kashin, Dmitry Khazanovich, Peter Kisner, Krista Lance, Marcia Lara, William Lee, Niall Lennon, Frances Letendre, Rosie LeVine, Alex Lipovsky, Xiaohong Liu, Jinlei Liu, Shangtao Liu, Tashi Lokyitsang, Yeshi Lokyitsang, Rakela Lubonja, Annie Lui, Pen MacDonald, Vasilia Magnisalis, Kebede Maru, Charles Matthews, William McCusker, Susan McDonough, Teena Mehta, James Meldrim, Louis Meneus, Oana Mihai, Atanas Mihalev, Tanya Mihova, Rachel Mittelman, Valentine Mlenga, Anna Montmayeur, Leonidas Mulrain, Adam Navidi, Jerome Naylor, Tamrat Negash, Thu Nguyen, Nga Nguyen, Robert Nicol, Choe Norbu, Nyima Norbu, Nathaniel Novod, Barry O'Neill, Sahal Osman, Eva Markiewicz, Otero L. Oyono, Christopher Patti, Pema Phunkhang, Fritz Pierre, Margaret Priest, Sujaa Raghuraman, Filip Rege, Rebecca Reyes, Cecil Rise, Peter Rogov, Keenan Ross, Elizabeth Ryan, Sampath Settipalli, Terry Shea, Ngawang

Sherpa, Lu Shi, Diana Shih, Todd Sparrow, Jessica Spaulding, John Stalker, Nicole Stange-Thomann, Sharon Stavropoulos, Catherine Stone, Christopher Strader, Senait Tesfaye, Talene Thomson, Yama Thoulutsang, Dawa Thoulutsang, Kerri Topham, Ira Topping, Tsamla Tsamla, Helen Vassiliev, Andy Vo, Tsering Wangchuk, Tsering Wangdi, Michael Weiand, Jane Wilkinson, Adam Wilson, Shailendra Yadav, Geneva Young, Qing Yu, Lisa Zembek, Danni Zhong, Andrew Zimmer, Zac Zwirko, Pablo Alvarez, Will Brockman, Jonathan Butler, CheeWhye Chin, Manfred Grabherr, Michael Kleber, Evan Mauceli, Iain MacCallum, Consor Drosophila 12 Genomes, Sequencing Broad Inst Genome, and Ass Broad Inst Whole Genome. 2007. 'Evolution of genes and genomes on the Drosophila phylogeny', *Nature*, 450: 203-18.

Czabotar, Peter E., Guillaume Lessene, Andreas Strasser, and Jerry M. Adams. 2014. 'Control of apoptosis by the BCL-2 protein family: implications for physiology and therapy', *Nature Reviews Molecular Cell Biology*, 15: 49-63.

Dada, Oluwatosin O., Bonnie J. Huge, and Norman J. Dovichi. 2012. 'Simplified sheath flow cuvette design for ultrasensitive laser induced fluorescence detection in capillary electrophoresis', *Analyst*, 137: 3099-101.

Delamarche, E., A. Bernard, H. Schmid, B. Michel, and H. Biebuyck. 1997. 'Patterned delivery of immunoglobulins to surfaces using microfluidic networks', *Science*, 276: 779-81.

Di Carlo, D., K. H. Jeong, and L. P. Lee. 2003. 'Reagentless mechanical cell lysis by nanoscale barbs in microchannels for sample preparation', *Lab on a Chip*, 3: 287-91.

Dong, Mingming, Minghuo Wu, Fangjun Wang, Hongqiang Qin, Guanghui Han, Jing Gong, Ren'an Wu, Mingliang Ye, Zhen Liu, and Hanfa Zou. 2010. 'Coupling Strong Anion-Exchange Monolithic Capillary with MALDI-TOF MS for Sensitive Detection of Phosphopeptides in Protein Digest', *Analytical Chemistry*, 82: 2907-15.

Doucette, A., D. Craft, and L. Li. 2003. 'Mass spectrometric study of the effects of hydrophobic surface chemistry and morphology on the digestion of surface-bound proteins', *Journal of the American Society for Mass Spectrometry*, 14: 203-14.

Eyer, K., S. Stratz, P. Kuhn, S. K. Kuester, and P. S. Dittrich. 2013. 'Implementing Enzyme-Linked Immunosorbent Assays on a Microfluidic Chip To Quantify Intracellular Molecules in Single Cells', *Analytical Chemistry*, 85: 3280-87.

Eyer, Klaus, Phillip Kuhn, Conni Hanke, and Petra S. Dittrich. 2012. 'A microchamber array for single cell isolation and analysis of intracellular biomolecules', *Lab on a Chip*, 12: 765-72.

Fan, Yi, Chang Young Lee, Stanislav S. Rubakhin, and Jonathan V. Sweedler. 2013. 'Stimulation and release from neurons via a dual capillary collection device interfaced to mass spectrometry', *Analyst*, 138: 6337-46.

Ferrell, J. E., and E. M. Machleder. 1998. 'The biochemical basis of an all-or-none cell fate switch in Xenopus oocytes', *Science*, 280: 895-98.

Freer, Giulia, and Laura Rindi. 2013. 'Intracellular cytokine detection by fluorescence-activated flow cytometry: Basic principles and recent advances', *Methods*, 61: 30-38.

Fuller, R. R., L. L. Moroz, R. Gillette, and J. V. Sweedler. 1998. 'Single neuron analysis by capillary electrophoresis with fluorescence spectroscopy', *Neuron*, 20: 173-81.

Gabriel, B., and J. Teissie. 1999. 'Time courses of mammalian cell electropermeabilization observed by millisecond imaging of membrane property changes during the pulse', *Biophysical Journal*, 76: 2158-65.

Graf, Thomas, and Matthias Stadtfeld. 2008. 'Heterogeneity of Embryonic and Adult Stem Cells', *Cell Stem Cell*, 3: 480-83.

Han, F. T., Y. Wang, C. E. Sims, M. Bachman, R. S. Chang, G. P. Li, and N. L. Allbritton. 2003. 'Fast electrical lysis of cells for capillary electrophoresis', *Analytical Chemistry*, 75: 3688-96.

Hanke, Stefan, Hueseyin Besir, Dieter Oesterhelt, and Matthias Mann. 2008. 'Absolute SILAC for accurate quantitation of proteins in complex mixtures down to the attomole level', *Journal of Proteome Research*, 7: 1118-30.

Harwood, Melissa M., Joan V. Bleecker, Peter S. Rabinovitch, and Norman J. Dovichi. 2007. 'Cell cycle-dependent characterization of single MCF-7 breast cancer cells by 2-D CE', *Electrophoresis*, 28: 932-37.

Hirschi, Karen K., Song Li, and Krishnendu Roy. 2014. 'Induced Pluripotent Stem Cells for Regenerative Medicine', *Annual Review of Biomedical Engineering, Vol 16*, 16: 277-94.

Hofstadler, S. A., J. C. Severs, R. D. Smith, F. D. Swanek, and A. G. Ewing. 1996. 'High performance Fourier transform ion cyclotron resonance mass spectrometric detection for capillary electrophoresis', *Hrc-Journal of High Resolution Chromatography*, 19: 617-21.

Irish, J. M., R. Hovland, P. O. Krutzik, O. D. Perez, O. Bruserud, B. T. Gjertsen, and G. P. Nolan. 2004. 'Single cell profiling of potentiated phospho-protein networks in cancer cells', *Cell*, 118: 217-28.

Jain, Kewal K. 2010. *The Handbook of Biomarkers* (Humana Press).

Janicki, S. M., T. Tsukamoto, S. E. Salghetti, W. P. Tansey, R. Sachidanandam, K. V. Prasanth, T. Ried, Y. Shav-Tal, E. Bertrand, R. H. Singer, and D. L. Spector. 2004. 'From silencing to gene expression: Real-time analysis in single cells', *Cell*, 116: 683-98.

Jo, Kyubong, Michael L. Heien, Lucas B. Thompson, Ming Zhong, Ralph G. Nuzzo, and Jonathan V. Sweedler. 2007. 'Mass spectrometric imaging of peptide release from neuronal cells within microfluidic devices', *Lab on a Chip*, 7: 1454-60.

Kalisky, Tomer, Paul Blainey, and Stephen R. Quake. 2011. 'Genomic Analysis at the Single-Cell Level', *Annual Review Genetics, Vol 45*, 45: 431-45.

Kandouz, M., M. Siromachkova, D. Jacob, B. C. Marquet, A. Therwath, and A. Gompel. 1996. 'Antagonism between estradiol and progestin on Bcl-2 expression in breast-cancer cells', *International Journal of Cancer*, 68: 120-25.

Karas, M., D. Bachmann, U. Bahr, and F. Hillenkamp. 1987. ' Matrix-assisted ultraviolet-laser desorption of nonvolatile compounds ', *International Journal of Mass Spectrometry and Ion Processes*, 78: 53-68.

Kim, Dohyun, and Amy E. Herr. 2013. 'Protein immobilization techniques for microfluidic assays', *Biomicrofluidics*, 7.

Krenkova, J., and F. Foret. 2004. 'Immobilized microfluidic enzymatic reactors', *Electrophoresis*, 25: 3550-63.

Kurn, N., P. C. Chen, J. D. Heath, A. Kopf-Sill, K. M. Stephens, and S. L. Wang. 2005. 'Novel isothermal, linear nucleic acid amplification systems for highly multiplexed applications', *Clinical Chemistry*, 51: 1973-81.

Kvastad, L., B. Werne Solnestam, E. Johansson, A. O. Nygren, N. Laddach, P. Sahlen, S. Vickovic, Schirmer C. Bendigtsen, M. Aaserud, L. Floer, E. Borgen, C. Schwind, R. Himmelreich, D. Latta, and J. Lundeberg. 2015. 'Single cell analysis of cancer cells using an improved RT-MLPA method has potential for cancer diagnosis and monitoring', *Scientific Reports*, 5.

Lambolez, B., E. Audinat, P. Bochet, F. Crepel, and J. Rossier. 1992. 'Ampa receptor subunits expressed by single purkinje-cells', *Neuron*, 9: 247-58.

Lee, H. Y., H. S. Jung, K. Fujikawa, J. W. Park, J. M. Kim, T. Yukimasa, H. Sugihara, and T. Kawai. 2005. 'New antibody immobilization method via functional liposome layer for specific protein assays', *Biosensors & Bioelectronics*, 21: 833-38.

Lee, Ji Eun, Jeong Hyun Seo, Chang Sup Kim, Yunkyeoung Kwon, Jeong Hyub Ha, Suk Soon Choi, and Hyung Joon Cha. 2013. 'A comparative study on antibody immobilization strategies onto solid surface', *Korean Journal of Chemical Engineering*, 30: 1934-38.

Lee, T. T., and E. S. Yeung. 1992. 'High-sensitiviy laser-induced fluorescence detection of native proteins in capillary electrophoresis', *Journal of Chromatography*, 595: 319-25.

Li, H. H., U. B. Gyllensten, X. F. Cui, R. K. Saiki, H. A. Erlich, and N. Arnheim. 1988. 'Amplification and analysis of DNA-sequences in single human-sperm and diploid-cells', *Nature*, 335: 414-17.

Li, L., R. E. Golding, and R. M. Whittal. 1996. 'Analysis of single mammalian cell lysates by mass spectrometry', *Journal of the American Chemical Society*, 118: 11662-63.

Li, Y. L., M. L. Gross, and F. F. Hsu. 2005. 'Ionic-liquid matrices for improved analysis of phospholipids by MALDI-TOF mass spectrometry', *Journal of the American Society for Mass Spectrometry*, 16: 679-82.

Lorincz, M. C., M. K. Parente, M. Roederer, G. P. Nolan, Z. J. Diwu, D. I. K. Martin, L. A. Herzenberg, and J. H. Wolfe. 1999. 'Single cell analysis and selection of living retrovirus vector-corrected mucopolysaccharidosis VII cells using a fluorescence-activated cell sorting-based assay for mammalian beta-glucuronidase enzymatic activity', *Journal of Biological Chemistry*, 274: 657-65.

Lottspeich, F. 1999. 'Proteome analysis: A pathway to the functional analysis of proteins', *Angewandte Chemie-International Edition*, 38: 2477-92.

Lu, Jang-Jih, Fuu-Jen Tsai, Cheng-Mao Ho, Yu-Ching Liu, and Chao-Jung Chen. 2012. 'Peptide Biomarker Discovery for Identification of Methicillin-Resistant and Vancomycin-Intermediate Staphylococcus aureus Strains by MALDI-TOF', *Analytical Chemistry*, 84: 5685-92.

Lu, Kuan-Ying, Andrew M. Wo, Ying-Jie Lo, Ken-Chao Chen, Cheng-Ming Lin, and Chii-Rong Yang. 2006. 'Three dimensional electrode array for cell lysis via electroporation', *Biosensors & Bioelectronics*, 22: 568-74.

Majewski, Ian J., and Rene Bernards. 2011. 'Taming the dragon: genomic biomarkers to individualize the treatment of cancer', *Nature Medicine*, 17: 304-12.

Martinkova, Jirina, Suresh Jivan Gadher, Marian Hajduch, and Hana Kovarova. 2009. 'Challenges in cancer research and multifaceted approaches for cancer biomarker quest', *FEBS Letters*, 583: 1772-84.

Massimo Cristofanilli, Thomas Budd, Matthew J. Ellis, Alison Stopeck, Jeri Matera. 2004. 'Circulating Tumor Cells, Disease Progression, and Survival in Metastatic Breast Cancer', *The New England Journal of Medicine*, 351: 11.

Mazutis, Linas, John Gilbert, W. Lloyd Ung, David A. Weitz, Andrew D. Griffiths, and John A. Heyman. 2013. 'Single-cell analysis and sorting using droplet-based microfluidics', *Nature Protocols*, 8: 870-91.

McMahon, Robert J. 2008. *Avidin-Biotin Interactions* (Humana Press).

Merali, Zamir, Meah MingYang Gao, Tim Bowes, Jian Chen, Kenneth Evans, and Andrea Kassner. 2014. 'Neuroproteome Changes after Ischemia/Reperfusion Injury and Tissue Plasminogen Activator Administration in Rats: A Quantitative iTRAQ Proteomics Study', *Plos One*, 9.

Miura, Daisuke, Yoshinori Fujimura, Hirofumi Tachibana, and Hiroyuki Wariishi. 2010. 'Highly Sensitive Matrix-Assisted Laser Desorption Ionization-Mass Spectrometry for High-Throughput Metabolic Profiling', *Analytical Chemistry*, 82: 498-504.

Mohan, Ritika, Benjamin R. Schudel, Amit V. Desai, Joshua D. Yearsley, Christopher A. Apblett, and Paul J. A. Kenis. 2011. 'Design considerations for elastomeric normally closed microfluidic valves', *Sensors and Actuators B-Chemical*, 160: 1216-23.

Moon, Hyejin, Aaron R. Wheeler, Robin L. Garrell, Joseph A. Loo, and Chang-Jin C. J. Kim. 2006. 'An integrated digital microfluidic chip for multiplexed proteomic sample preparation and analysis by MALDI-MS', *Lab on a Chip*, 6: 1213-19.

Mull, Amber N., Ashwini Zolekar, and Yu-Chieh Wang. 2015. 'Understanding Melanocyte Stem Cells for Disease Modeling and Regenerative Medicine Applications', *International Journal of Molecular Sciences*, 16: 30458-69.

Nakajima-Takagi, Yaeko, Mitsujiro Osawa, and Atsushi Iwama. 2014. 'Manipulation of Hematopoietic Stem Cells for Regenerative Medicine', *Anatomical Record-Advances in Integrative Anatomy and Evolutionary Biology*, 297: 111-20.

Nashimoto, Yuji, Yasufumi Takahashi, Takeshi Yamakawa, Yu-Suke Torisawa, Tomoyuki Yasukawa, Takahiro Ito-Sasaki, Masaki Yokoo, Hiroyuki Abe, Hitoshi Shiku, Hideki Kambara, and Tomokazu Matsue. 2007. 'Measurement of gene expression from single adherent cells and spheroids collected using fast electrical lysis', *Analytical Chemistry*, 79: 6823-30.

Nelson, Wyatt C., Ivory Peng, Geun-An Lee, Joseph A. Loo, Robin L. Garrell, and Chang-Jin C. J. Kim. 2010. 'Incubated Protein Reduction and Digestion on an Electrowetting-on-Dielectric Digital Microfluidic Chip for MALDI-MS', *Analytical Chemistry*, 82: 9932-37.

Nemes, Peter, Ann M. Knolhoff, Stanislav S. Rubakhin, and Jonathan V. Sweedler. 2011. 'Metabolic Differentiation of Neuronal Phenotypes by Single-cell Capillary Electrophoresis-Electrospray Ionization-Mass Spectrometry', *Analytical Chemistry*, 83: 6810-17.

Nemes, Peter, Ann M. Knolhoff, Stanislav S. Rubakhin, and Jonathan V. Sweedler. 2012. 'Single-Cell Metabolomics: Changes in the Metabolome of Freshly Isolated and Cultured Neurons', *Acs Chemical Neuroscience*, 3: 782-92.

Ng, H. T., A. P. Fang, L. Q. Huang, and S. F. Y. Li. 2002. 'Protein microarrays on ITO surfaces by a direct covalent attachment scheme', *Langmuir*, 18: 6324-29.

Noirel, Josselin, Caroline Evans, Malinda Salim, Joy Mukherjee, Saw Yen Ow, Jagroop Pandhal, Pham Trong Khoa, Catherine A. Biggs, and Phillip C. Wright. 2011. 'Methods in Quantitative Proteomics: Setting iTRAQ on the Right Track', *Current Proteomics*, 8: 17-30.

Nordhoff, Eckhard, Hans Lehrach, and Johan Gobom. 2007. 'Exploring the limits and losses in MALDI sample preparation of attomole amounts of peptide mixtures', *International Journal of Mass Spectrometry*, 268: 139-46.

Ocvirk, G., H. Salimi-Moosavi, R. J. Szarka, E. A. Arriaga, P. E. Andersson, R. Smith, N. J. Dovichi, and D. J. Harrison. 2004. 'beta-galactosidase assays of single-cell lysates on a microchip: A complementary method for enzymatic analysis of single cells', *Proceedings of the Ieee*, 92: 115-25.

Odowd, D. K., and M. A. Smith. 1996. 'Single-cell analysis of gene expression in the nervous system - Measurements at the edge of chaos', *Molecular Neurobiology*, 13: 199-211.

Page, J. S., S. S. Rubakhin, and J. V. Sweedler. 2002. 'Single-neuron analysis using CE combined with MALDI MS and radionuclide detection', *Analytical Chemistry*, 74: 497-503.

Pan, S., H. Zhang, J. Rush, J. Eng, N. Zhang, D. Patterson, M. J. Comb, and R. Aebersold. 2005. 'High throughput proteome screening for biomarker detection', *Molecular & Cellular Proteomics*, 4: 182-90.

Pedreira, Carlos E., Elaine S. Costa, Quentin Lecrevisse, Jacques J. M. van Dongen, Alberto Orfao, and Consortium EuroFlow. 2013. 'Overview of clinical flow cytometry data analysis: recent advances and future challenges', *Trends in Biotechnology*, 31: 415-25.

Peluso, P., D. S. Wilson, D. Do, H. Tran, M. Venkatasubbaiah, D. Quincy, B. Heidecker, K. Poindexter, N. Tolani, M. Phelan, K. Witte, L. S. Jung, P. Wagner, and S. Nock. 2003. 'Optimizing antibody immobilization strategies for the construction of protein microarrays', *Analytical Biochemistry*, 312: 113-24.

Perez-Almodovar, Ernie X., and Giorgio Carta. 2009. 'IgG adsorption on a new protein A adsorbent based on macroporous hydrophilic polymers. I. Adsorption equilibrium and kinetics', *Journal of Chromatography A*, 1216: 8339-47.

Perez, O. D., and G. P. Nolan. 2002. 'Simultaneous measurement of multiple active kinase states using polychromatic flow cytometry', *Nature Biotechnology*, 20: 155-62.

Perkins, D. N., D. J. C. Pappin, D. M. Creasy, and J. S. Cottrell. 1999. 'Probability-based protein identification by searching sequence databases using mass spectrometry data', *Electrophoresis*, 20: 3551-67.

Petricoin, E. F., K. C. Zoon, E. C. Kohn, J. C. Barrett, and L. A. Liotta. 2002. 'Clinical proteomics: Translating benchside promise into bedside reality', *Nature Reviews Drug Discovery*, 1: 683-95.

Qi, Xingmei, Yifan Sun, and Sidong Xiong. 2015. 'A single freeze-thawing cycle for highly efficient solubilization of inclusion body proteins and its refolding into bioactive form', *Microbial Cell Factories*, 14.

Rau, K. R., A. Guerra, A. Vogel, and V. Venugopalan. 2004. 'Investigation of laser-induced cell lysis using time-resolved imaging', *Applied Physics Letters*, 84: 2940-42.

Rau, K. R., P. A. Quinto-Su, A. N. Hellman, and V. Venugopalan. 2006. 'Pulsed laser microbeam-induced cell lysis: Time-resolved imaging and analysis of hydrodynamic effects', *Biophysical Journal*, 91: 317-29.

Renart, J., J. Reiser, and G. R. Stark. 1979. ' Transfer of proteins from gels to diazobenzyloxymethyl-paper and detection with antisera-method for studying antibody specificity and antigen structure ', *Proceedings of the National Academy of Sciences of the United States of America*, 76: 3116-20.

Roman, Gregory T., Yanli Chen, Pernilla Viberg, Anne H. Culbertson, and Christopher T. Culbertson. 2007. 'Single-cell manipulation and analysis using microfluidic devices', *Analytical and Bioanalytical Chemistry*, 387: 9-12.

Roman, Gregory T., and Robert T. Kennedy. 2007. 'Fully integrated microfluidic separations systems for biochemical analysis', *Journal of Chromatography A*, 1168: 170-88.

Roncador, G., P. J. Brown, L. Maestre, S. Hue, J. L. Martinez-Torrecuadrada, K. L. Ling, S. Pratap, C. Toms, B. C. Fox, V. Cerundolo, F. Powrie, and A. H. Banham. 2005. 'Analysis of FOXP3 protein expression in human CD4(+)CD25(+) regulatory T cells at the single-cell level', *European Journal of Immunology*, 35: 1681-91.

Ross, P. L., Y. L. N. Huang, J. N. Marchese, B. Williamson, K. Parker, S. Hattan, N. Khainovski, S. Pillai, S. Dey, S. Daniels, S. Purkayastha, P. Juhasz, S. Martin, M. Bartlet-Jones, F. He, A. Jacobson, and D. J. Pappin. 2004. 'Multiplexed protein quantitation in Saccharomyces cerevisiae using amine-reactive isobaric tagging reagents', *Molecular & Cellular Proteomics*, 3: 1154-69.

Rowe, C. A., S. B. Scruggs, M. J. Feldstein, J. P. Golden, and F. S. Ligler. 2003. 'An array immunosensor for simultaneous detection of clinical analytes (vol 71, pg 433, 1999)', *Analytical Chemistry*, 75: 1225-25.

Rubakhin, S. S., W. T. Greenough, and J. V. Sweedler. 2003. 'Spatial profiling with MALDI MS: Distribution of neuropeptides within single neurons', *Analytical Chemistry*, 75: 5374-80.

Rubakhin, Stanislav S., James D. Churchill, William T. Greenough, and Jonathan V. Sweedler. 2006. 'Profiling signaling peptides in single mammalian cells using mass spectrometry', *Analytical Chemistry*, 78: 7267-72.

Rubakhin, Stanislav S., and Jonathan V. Sweedler. 2008. 'Quantitative measurements of cell-cell signaling peptides with single-cell MALDI MS', *Analytical Chemistry*, 80: 7128-36.

Rusmini, Federica, Zhiyuan Zhong, and Jan Feijen. 2007. 'Protein immobilization strategies for protein biochips', *Biomacromolecules*, 8: 1775-89.

Seeley, Erin H., and Richard M. Caprioli. 2008. 'Molecular imaging of proteins in tissues by mass spectrometry', *Proceedings of the National Academy of Sciences of the United States of America*, 105: 18126-31.

Shapiro, G. I., C. D. Edwards, L. Kobzik, J. Godleski, W. Richards, D. J. Sugarbaker, and B. J. Rollins. 1995. ' Reciprocal Rb inactivation and P16INK4 expression in primary lung cancers and cell-lines', *Cancer Research*, 55: 505-09.

Shen, Guangyu, Chenbo Cai, Kun Wang, and Jilin Lu. 2011. 'Improvement of antibody immobilization using hyperbranched polymer and protein A', *Analytical Biochemistry*, 409: 22-27.

Sims, Christopher E., and Nancy L. Allbritton. 2007. 'Analysis of single mammalian cells on-chip', *Lab on a Chip*, 7: 423-40.

Sobhani, Kimia, Susan L. Fink, Brad T. Cookson, and Norman J. Dovichi. 2007. 'Repeatability of chemical cytometry: 2-DE analysis of single RAW 264.7 macrophage cells', *Electrophoresis*, 28: 2308-13.

Stratz, Simone, Klaus Eyer, Felix Kurth, and Petra S. Dittrich. 2014. 'On-Chip Enzyme Quantification of Single Escherichia coli Bacteria by Immunoassay-based Analysis', *Analytical Chemistry*, 86: 12375-81.

Stuart, J. N., and J. V. Sweedler. 2003. 'Single-cell analysis by capillary electrophoresis', *Analytical and Bioanalytical Chemistry*, 375: 28-29.

Takahashi, Kazutoshi, Koji Tanabe, Mari Ohnuki, Megumi Narita, Tomoko Ichisaka, Kiichiro Tomoda, and Shinya Yamanaka. 2007. 'Induction of pluripotent stem cells from adult human fibroblasts by defined factors', *Cell*, 131: 861-72.

Tanaka, Hiroyuki, Minako Hanasaki, Tatsushi Isojima, Hisao Takeuchi, Toshifumi Shiroya, and Haruma Kawaguchi. 2009. 'Enhancement of sensitivity of SPR protein microarray using a novel 3D protein immobilization', *Colloids and Surfaces B-Biointerfaces*, 70: 259-65.

Thierry, Benjamin, Mahaveer Kurkuri, Jun Yan Shi, Ei Mon Phyo Lwin, and Dennis Palms. 2010. 'Herceptin functionalized microfluidic polydimethylsiloxane devices for the capture of human epidermal growth factor receptor 2 positive circulating breast cancer cells', *Biomicrofluidics*, 4.

Tholey, A., M. Zabet-Moghaddam, and E. Heinzle. 2006. 'Quantification of peptides for the monitoring of protease-catalyzed reactions by matrix-assisted laser desorption/ionization mass spectrometry using ionic liquid matrixes', *Analytical Chemistry*, 78: 291-97.

Toriello, Nicholas M., Erik S. Douglas, Numrin Thaitrong, Sonny C. Hsiao, Matthew B. Francis, Carolyn R. Bertozzi, and Richard A. Mathies. 2008. 'Integrated microfluidic bioprocessor for single-cell gene expression analysis', *Proceedings of the National Academy of Sciences of the United States of America*, 105: 20173-78.

Treumann, Achim, and Bernd Thiede. 2010. 'Isobaric protein and peptide quantification: perspectives and issues', *Expert Review of Proteomics*, 7: 647-53.

Ullal, Adeeti V., Vanessa Peterson, Sarit S. Agasti, Suan Tuang, Dejan Juric, Cesar M. Castro, and Ralph Weissleder. 2014. 'Cancer Cell Profiling by Barcoding Allows Multiplexed Protein Analysis in Fine-Needle Aspirates', *Science Translational Medicine*, 6.

Unger, M. A., H. P. Chou, T. Thorsen, A. Scherer, and S. R. Quake. 2000. 'Monolithic microfabricated valves and pumps by multilayer soft lithography', *Science*, 288: 113-16.

'The Uniprot Consortium'. 2012. *Nucleic Acids Research*, 40: 5.

Verbeek, B. S., T. M. Vroom, S. S. AdriaansenSlot, A. E. OttenhoffKalff, J. G. N. Geertzema, A. Hennipman, and G. Rijksen. 1996. 'c-Src protein expression is increased in human breast cancer. An immunohistochemical and biochemical analysis', *Journal of Pathology*, 180: 383-88.

Wang, Daojing, and Steven Bodovitz. 2010. 'Single cell analysis: the new frontier in 'omics'', *Trends in Biotechnology*, 28: 281-90.

Wang, Ying-Chih, and Jongyoon Han. 2008. 'Pre-binding dynamic range and sensitivity enhancement for immuno-sensors using nanofluidic preconcentrator', *Lab on a Chip*, 8: 392-94.

Weinberg, Robert A. 2013. *The Biology of Cancer* (Garland Science).

Wheeler, A. R., H. Moon, C. A. Bird, R. R. O. Loo, C. J. Kim, J. A. Loo, and R. L. Garrell. 2005. 'Digital microfluidics with in-line sample purification for proteomics analyses with MALDI-MS', *Analytical Chemistry*, 77: 534-40.

Whitesides, George M. 2006. 'The origins and the future of microfluidics', *Nature*, 442: 368-73.

Wiese, Sebastian, Kai A. Reidegeld, Helmut E. Meyer, and Bettina Warscheid. 2007. 'Protein labeling by iTRAQ: A new tool for quantitative mass spectrometry in proteome research', *Proteomics*, 7: 340-50.

Wu, Meiye, and Anup K. Singh. 2012. 'Single-cell protein analysis', *Current Opinion in Biotechnology*, 23: 83-88.

Xie, Weiyi, Dan Gao, Feng Jin, Yuyang Jiang, and Hongxia Liu. 2015. 'Study of Phospholipids in Single Cells Using an Integrated Microfluidic Device Combined with Matrix-Assisted Laser Desorption/Ionization Mass Spectrometry', *Analytical Chemistry*, 87: 7052-59.

Xie, X. Sunney, Paul J. Choi, Gene-Wei Li, Nam Ki Lee, and Giuseppe Lia. 2008. 'Single-molecule approach to molecular biology in living bacterial cells', *Annual Review of Biophysics*, 37: 417-44.

XiXi Chen, Fan Bai. 2015. 'single-cell analyses of circulating tumor cells', *Cancer Biology&Medicine*, 12: 9.

Yang, Mian, Tzu-Chiao Chao, Randall Nelson, and Alexandra Ros. 2012. 'Direct detection of peptides and proteins on a microfluidic platform with MALDI mass spectrometry', *Analytical and Bioanalytical Chemistry*, 404: 1681-89.

Zabet-Moghaddam, M., E. Heinzle, and A. Tholey. 2004. 'Qualitative and quantitative analysis of low molecular weight compounds by ultraviolet matrix-assisted laser

desorption/ionization mass spectrometry using ionic liquid matrices', *Rapid Communications in Mass Spectrometry*, 18: 141-48.

Zhang, H., and W. R. Jin. 2004. 'Determination of different forms of human interferon-gamma in single natural killer cells by capillary electrophoresis with on-capillary immunoreaction and laser-induced fluorescence detection', *Electrophoresis*, 25: 1090-95.

Zhang, H., and W. R. Jin. 2006. 'Single-cell analysis by intracellular immuno-reaction and capillary electrophoresis with laser-induced fluorescence detection', *Journal of Chromatography A*, 1104: 346-51.

Zhang, W.Y., G. S. Ferguson, and S. Tatic-Lucic. 2004. 'Elastomer-supported cold welding for room temperature wafer-level bonding', *Micro Electro Mechanical Systems*: 4.

APPENDIX A

SUPPLEMENTAL MATERIAL FOR CHAPTER 4

Appendix A 1: Influence of iTRAQ ratios on the quantification of Bcl-2

The quantification of Bcl-2 on-chip was achieved by using two iTRAQ tags. The MS/MS analysis allows for the detection of the iTRAQ labels whereas the peak area ratio of 114 tag /117 tag is used to determine unknown concentrations of the peptides and thus the corresponding protein. To demonstrate the applicability of the peptide tagging by iTRAQ for Bcl-2, digests were differentially labeled with 114 tag and 117 tag. Accordingly, 2 μL of 1.4×10^{-6} M Bcl-2 was mixed with 8 μL iTRAQ dissolution buffer, 2 μL trypsin solution (0.1mg/mL) and 8 μL iTRAQ tag solution (either 114 tag or 117 tag). These solutions were incubated at 37 ℃ overnight. The resulting Bcl-2 concentration was 1.4×10^{-7} M which was the same as the reference tag for Bcl-2 in the main manuscript. Subsequently, Bcl-2 digests with two labels were mixed in various volume ratios. MALDI matrix was added and spotted onto a MALDI target plate. The spots were analyzed by using MALDI-TOF/TOF. Figure A 1 shows the peak area ratios derived from our experiments versus the expected amount ratios of Bcl-2 digest. An average SD of 13.5% was determined which is in good agreement with Wiese et al (Wiese et al. 2007).

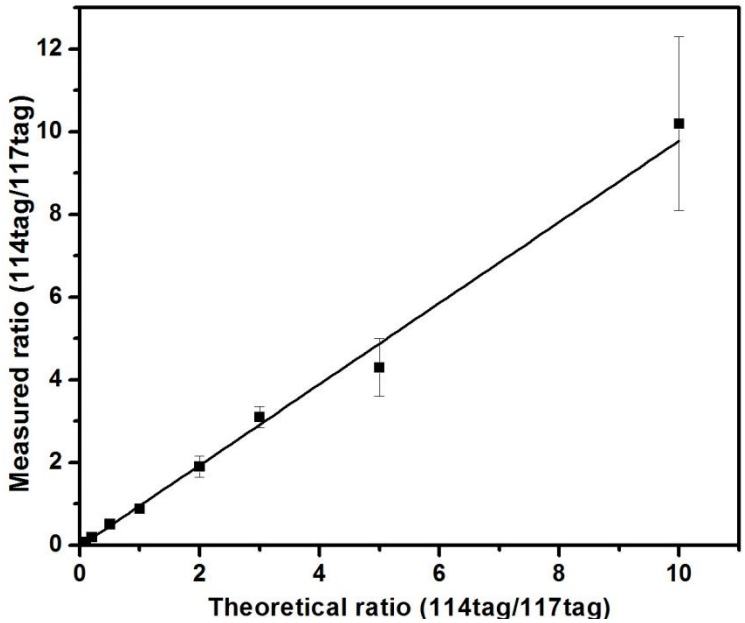

Figure A 1: Linear range between measured peak area ratios of iTRAQ reporter ions (m/Z 114.1 and m/Z 117.1) and theoretical amount ratios of differentially labeled Bcl-2 digest with a slope of 0.98 ±0.054 and R2 of 0.9923. An average SD of 17% was determined (insert: Bcl-2 measurements for different ratios of 114 and 117 tag).

Appendix A 2: Detection Sensitivity for Bcl-2

The concentration range for Bcl-2 detectiction was tested over three orders of magnitude. First, direct detection of digested Bcl-2 was performed. Bcl-2 at three different concentrations (100 nM, 10 nM, 1 nM) was digested by trypsin. Digests were detected by MALDI MS and results are shown in Figure A-3. Second, Bcl-2 in different concentrations (100 nM, 10 nM, 1 nM) was used for the Bcl-2 immunoassay and digestion experiment on chip (Method details were described in Experimental Section in the main manuscript). Results are shown in Figure A 2 and A 3.

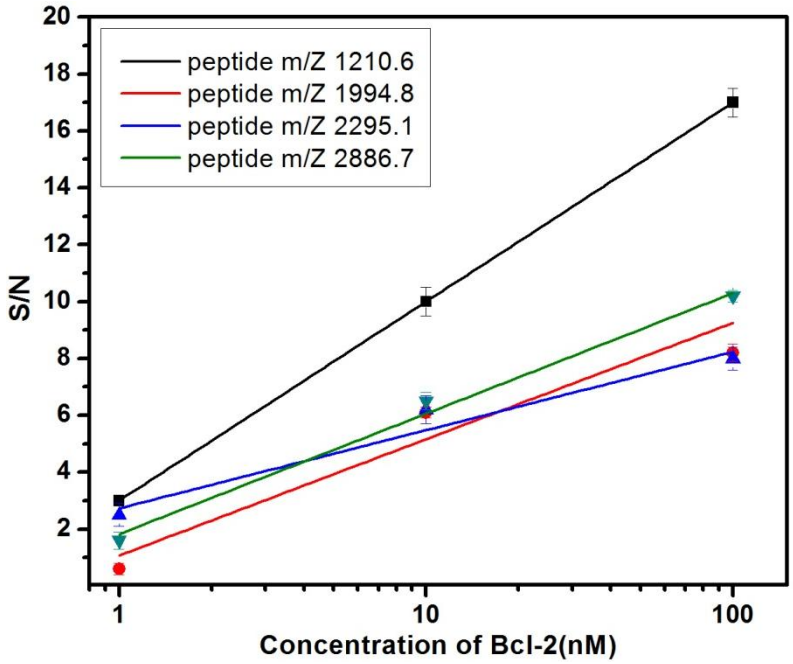

Figure A 2: Signal to noise ratio of Bcl-2 peptides after trypsin digest vs. concentration for various concentrations of Bcl-2.

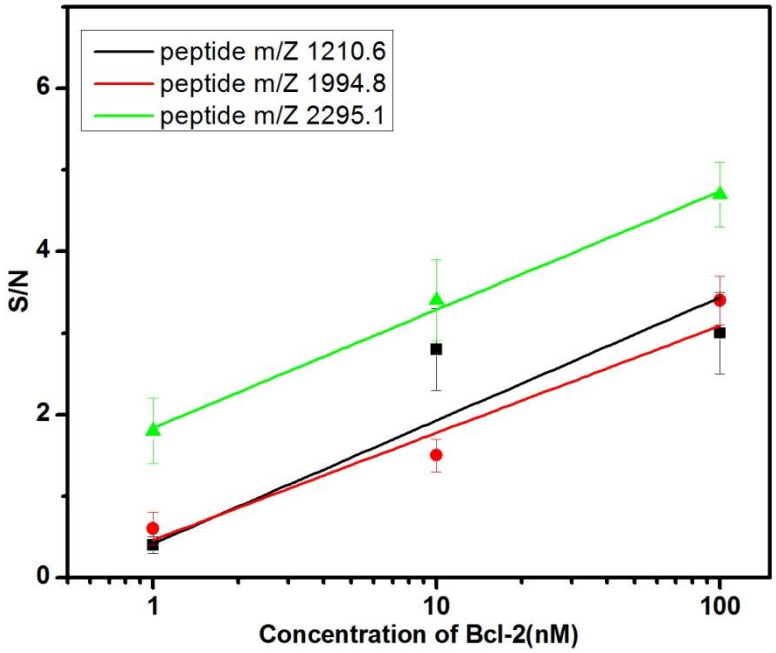

Figure A 3: Signal to noise ratio of Bcl-2 peptides after affinity capture and digestion on chip vs. concentration of Bcl-2.